University of Minnesota
St. Anthony Falls Hydraulic Laboratory

Project Report No. 270

HYDRAULIC TRANSIENT MODELING OF TARP SYSTEMS

by

Charles C. S. Song,

Qizhong Guo

and

Yifan Zheng

Prepared for

METROPOLITAN SANITARY DISTRICT OF GREATER CHICAGO
Chicago, Illinois 60611

March 1988

TABLE OF CONTENTS

LIST OF FIGURES

Figure No.

I. INTRODUCTION

Under the agreement of November 1, 1986, between the Metropolitan Sanitary District of Greater Chicago and the University of Minnesota, the St. Anthony Falls Hydraulic Laboratory of the University conducted mathematical modeling of the recently completed portions of the Tunnel and Reservoir Plan (TARP), both the Mainstream System and the Calumet System of Greater Chicago, for the purpose of establishing optimum operating procedures and additional structures to control hydraulic transient problems. The scope of the work was later extended to include the Des Plaines System and the 13A tunnel when operated independently of the Mainstream System.

The fully dynamic transient mixed flow mathematical model (MXTRANS) developed at the University of Minnesota was used for this study. In order to enhance the confidence level of the modeling results, attempts were first made to reproduce the transient phenomena observed in the Mainstream System during the storm events of October 3, 1986, September 26, 1986, and October 18, 1985. The work is described in Section III, Calibration of Mainstream Model.

After studying the detailed mechanisms of the air blow-off and geyser process in the Mainstream System, a set of safety criteria were established. These criteria were later used to determine the effectivenss of various solution alternatives. General transient characteristics and the safety criteria are described in Section IV.

Various short-term and long-term solution alternatives for all four systems were studied, and the results described in Sections V, VI, VII, and VIII. Short-term solutions are based mainly on inflow controls using the structures that exist at the present time along with proposed orifice controls. Because only limited means are available, the solutions are mostly effective to storms that are less than the maximum design storm. Long-term solutions are based on the condition after the planned storage reservoirs at the downstream ends of the Mainstream System and Calumet System have been completed. These solutions may include inflow control, additional construction of surge structures, and some structural modification.

This report summarizes the work completed under this contract.

II. THE MIXED TRANSIENT FLOW MODEL

The flow to be simulated is very unsteady and contains highly dynamic phenomena such as pressurization surge and resonance. The model used must be able to simultaneously calculate unsteady open channel flows and unsteady pressurized flow including the abrupt change that occurs at the shock or the surge front.

The well-known St. Venant equations

$$\frac{\partial y}{\partial t} + v \frac{\partial y}{\partial x} + \frac{c^2}{g} \frac{\partial v}{\partial x} = 0 \tag{1}$$

$$g \frac{\partial y}{\partial x} + \frac{\partial v}{\partial t} + v \frac{\partial v}{\partial x} + g(s_f - s_o) = 0 \tag{2}$$

are used to represent the unsteady open channel flow. In the above equations, y is the flow depth, v is the flow velocity, c is the gravity wave speed, S_o is the channel slope, S_f is the energy slope, and g is the acceleration due to gravity.

The corresponding equations for unsteady pressurized flow are:

$$\frac{\partial y}{\partial t} + v \frac{\partial y}{\partial x} + \frac{a^2}{g} \frac{\partial v}{\partial x} = 0 \tag{3}$$

$$g \frac{\partial y}{\partial x} + \frac{\partial v}{\partial t} + v \frac{\partial v}{\partial x} + g(s_f - s_o) = 0 \tag{4}$$

in which a is the pressure wave speed while y takes the meaning of piezometric head measured from the tunnel invert.

The systems of equations (1) ~ (4) are solved by the method of characteristics. Because the transition from the open channel flow condition to pressurized flow condition must be abrupt, as in the case of a hydraulic jump, the special shock boundary conditions must be applied. It was shown by Song[1], for a pressurization surge or a positive surge, where three characteristic equations plus two shock boundary conditions can be used to calculate five unknowns at the interface. These five unknowns are

---

[1]Charles C. S. Song, "Modeling of Mixed-Transient Flow," Proceedings, Vol. I, SECTAM XII, Auburn University, May 10-11, 1984.

v and y on both sides of the interface and the speed of the interface movement. The model can also simulate the negative surge which occurs during the depressurization process.

A number of other boundary conditions representing junctions, dropshafts, reservoirs, and other accessories are also provided in the model. Inflow hydrographs, outflow conditions, and other active or passive flow control methods can also be included in the input data file. Velocity, depth, discharge, and other variables at any location and any time may be specified as outputs.

In principle, if all data are accurate, the model should require no calibration. In practice, however, there may be some uncertainties in the input data that some adjustment to the original input data may be necessary. In the case of the TARP system, the greatest uncertainty exists in the inflow data.

III. CALIBRATION OF MAINSTREAM MODEL

For the mathematical modeling purpose, the simplified Mainstream System configuration, as shown in Fig. 1, is used. The system consists of a main tunnel and six branch tunnels. Numbers shown in Fig. 1 are the station numbers used in the model for the purpose of defining different segments of the system. Each junction is represented by three stations for identification of three connecting segments. The entire system is divided into 242 finite segments of 1000 feet each. Some of the dropshafts located close to each other are combined so that a total of 82 shafts and inflow points are explicitly represented in the model. Each shaft is assumed to be directly attached to the tunnel, and the detailed geometry including the approach conduit is ignored.

Three storm events of October 3, 1986, September 26, 1986, and October 18, 1985, were used for calibration purposes. According to field personnel, the field data of the October 3, 1986, storm are most complete and reliable. There are some uncertainties on the actual gate settings during the October 18, 1985, storm. The September 26, 1986, storm was relatively small, and the transient was mild. Therefore, the October 3, 1986, data are the most useful data for calibration purposes. Inflow hydrographs for each storm were furnished by Mr. Clint J. Keifer, who generated the hydrograph with another model using the measured rainfall data as inputs. The Mainstream System Model, using the synthetic hydrographs and the field records of the actual gate operating procedure as inputs, calculates the time history of discharge and head at all stations. The Metropolitan Sanitary District also furnished the data on the head measured at the downstream end for each storm. The measured and the computed heads at the downstream end of the system were compared and used as the primary means of judging the accuracy of the model. It turned out that the model needed practically no adjustment.

The calculated water level at the downstream end of the Mainstream System due to the October 3, 1986, storm is compared with the measured values in Fig. 2. Similar comparisons for the September 26, 1986, storm are shown in Fig. 3. Because there are too many uncertainties on the gate operating conditions, no meaningful comparison for the October 18, 1985, storm is possible. There are good general agreements between the results of mathematical modeling and the measurements.

The two most important factors that affect the results of simulation are the inflow hydrographs and the amount of water initially stored in the system. Since there is no actual inflow data available, the synthetic inflow hydrographs were accepted as being accurate for calibration purposes. The initial storage in the system was estimated from the measured water level at the downstream end, assuming that the water was stationary and level. In reality, if the water is flowing, the water surface may not be level. Fortunately, the assumption is validated for the Mainstream System because the initial storages are the same for both sta-

tionary and flowing water in the early filling process. The error in the initial storage volume may significantly affect the timing of the sharp rises in water level, each signaling the complete pressurization of the main tunnel or a branch tunnel.

IV. GENERAL TRANSIENT CHARACTERISTICS

A. The Filling Process

1. Mainstream System--existing condition

A series of computer simulations were carried out based on the system configuration as shown in Fig. 1, representing the existing condition of the Mainstream System. The results along the main tunnel as shown in Fig. 4 are studied in detail. Depending on the amount of water initially stored in the tunnel, a downstream portion of the tunnel is pressurized at the beginning of the inflow. As the tunnel continues to fill and the pressurized portion expands, surge develops at the interface between the pressurized zone and the free surface zone. The magnitude of the surge (jump in head) increases as the inflow rate increases. This situation is illustrated by the three instantaneous hydraulic gradelines shown in Fig. 5. Note that the station number shown in this figure refers to that of Fig. 4.

Water is flowing in the opposite direction across the surge front. Water is flowing in the downstream direction ahead of the surge but flowing in the upstream direction behind the surge. The water surface is far from level, and water is rushing towards the upstream end. When the surge front first arrives at the upstream end, at 157 min. as shown in Fig. 6, a large amount of backflow causes water to be squeezed into the dropshaft, raising the water level very rapidly. The smaller the diameter of the shaft, the higher the water level will rise due to this first surge. This high head thus generated at the upstream end now travels downstream as a reflected surge, causing head in the tunnel to surge up once again. At about 159 min., a somewhat weaker surge develops at the downstream end and starts to move upstream. When the two surges, one from upstream and one from downstream, collide at about 163 min., head near DS 52 and DS 53 rises very rapidly. When the reflected surge arrives at the downstream end at about 175 min., it is reflected again and starts to move upstream. Instantaneous hydraulic gradelines after this time are shown in Fig. 7. Clearly, the water in the tunnel rocks as the tunnel is being filled to the ground level.

When the first pressurization surge arrives at a junction, it may break up into two surges; one continues to move along the main tunnel and the other moves along the branch tunnel. Due to the same mechanism just described for the main tunnel, the upstream end of the branch channel may also reflect the surge. Thus, each branch also contributes to surging and rocking of certain characteristic periods. Since the South Fork branch usually fills first, any station downstream experiences first pressure peak due to the filling of this branch. This phenomenon was quite prominent during the October 18, 1985, storm which started when storage was relatively small.

2. Mainstream System--with reservoir at downstream end

A reservoir having the total storage capacity of 32,000 acre-feet and the depth of 196 feet is assumed to exist at the downstream end of the system as shown in Fig. 1. In this case the detailed filling process will depend on the storm size and the amount of water initially stored in the reservoir. If the reservoir water level is initially at or near the crown of the tunnel and the October 3, 1986, storm is the input, then the tunnel will fill from the downstream end and proceed upstream. The pressurization surge intensity will increase in the upstream direction creating significant transient conditions. As shown in Fig. 8, surge conditions still exist in midstream and upstream portions of the tunnel. Insufficient conveyance capacity caused by the backwater effect is responsible for the strong surge.

When the reservoir is initially empty and inflow is larger, then pressurization may initiate somewhere in the midstream of the tunnel due to inadequate conveyance. A simulation run was made with a partially controlled maximum storm hydrograph as shown in Fig. 9. As indicated by the instantaneous hydraulic gradelines plotted in Fig. 10, two pressurization surges, one moving upstream and the other moving downstream, are generated. The surge that moves upstream will collide with the upstream end and cause a rapid head increase at t=110 minutes. The downstream moving surge behaves quite differently because of the reservoir. When the positive surge first arrives at the downstream end, it is immediately eliminated, and the head is reduced to that of the reservoir. At this time the reservoir reflects a negative surge which will travel upstream. This negative surge cannot travel very far upstream before its direction is reversed and becomes a positive surge again because of the large pressure gradient. The reservoir will eliminate the second positive surge and reflect another negative surge. The process repeats itself until the reservoir water level reaches the crown of the tunnel. The pressurization is thus completed.

3. Calumet System

The simplified configuration for modeling purposes of the existing calumet system is shown in Fig. 11. The system consists of the main tunnel and three branches. The entire system is divided into 219 finite elements of 500 ft each. Because the proposed Thornton reservoir is approximately 22,500 ft away from the main tunnel, the model configuration for future conditions is changed as shown in Fig. 12.

The overall slope of the main tunnel of the Calumet System is many times greater than the slope of the Mainstream System. Increased conveyance due to increased slope make the Calumet System unlikely to pressurize from the midsection of the tunnel. Pressurization invariably initiates at the downstream end, with or without the proposed reservoir.

4. Storage Volume--stage relationship

Inflow control is a possible means of preventing surge related problems. Since the surge intensity is strongly related to the total inflow rate during the final stage of the filling process, it is necessary to limit the inflow rate as the tunnel approaches the full condition. The real time information on the amount of water stored in the system is needed to operate the inflow control gates. At the present time the volume of water stored is calculated from the water level data taken at the downstream end of the Mainstream System and by assuming that the water surface is level over the entire system, i.e. hydrostatic condition.

Under a dynamic condition the water surface profile in an open channel flow portion is not level and actual volume may be quite different from that estimated by the depth data at the downstream end alone. The correlations between the storage volume and the water depth at the downstream end under three different conditions for the Mainstream System are shown in Fig. 13. Similar plots for the Calumet System are shown in Fig. 14. In each of these figures, the solid line represents the case when the volume was calculated by assuming static conditions, the broken line represents the storage volume calculated by the model under the dynamic condition of October 3, 1986, storm, and the dashed line represents the dynamic condition of the September 26, 1986, storm.

According to Fig. 13, static approach for the Mainstream System may overpredict the storage by as much as 10 percent while, according to Fig. 14, static approach for the calumet system may underpredict the storage by as much as 65 percent. The different trend shown for the two systems may be explained by the difference in the slope of the tunnels. Qualitative sketches of water surface profiles under the static condition and under a dynamic condition for the two systems are shown in Fig. 15. For the Mainstream System which has a very small slope, the static-free surface extends very far upstream resulting in overprediction. In contrast, for the Calumet System which has a large slope, much of the upstream portion may contain no water under static conditions, but will have flowing water under a dynamic condition. The differences between static prediction and the actual dynamic storage are likely to be greater for longer storms and vice versa.

Real time depth data at more than one station along the main tunnel are clearly required to improve the storage estimation. Numerical experimentations were carried out to determine the method of improving the storage volume calculation. It was found that depth data at two stations, one at the downstream end and one near the upstream end, would be sufficient to make very accurate storage volume calculations. The basic form of the equation needed is given as follows.

$$\hat{V} = \hat{V}_o(y_1) + \hat{V}_1(y_1, y_2) \tag{5}$$

in which

$\hat{V}$ = total estimated storage

$\hat{V}_o(y_1)$ = static storage volume

$\hat{V}_1(y_1, y_2)$ = correction due to dynamic effect

The correction term in Eq. 5 for the Mainstream System is given by

$$\hat{V}_1(y_1, y_2) = -15{,}000\ y_2\sqrt{|14.6 + y_2 - y_1|}\ , \text{ if } y_2 < D_2 \qquad (6)$$

$$\hat{V}_1(y_1, y_2) = -15{,}000\ D_2\sqrt{|14.6 + y_2 - y_1|}\ , \text{ if } y_2 > D_2 \qquad (7)$$

The corresponding equations for the Calumet System are:

$$\hat{V}_1(y_1, y_2) = 70{,}000\ y_2\sqrt{|100 + y_2 - y_1|}\ , \text{ if } y_2 < D_2 \qquad (8)$$

$$\hat{V}_1(y_1, y_2) = 70{,}000\ D_2\sqrt{|100 + y_2 - y_1|}\ , \text{ if } y_2 > D_2 \qquad (9)$$

In the above equations, y_1 is the measured water depth or piezometric head at the downstream end of each system, and y_2 is the measured water depth or piezometric head at the Roosevelt Road construction shaft for the Mainstream System and at St. 3+90 for the Calumet System. D_2 is the diameter of the tunnel at the location where y_2 is being measured.

To visualize the improvement on the storage volume calculation due to the inclusion of the correction term $\hat{V}_1(y_1, y_2)$ in Eq. 5, Figs. 16, 17, 18, and 19 are prepared. Figure 16 shows the correlation between the static storage value $\hat{V}_o(y_1)$ and the actual value V calculated by the dynamic model for two storm conditions for the Mainstream System, without downstream reservoir present. Figure 16 shows the correlation between the corrected storage volume $\hat{V}$ given by Eq. 5 and the actual volume V. The deviations of these curves from the straight diagonal line represent the error of estimation. Similar curves for the Calumet System are shown in Figs. 18 and 19. Considerable improvement of $\hat{V}$ over $\hat{V}_o$ is quite evident. It should be noted that Eqs. 5 ~ 9 are applicable to any storm but only to the system with no reservoir. New equations have to be derived after the reservoirs are constructed.

B. Some Transient Problems

1. The air blow-off phenomenon

When a pressurization surge reaches an upstream end during the filling process, water will rise rapidly in the dropshafts near the upstream end. Water levels in other dropshafts will also rise as the surge reflected by the upstream end travels downstream.

The rising water will then push air inside the dropshaft upward, exerting pressure on the cover. The magnitude of the air pressure depends on the speed of the rising water level and the type of cover grating. Extremely large pressure can be generated if the cover is air tight. Since all covers in the Mainstream System are either fully grated with area ratios of 0.54 or half grated with area ratio of 0.27, it is unlikely that air pressure alone can cause damaging effects.

Assuming steady amounts of air flowing through the cover grating, the force acting on the cover due to the air flow may be calculated by

$$F = \frac{1}{2} \rho_a V_a^2 \; C_D A \; (1 - f) \tag{10}$$

where $$C_D = \left[1 + 0.707 \sqrt{(1-f)} \right]^2 / f^2 \tag{11}$$

f = area ratio.

ρ_a = density of air

V_a = average air speed in dropshaft

A = total cover area

According to Eqs. 10 and 11, air flow velocity required to lift unsecured cover is 131 fps for the fully grated case and 31 fps for the half grated case. The three storms used for calibration did not generate large enough air speed to uplift the cover.

2. The Geyser process

When a water column in a dropshaft rises very slowly to the levels of the connecting pipe, the water may back into the connecting pipe. But if the water column rises too rapidly, it may overshoot the connecting pipe and impact the cover. The impact force is given by

$$F = \rho a \, V(1-f)A \tag{12}$$

where ρ = density of water, and a = speed of pressure wave. According to this equation, the velocity of the water column needed to uplift the half grated and unsecured cover is only 0.1 fps.

If Eq. 12 is not a relevant estimation of the lift force, then the steady flow velocity needed to lift the cover based on Eqs. 10 and 11, with appropriate change in variables from those of air to water, are 4.6 fps for the fully grated cover and 1.1 fps for the half grated cover. Clearly,

only a very small water velocity is needed to lift the cover once water level exceeds the cover level.

An independent mathematical model of a Dropshaft-Drift Tube System as sketched in Fig. 20 was constructed and used to quantify the geyser problem. This model assumes that the surge in the main tunnel imposes a sudden rise in pressure at the downstream end of the drift tube. The surge pressure transmitting through the drift tube acts on the water column in the dropshaft and causes it to move.

The motion of water column in the dropshaft can be described by the following continuity and momentum equations.

$$A_s \frac{dH}{dt} = Q_i - V_d A_d \tag{13}$$

$$\rho A_s H \frac{d^2H}{dt^2} = -\rho g H A_s - \tau_o A_p + P_d A_s \tag{14}$$

where A_s = cross-sectional area of dropshaft

A_d = cross-sectional area of drift tube

A_p = wetted area of dropshaft

H = water column height

P_d = pressure at the bottom of dropshaft

V_d = velocity at drift tube entrance

τ_o = shear stress on wetted area of dropshaft

Q_i = inflow rate from connecting pipe

The drift tube of length L is divided into a number of finite elements. The flow in each of the elements is equivalent to a finite difference model of the drift tube with its upstream condition described by Eqs. 13 and 14. The time dependent pressure calculated by the Mainstream System model at the corresponding location is used as the downstream end boundary condition of the drift tube-dropshaft model.

Figure 21 shows a typical time variation of water depth in a dropshaft due to a fairly slow rise in the tunnel pressure. It shows that a linear increase in the tunnel pressure results in an oscillatory increase in the water depth in the dropshaft. Figure 22 shows a similar result when the tunnel pressure rises more rapidly due to surge. All other conditions being equal, more rapid rise in tunnel pressure produces larger amplitude oscillation of the water depth. Clearly, large intensity surge in the tunnel will cause a geyser due to oscillation, even if the final equilibrium condition may indicate no overflow.

Figure 23 shows a special case when there is a resonance condition due to matching of the natural frequency of the water column in the

dropshaft and the natural frequency of the drift tube. Even with a fairly slow rise in the tunnel pressure, the water column oscillation may grow large enough to cause a geyser.

The natural frequency of a water column of height H_m is given by

$$f_s = \frac{1}{2\pi}\sqrt{\frac{g}{H_m}} \tag{15}$$

The natural frequency of a drift tube of length L and pressure wave speed a is

$$f_d = \frac{a}{4L} \tag{16}$$

Clearly, the resonance condition

$$\frac{2}{\pi}\sqrt{\frac{g}{H_m}}\ \frac{L}{a} = 1 \tag{17}$$

must be avoided. According to Eq. 17, the resonance condition is determined by three variables H_m , L, and a. Out of these variables H_m and L are readily determined from the physical dimensions. On the other hand the wave speed a is highly dependent on the air content of the flow and difficult to determine. Figure 73 shows the relationship between the air content and the wave speed length of drift tunnel at resonance condition.

3. The Safety Criterion

The analysis of the previous section clearly indicates that the geyser phenomenon depends on the surge intensity as well as other factors. Since the Mainstream and other system models do not include the detailed dropshaft-drift tube configuration, a simplified and general safety criterion is needed to determine the effectiveness of any surge mitigation method. Let,

$$H = H_m + h \tag{18}$$

and $$P_d = \rho g\ (H_m + y) \tag{19}$$

where H and H_m are the instantaneous and the mean values of the water depth in the dropshaft and P_d is the instantaneous pressure at the base of the dropshaft. In this way, h and y are the fluctuating components of the water depth and the pressure head, respectively. By substituting Eqs. 18 and 19 into Eqs. 13 and 14 and linearizing, the following equation is obtained:

$$\frac{d^2h}{dt^2} + 2\zeta \frac{dh}{dt} + k^2 h = \frac{gy}{H_m} \tag{20}$$

where

$$\zeta = \frac{f}{4D_s} \frac{dh}{dt} = \text{damping factor}$$

$$k = \sqrt{\frac{g}{H_m}} = 2\pi f_s$$

f = Darcy-Weisbach friction coefficient.

Assuming an oscillatory forcing function, we may write

$$y = y_o \sin \omega t \tag{21}$$

where $\omega = 2\pi f_d$ (22)

This assumption is justified by the results of the mathematical model described in the last section indicating that the drift tube modifies any pressure change in the tunnel to an oscillatory force of frequency f_d.

Equation 20 is the differential equation of a typical vibrating mass-spring system with a variable damping factor. If we ignore the variability of ζ and take it to be a constant, then it is possible to write the general solution of Eq. 20 in a closed form. Assuming that the exiting head is a harmonic function

$$y = y_o \sin \omega t \tag{23}$$

the general solution of Eq. 20 is

$$h = e^{-\zeta t}(C_1 \cos \sqrt{k^2 - \zeta^2}\, t + C_2 \sin \sqrt{k^2 - \zeta^2}\, t) + B \sin (\omega t - \phi) \tag{24}$$

where

$$B = \frac{gy_o}{H_m} \left[(k^2 - \omega^2)^2 + 4\zeta^2\omega^2 \right]^{-1/2} \tag{25}$$

$$\phi = \tan \frac{2\zeta\omega}{k^2 - \omega^2} \tag{26}$$

The constants of integration C_1 and C_2 may be determined by the initial conditions, i.e.

$$h = h_o \quad \text{and} \quad \frac{dh}{dt} = u_o \quad \text{at} \quad t = 0 \tag{27}$$

Two special cases are important to the gysering problem. These are described as follows:

1) Free oscillations

Assuming that the geometry of the dropshaft and the drift tunnel is such that $k \neq \omega$ and resonance does not exist, the water column in the dropshaft will undergo a free oscillation when excited by a surge in the main tunnel. Its motion is described by the first term on the right-hand side of Eq. 24, and the maximum amplitude of oscillation is given by

$$h_{max} = \frac{u_o}{k} = C_1 \sqrt{\frac{H_m}{g}}\ U_m \tag{28}$$

where U_m is the speed of head rise in the main tunnel and C_1 is a constant that must be determined by calibration. Referring to Fig. 20, the oscillatory water column will touch the cover if

$$H_m + h_{max} > H_s \tag{29}$$

where H_s is the cover elevation. By comparing Eqs. 28 and 29, it is possible to derive the following safety equation

$$N_f = \frac{C_1}{H_s - H_m} \sqrt{\frac{H_m}{g}}\ U_m \tag{30}$$

If N_f is greater than one, then a free oscillation of the water column caused by the surge will produce a geyser.

2) Resonance oscillation

If the natural frequencies of the dropshaft k matches the frequency of the forcing function ω (which is also equal to the natural frequency of the drift tunnel) then the maximum amplitude of oscillation is determined by the second term on the right side of Eq. 24. It is given by

$$h_{max} = \frac{g y_o}{2\zeta k H_m} \tag{31}$$

By comparing this equation with Eq. 29 the following safety equation is obtained.

$$N_r = \frac{C_2}{H_s - H_m} D_s^{1/2} \left(\frac{H_m}{g} \right)^{1/4} U_m^{1/2} \tag{32}$$

where C_2 is a constant to be determined by calibration. Using the event of October 3, 1986, it was determined that $C_1 = 4.6$ and $C_2 = 40$.

V. SOLUTION ALTERNATIVES FOR MAINSTREAM SYSTEM

Effective solution alternatives depend very much on the storm size to be considered. In order to assist the decision making process, the following three storms are used in the analysis.

Storm A: The largest of the three calibration storms, October 18, 1985 storm, is used as a standard storm.

Storm B: A storm that causes maximum design inflow for 3.5 hours.

Storm C: A storm that causes maximum design inflow for indefinite periods of time.

For the analysis that follows, the 13A, Nashville and Lawrence Avenue Branch tunnels are assumed to be closed, and the Mainstream System excluding these three branches is shown in Fig. 24.

The safety criterion given in Section IV-B is used to determine the effectiveness of any surge mitigation method. N_f is applied at upstream ends, and N_r is applied at DS-53.

A. Short Term Solutions

Presently there are flow control gates located at DS.3, 8, 9, 10, 11, 12, 13, 14, 15, 17, 19, 20, 21, 25, 26, 27, 28, 29, 30, 35, 38, 39, 40, 41, 45, 47, 49, 50, 51, 52, 53, 54, 55, 57, 58, 60, 61, 61A, 64, 66 67R, 70 73, 75, 76, 79, 80, 82, 83, 84, 85, 86, 88, 90, 91, 97, 100, 104, 106, 107, and 109. 92% of the potential inflow can be eliminated when these gates are all closed. In addition fixed orifices are being planned for dropshaft Nos. 16, 22, 42, 43, 71, 81, 87, 89, 93, 94, 95, 96, 98, 99, and 105 to limit inflow to a maximum of 1/3, the maximum inflow rate possible at each site.

1. Storm A

It is possible to mitigate the surge problem by limiting inflow using the existing gates. The gates at dropshafts Nos. 27, 28, and 29 (Racine Ave. pumping station) should start to close when the system is 50 percent full. All other control gates are closed at 70 percent full. All gates are assumed to require 10 minutes to complete closing.

The total inflow hydrograph for this operation is plotted in Fig. 25. The variation of water depth at the upstream end and the downstream end are plotted in Fig. 26. The water depth variation at St. 93 (DS-53) is compared with that of the upstream end in Fig. 27. These figures clearly show the existence of surges as the system is being filled.

The computed surge oscillation numbers are N_f = 0.88 and N_r = 1.0 indicating only DS-53 is at a marginal condition.

2. Storm B

The modeling results indicate that the existing control gates are not sufficient to prevent geysering. It requires two additional control gates at DS-1 and DS-114. It also requires all the planned fixed orifices to be in place.

The gates at dropshafts Nos. 27, 28, and 29 should start to close when the tunnel is 30 percent full. All other control gates should be closed at 40 percent full. The gate closing time is 10 minutes.

Total inflow hydrograph for this case is plotted in Fig. 28. The variation of water depth with time at the downstream end and upstream end are plotted in Fig. 29. The surge oscillation numbers are N_f = 0.80 and N_r = 1.0.

3. Storm C

Fixed orifices must be provided for all ungated dropshafts or, alternatively, some additional controllable gates are needed. The results of simulation with existing control gates plus fixed orifices at all ungated dropshafts are presented here.

The gate operating procedure is identical to that of Storm B.

Total inflow hydrograph for this case is shown in Fig. 30. Because of the increased number of fixed orifices, the restricted inflow after gates closure for this case is smaller than that of Storm B. Reduced inflow rate compensates for increase duration. Time variation of water depth at upstream and downstream ends are shown in Fig. 31. A similar plot for DS-53 is shown in Fig. 32. The surge oscillation factors are N_f = 0.32 and N_r = 1.0.

It should be noted that for all three storms analyzed the critical condition is determined by the resonance condition at dropshaft No. 53.

B. Long Term Solutions

A 32,000 acre-feet reservoir using the McCook Quarry is planned for the purpose of increasing storage capacity and reducing flooding problems. Because of the conveyance limitation as described previously, however, the surge and geyser problems cannot be completely eliminated without further controls.

1. Storm A with Gate Control - reservoir initially empty

The filling process is somewhat different for different initial storage conditions. When the reservoir is initially empty, then the tunnel is at its full conveyance capacity and the reservoir can contribute to surge reduction.

In this case only the gates at dropshaft Nos. 27, 28, and 29 need to be closed when the tunnel, excluding the reservoir, is 75 percent full. The total inflow hydrograph for this case is shown in Fig. 33. The time variation of water depths at the upstream end, downstream end, and DS-53 are shown in Fig. 34. This figure indicates that the tunnel at both ends remains open (not pressurized) for the entire duration of the storm. Due to the conveyance limitation, however, the midportion of the tunnel is pressurized and the resonance condition at DS-53 dictates the safety of the system. The surge oscillation numbers are $N_f \approx 0$ and $N_r = 0.65$.

2. Storm A with Gate Control - reservoir partially full

The condition considered here is the case when the water level in the reservoir is just at the crown of the tunnel at the downstream end. Reductions in conveyance and the remaining storage capacity in the tunnel causes more severe surge problems in the middle portion of the system.

To avoid the geyser problem at DS-53, it is necessary to start closing all gates when the tunnel is 80 percent full. Figure 35 shows the total inflow hydrograph, and Fig. 36 shows the corresponding time variations of water depths at three stations. The surge oscillation numbers are $N_f \approx 0$ and $N_r \approx 0.71$.

3. Storms B and C with Gate Control - reservoir initially empty

Gate closure should start when the tunnel is 50 percent full to cut off 80 percent of flow coming in from the gated dropshaft. This can be accomplished by completely closing the gates responsible for 80 percent of gated inflow.

The total inflow rate is shown in Fig. 37. The time variation of water depths at three stations are shown in Fig. 38. Instantaneous hydraulic gradelines showing the movement of surges are plotted in Fig. 39. This figures clearly show that the problem is in the midsection of the tunnel. The oscillation numbers are $N_f \approx 0$ and $N_r \approx 1.0$.

4. Storm C with Surge Structure - modified DS-53

Previous analysis has clearly indicated that the resonance instability of DS-53 is always most critical after the construction of the reservoir. Therefore, the first priority of structural modification is the removal of the resonance condition at DS-53. After this is done, it is necessary to enlarge the shaft diameter at the upstream end to 100 feet.

With the structural modification described above, the total Storm C hydrographs are allowed to enter the system. Time variation of water depth at three key locations are shown in Fig. 40. The critical location now shifts to the upstream end (Station 1 in Fig. 40). The relevant oscillation number is $N_f = 1.0$ in this case.

5. Storm C, trade-off between surge structure and gate control

The purpose of this run is to provide additional information on the relative effectiveness of surge structure and inflow control in surge mitigation. It is assumed that the diameter of the shaft at the upstream end is equal to 70 feet and the resonant condition has been removed.

In this case the inflow from the gated dropshafts should be reduced 50 percent when the tunnel is 50 percent full. The corresponding total inflow hydrograph is shown in Fig. 9 and the time variation of water depth at three key stations are shown in Fig. 41. It is interesting to note that there are positive and negative surges near the reservoir that alternately move downstream and upstream.

VI. SOLUTION ALTERNATIVES FOR CALUMET SYSTEM

The Calumet system is presently accepting only small amounts of inflow and has not experienced any surge related problem. However,the potential for a geyser problem cannot be ruled out when the system becomes fully operational in the near future. A storage reservoir is also planned for this system sometime in the future. Therefore, the short-term condition without reservoir and the long-term condition with reservoir are analyzed. The largest of the three past storms, September 26, 1986, storm, and the maximum design inflow rates were considered. In the following tests, all tunnels are assumed to be connected and the whole system operates as a unit.

A. Short Term Solutions

1. Sepember 26, 1986 storm

The total inflow hydrograph due to the September 26, 1986, storm is shown in Fig. 42. The tunnel is assumed to be initially empty. River water level is assumed to be at elevation +2 and overflow is allowed when the level in certain dropshafts exceed the river level. Time variation of water depth at three key stations are plotted in Fig. 43. This figure clearly indicates the existence of surges in the system. However, the oscillation coefficient is substantially less than one (N_f = 0.411) indicating that surge is not strong enough to produce a geyser. The tunnel will eventually fill up and overflow will occur. Total overflow hydrograph is shown in Fig. 44.

No inflow control is necessary in this case.

2. Maximum design storm

The analysis indicates that the surge will be severe enough (N_f = 1.45) to cause a geyser if the maximum design storm is allowed to enter unrestricted.

Presently there are six gated dropshafts (CS - 7, 8, 10, 11, 12, 13) which can be used to control the inflow. By trial, it was determined that the geyser problem will not exist if all six gates are closed within 10 minutes after the tunnel is 75% filled. The corresponding total inflow hydrograph is shown in Fig. 45. Time variation of water depth of five key stations are shown in Fig. 46. The calculated oscillation number is N_f = 0.81.

B. Long-Term Solutions

The planned Thornton Reservoir enables the system to take all the inflows due to the September 26 storm without causing geyser problems. Geyser problems do not exist even for the maximum design flow if the reservoir is initially empty. The total inflow hydrograph used for this analysis is shown in Fig. 47. Here the inflow rate is allowed to linearly increase to the maximum value in 75 minutes. Time variation of six key locations are shown in Fig. 48. It is interesting to point out that the water level at the treatment plant rises very slowly due to the existence of the reservoir although there are surges indicated by rapid level rises at other stations further upstream. The time variation of water depth in the reservoir is shown in Fig. 49. The computed oscillation coefficient is $N_f = 0.15$.

It is reasonable to expect that, if the tunnel is initially 100 percent full, sudden and large amounts of inflow are not allowable, even when the reservoir is operational. The dynamics of surge would depend on the initial storage level, the rate of increase of the inflow rate, and the maximum inflow rate. Time and funding do not allow a complete parametric study. For the purpose of illustrating the type of analysis that may be carried out in the future, two additional example runs were made. Both runs assume the total inflow hydrograph to be as shown in Fig. 47. The tunnel was assumed to be initially 50 percent full for the first run and 75 percent full for the second run. Both cases indicated no geyser problem although the surge problem progressively worsened as the initial storage increased. The calculated values of N_f is 0.31 for the first run and 0.38 for the second.

VII. THE DES PLAINES SYSTEM

The Des Plaines System is to be constructed in three stages. These are the South System, South-Middle System, and the complete system. The system's configurations for modeling purposes are shown in Figs. 50, 51, and 52, respectively. Maximum design inflow rates were used for all three cases. All dropshafts are assumed to be fully gated. The purpose of the analysis is to determine the time of gate closure so that water will not reach the elevation of any flood gate at any time.

Since there are many possible combinations of individual gate closing schedules, a comprehensive study cannot be carried out at this time. All gates are assumed to be operated simultaneously and closed at the same time.

A. South System

The inflows are assumed to increase from zero to the maximum design values of 80 minutes. As the tunnel fills, the inflow will be cut down to zero in such a way that there will not be any excessive surge during the process and that the tunnel is filled at the end. Simulation results indicate that, if the maximum inflow is suddenly cut-off at a time when the tunnel is nearly full, strong oscillations will occur. The water column in some dropshafts may oscillate by as much as 50 feet. For structural safety it is desirable to avoid oscillations of this magnitude.

After a number of trial runs, a satisfactory gate closing procedure was found: start gate closing when the system is 50 percent full, cut-off two-thirds of the flow in 20 minutes, wait until the system is 75 percent full and resume gate closing, and complete the closing in 20 minutes. The resulting total inflow hydrograph is shown in Fig. 53. The calculated time dependent water depth at the upstream and downstream ends of the system are shown in Fig. 54. The oscillatory motion shown in this figure caused by gate closure may become unacceptably severe if the gate is closed too rapidly. Instantaneous hydraulic gradelines plotted in Fig. 55 show the surge movement.

The system is 94.5% full at the end of the operation.

B. South-Middle System

In addition to gate closure, it is assumed that a pump station located at the downstream end can be activated to withdraw 200 cfs from the system whenever necessary. For simplicity sake, the model assumes that the pumping rate of 200 cfs is used as soon as the inflow rate exceeds 200 cfs.

A satisfactory gate operating procedure is to start gate closing when the system is 75% full, cut off the two-thirds of the inflow in 10 minutes, resume gate closing when the system is 90% full, and close the gate until

total inflow is equal to 200 cfs. The corresponding total inflow hydrograph is plotted in Fig. 56. The time variation of water depth at two ends is shown in Fig. 57 and similar plots for two other stations are shown in Fig. 58. Instantaneous hydraulic gradelines are shown in Fig. 59.

The system is filled to 92.2% at the end of the operation.

C. Complete System

The operating procedure described for the South-Middle System is also satisfactory for the complete system.

Figure 60 shows the total inflow hydrograph. Time variation of water depth at the upstream ends of three branch tunnels is shown in Fig. 61. Instantaneous hydraulic gradelines along the main tunnel are shown in Fig. 62. Very steep slopes near the upstream end prevent the surge from reaching the upstream end. The tunnel is 95% filled at the end of the operation.

VIII. SOLUTION ALTERNATIVES FOR 13A SYSTEM

The outflow from the 13A tunnel to the Main Stream Tunnel is blocked and the branch tunnel is assumed to be independent. There is an overflow structure at the downstream end to relieve the tunnel and prevent flooding. The overflow structure consists of a 10.5'x13.5' exit conduit with invert elevation at -9.5'. There is a flap gate preventing river water from entering the tunnel. When the tunnel water level at DS61 exceeds that of river water, assumed to be at elevation 0, overflow is assumed to take place through an orifice.

Three sets of inflow rates: (1) existing estimated peak, (2) future planned peak, and (3) dropshaft design capacity were used as the inflow rates. The total flow rates are 1003 cfs, 1805 cfs, and 3322 cfs, respectively. The objectives of flow control are to limit the maximum water level at DS.61 to be less than 18 feet and to prevent geysering everywhere in the system.

The system configuration for modeling purposes is shown in Fig. 63.

A. Existing Estimated Peak Inflow Condition

The inflow rate at each dropshaft is assumed to be constant and equal to the existing estimated peak flow. The time variation of water surface elevation at the downstream end is shown in Fig. 64. The corresponding plot for DS.61 is shown in Fig. 65. At t = 100 minutes, the flow has attained an equilibrium condition and the water level becomes independent of time. Surge does not produce very sharp peaks and the water level at DS.61 stores under elevation 18 ft all the time. No possibility of a geyser is indicated. The overflow hydrograph is shown in Fig. 66.

B. Future Planned Peak Inflow Condition

The system overloads under restricted future planned peak inflow conditions. Two problems are noted in this case. Because of rather high inflow rates at Station 5 (DS.55), the junction becomes pressurized rather early and produces large air space between the junction and the surge front moving upstream from the downstream end. This situation should be avoided because large waterhammer pressure may be generated when two surge fronts collide. The second problem is the violation of water level constraint at DS.61 due to the inflow rate exceeding the overflow capacity. At the request of the client, the analysis was carried out based on an assumption that inflow control gates will be installed at all dropshafts.

After several trial runs, a satisfactory control procedure was found. First the inflow at DS.55 should be limited to 200 cfs by presetting the gate at the proper opening. Second, the inflow at station 40 (DS.1) should be reduced from the original 460 cfs to 230 cfs in ten minutes as soon as the water level at DS.61 reaches elevation 8.

Time variation of water surface elevation at the downstream end is shown in Fig. 67. The corresponding plot for DS.61 is shown in Fig. 68. The water surface approaches the limiting condition slowly without violating the constraint. The overflow hydrograph is plotted in Fig. 69. No geyser problem exists.

C. Dropshaft Design Capacity Inflow Condition

The total inflow in this case exceeds that of the last case by a large margin. Clearly, this amount of inflow is not acceptable.

Undoubtedly, there are a number of possible gate control procedures. After several trail runs, a possible control procedure, not necessarily optimum, was found. First, the inflow at DS.55, must be limited to 100 cfs from the beginning of the storm to prevent premature pressurization at the junction. Inflow from all dropshafts are cut-off in 10 minutes starting when the water surface at DS.61 reaches elevation -77 ft. According to the computer output, all gates will start closing at t = 23 minutes but the additional inflow taking place during the 10 minutes closing time is sufficient to fill the tunnel. If desirable, gate closing could start earlier but leave some inflow to continue after the gate operation.

Time dependent water surface elevation at the downstream end and at DS.61 are shown, respectively, in Figs. 70 and 71. The calculated overflow is shown in Fig. 72. Because of larger initial inflow rate, the flow is more dynamic in this case than the previous two cases. The flow oscillation causes overflow to take place in two separate time periods.

The system operates satisfactorily under the assumed operating condition.

IX. CONCLUSIONS AND RECOMMENDATIONS

The mechanisms of air blow-off and geysering have been identified and possible solutions recommended. Because the mathematical model outputs were compared with some field data and showed good agreement, the modeling results should be reasonably reliable. Following is a list of some significant conclusions:

1. Some air flowing out of the tunnel through dropshafts or air vent when tunnel is filling is inevitable. With existing grating of covers, no structural damage due to air flow should occur.

2. Geysering is basically caused by a rapid rise of water level in dropshafts due to pressurization surge. For a dropshaft with long drift tube, such as DS.53, resonance may magnify the problem of geysering.

3. For DS.53 of the Main Stream System, it appears that the resonance is made possible by a reduction in pressure wave speed due to entrained air bubbles. Estimated relationships between dropshaft height, drift table length, and the air concentration are shown in Fig. 73.

4. The transient problems can be controlled with proper inflow control. Satisfactory control procedures have been identified and described in this report. These control procedures are not necessarily optimum because optimum conditions depend on objectives and require considerable search efforts.

5. Inflow control or other surge mitigating is necessary for the Main Stream System even after the construction of the planned reservoir at the downstream end. This is due to insufficient coveyance.

6. There is a choice between a construction of a surge mitigating reservoir at the upstream end and the use of inflow control when the planned reservoir for the Main Stream System is in place.

7. The situation for the Calumet System is quite different from that of the Main Stream System. It has sufficient conveyance so that the presence of the planned reservoir can prevent the surge problem.

8. For the Des Plaines System, the gate closures may be carried out in two steps to avoid large amplitude oscillation while large amounts of flow can be captured and the system is nearly full at the end.

9. Because there is an overflow structure at the downstream end, the 13A tunnel is relatively easier to control. It needs no control with the existing estimated peak flow condition.

10. Because of the difference between dynamic and static conditions, the Main Stream System and the Calumet System controls should not be based on the water level measured at a single location. The control should be based on the actual volume of water stored in the system. Good estimates of storage volume can be made by using water surface elevations measured at two stations sufficiently far apart.

Some recommendations as listed below are offered.

1. The resonance problem at DS.53 should be solved on a priority basis because it is the most likely location for a geyser to occur.

2. More detailed analysis is needed for the actual solution of DS.53, short or disconnecting it from the Main Stream System.

3. All solution procedures described in the report are satisfactory from the transient point of view, but not necessarily optimum from operational or other possible viewpoints. Therefore, either the procedures should be further refined by analysis or field trials before regarded as final.

4. Any control procedure described in this report is based on a given inflow hydrograph. In actual conditions, the inflow rate is not known, and therefore, the control procedure based on storage volume alone may cause risks. Two types of risks may be considered. If the operating procedure based on large storms is adopted, then the risk is under utilization of the tunnel. On the other hand, if the operating procedure is based on small storms, then the risk is geysering and safety. For this reason a risk analysis is recommended.

5. One practical method of reducing the risk described above is to base the control on storage volume plus the rate of increase of the storage. Because the rate of increase of storage volume reflects the inflow rate which also reflects the storm size, the control method based on these two values should greatly reduce the risk. This method is recommended because it may be more practical than a method based on weather forecasts.

6. The storage volume-water surface elevation relationships given in this report apply only to the cases without reservoirs. The relationships should be redetermined in the future when reservoirs are constructed.

7. The long-term solutions for Main Stream and Calumet Systems are based on the assumption that the tunnels are connected to

the reservoirs at all times and there is no gate or valves to impede the flow. Further analysis is needed if the flow between the tunnel and reservoir is to be disrupted for draining or other reasons.

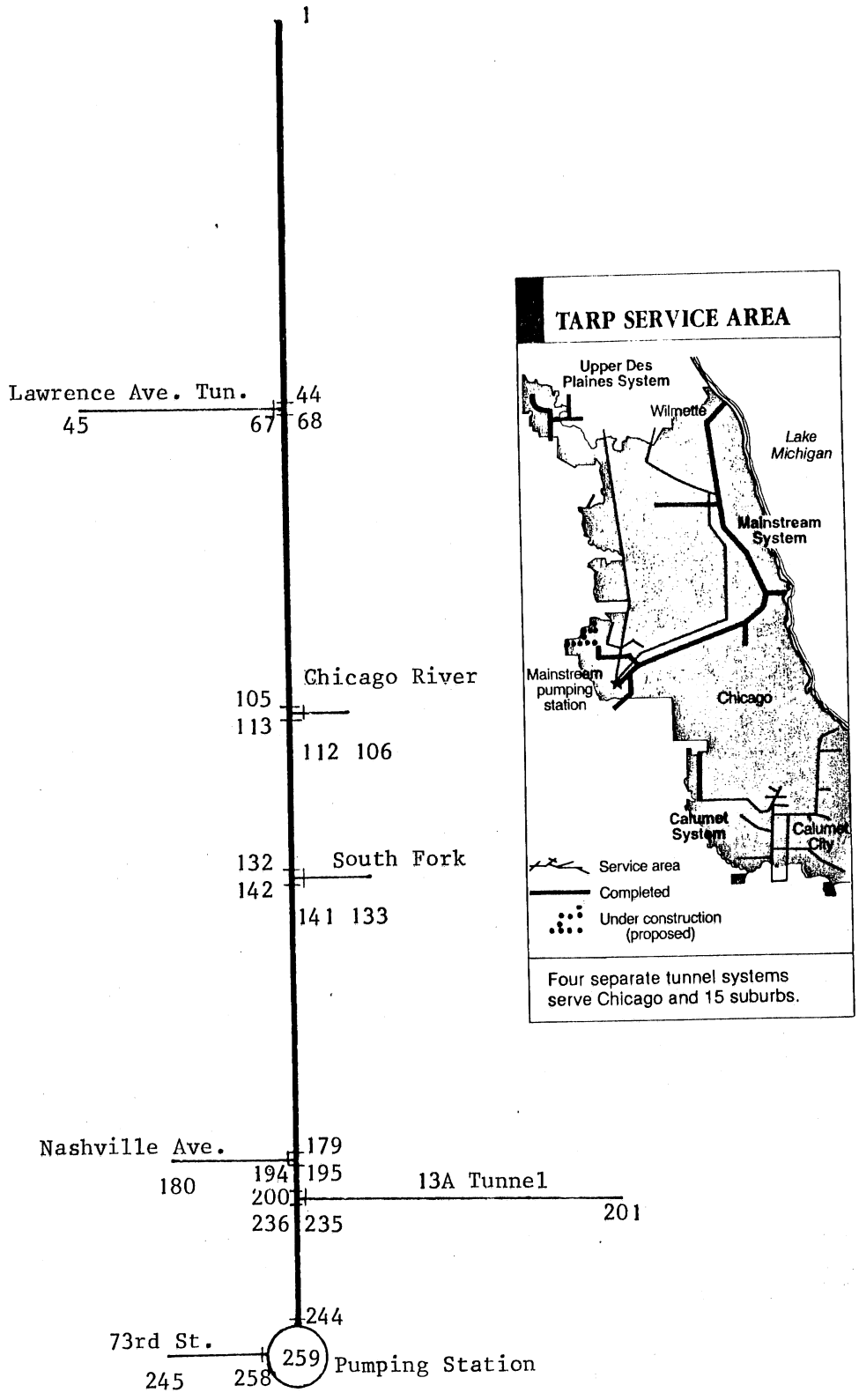

Figure 1. Mainstream system configuration and stationing for modeling purposes.

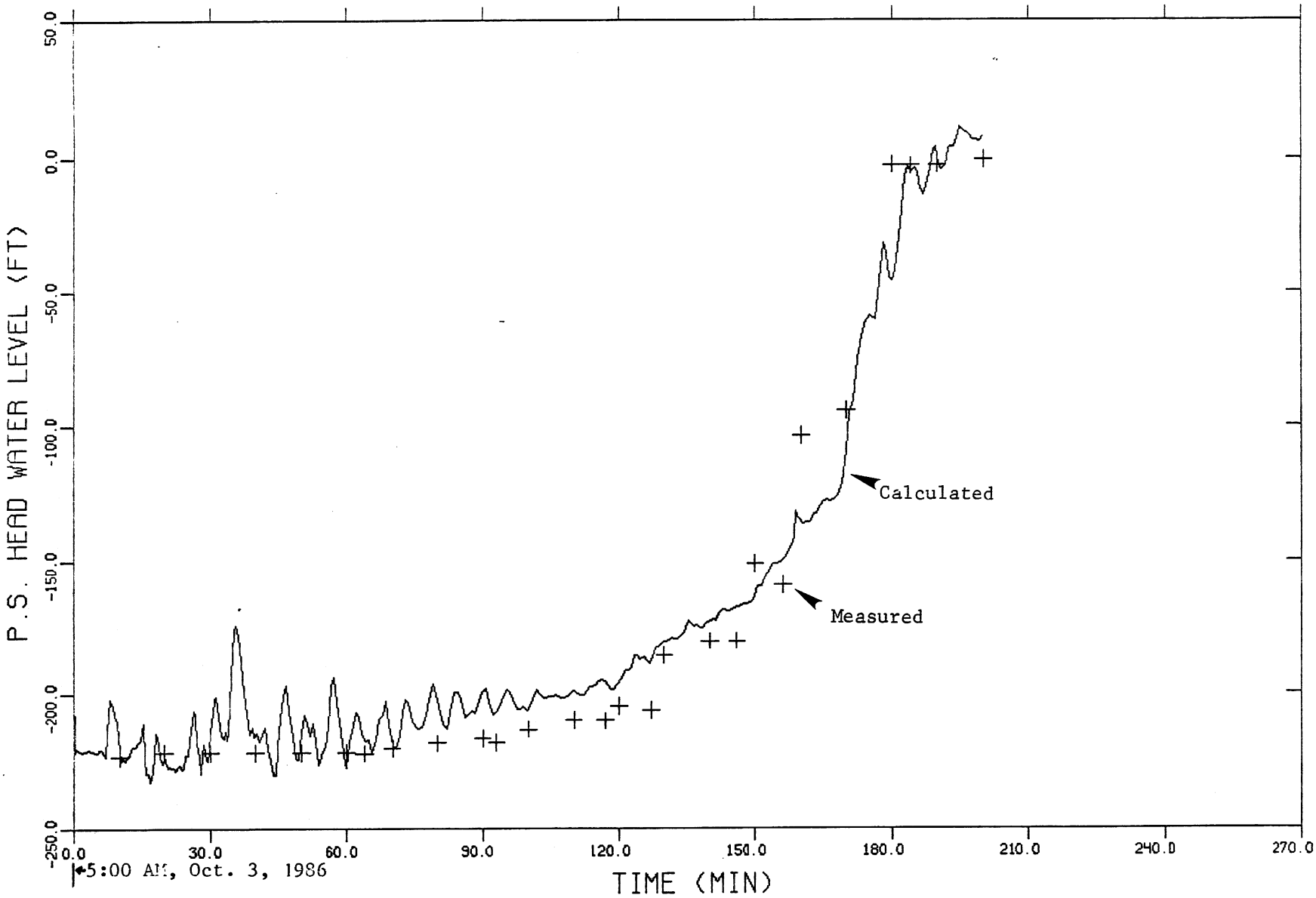

Figure 2. Comparison of measured and calculated water level at the downstream end, Oct. 3, 1986 storm.

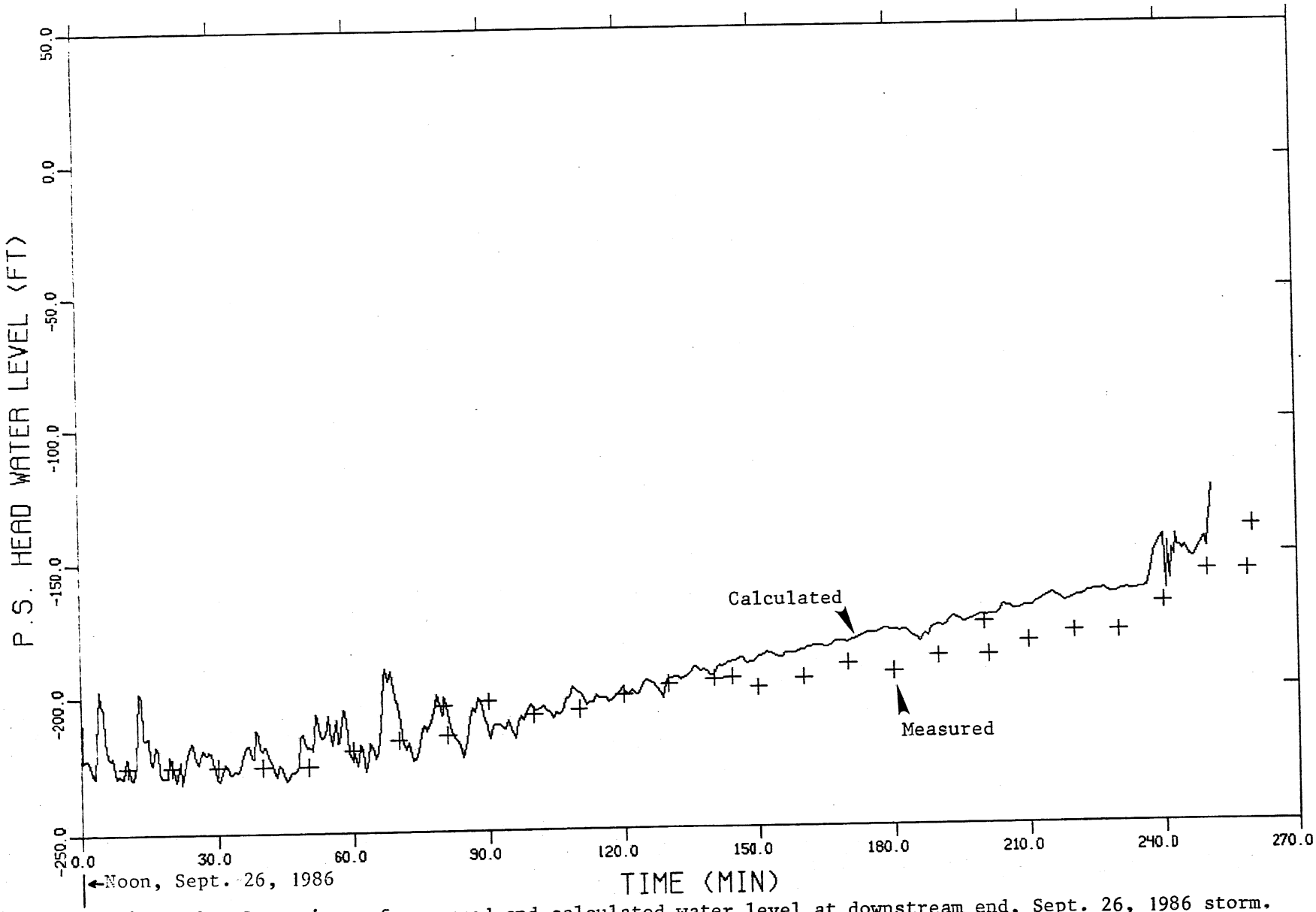

Figure 3. Comparison of measured and calculated water level at downstream end, Sept. 26, 1986 storm.

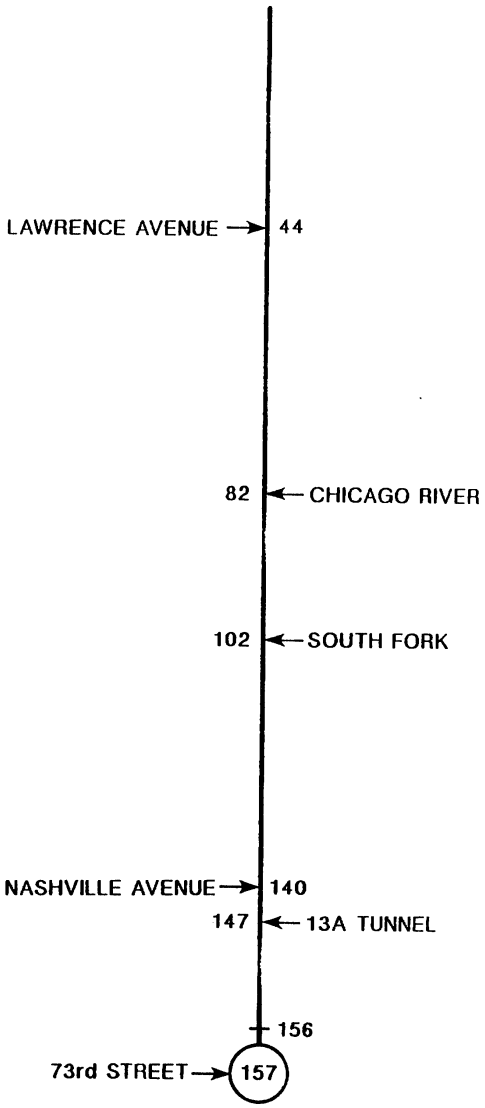

Fig. 4. Stationing of Mainstream System excluding all branch tunnels.

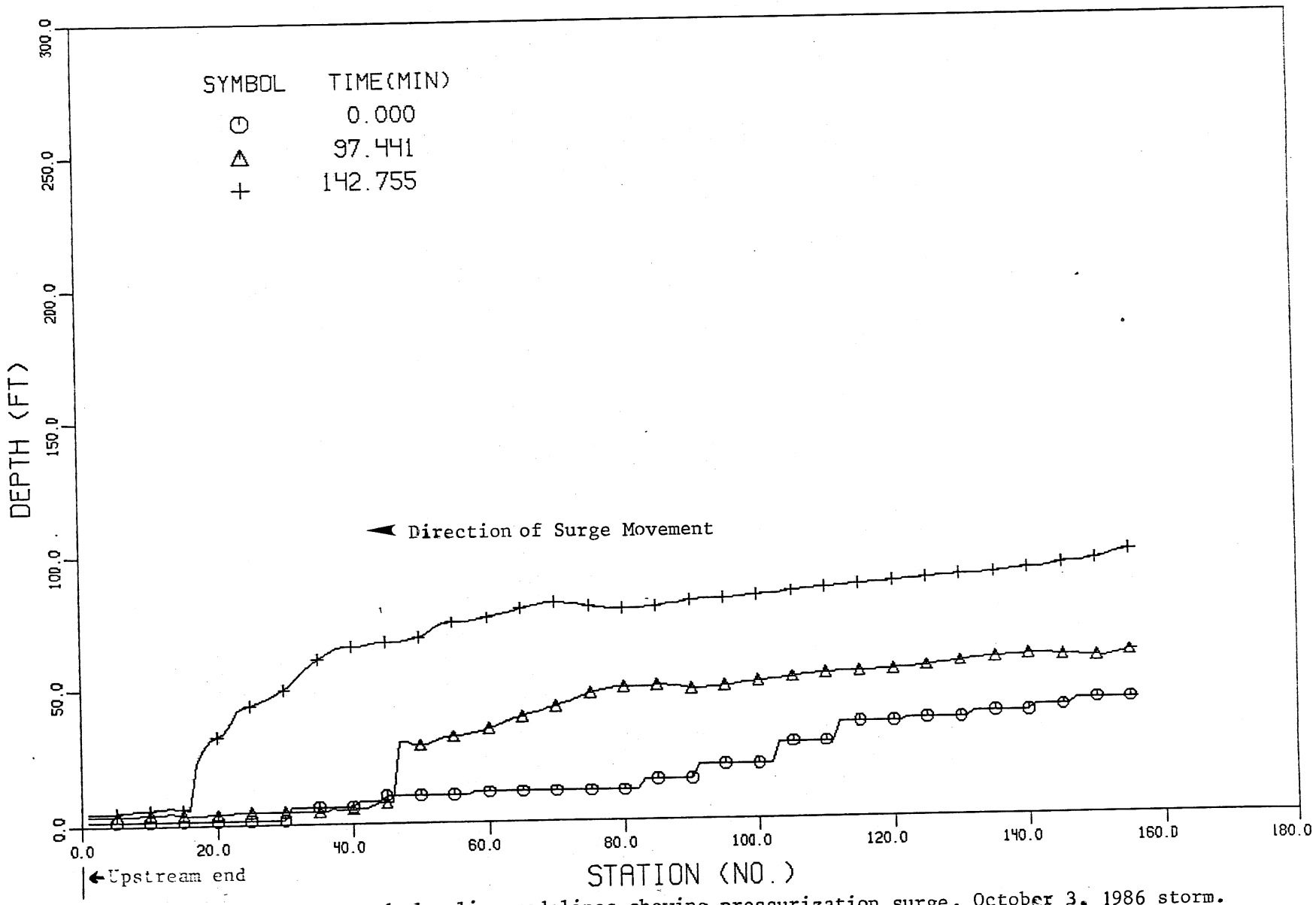

Figure 5. Instantaneous hydraulic gradelines showing pressurization surge, October 3, 1986 storm.

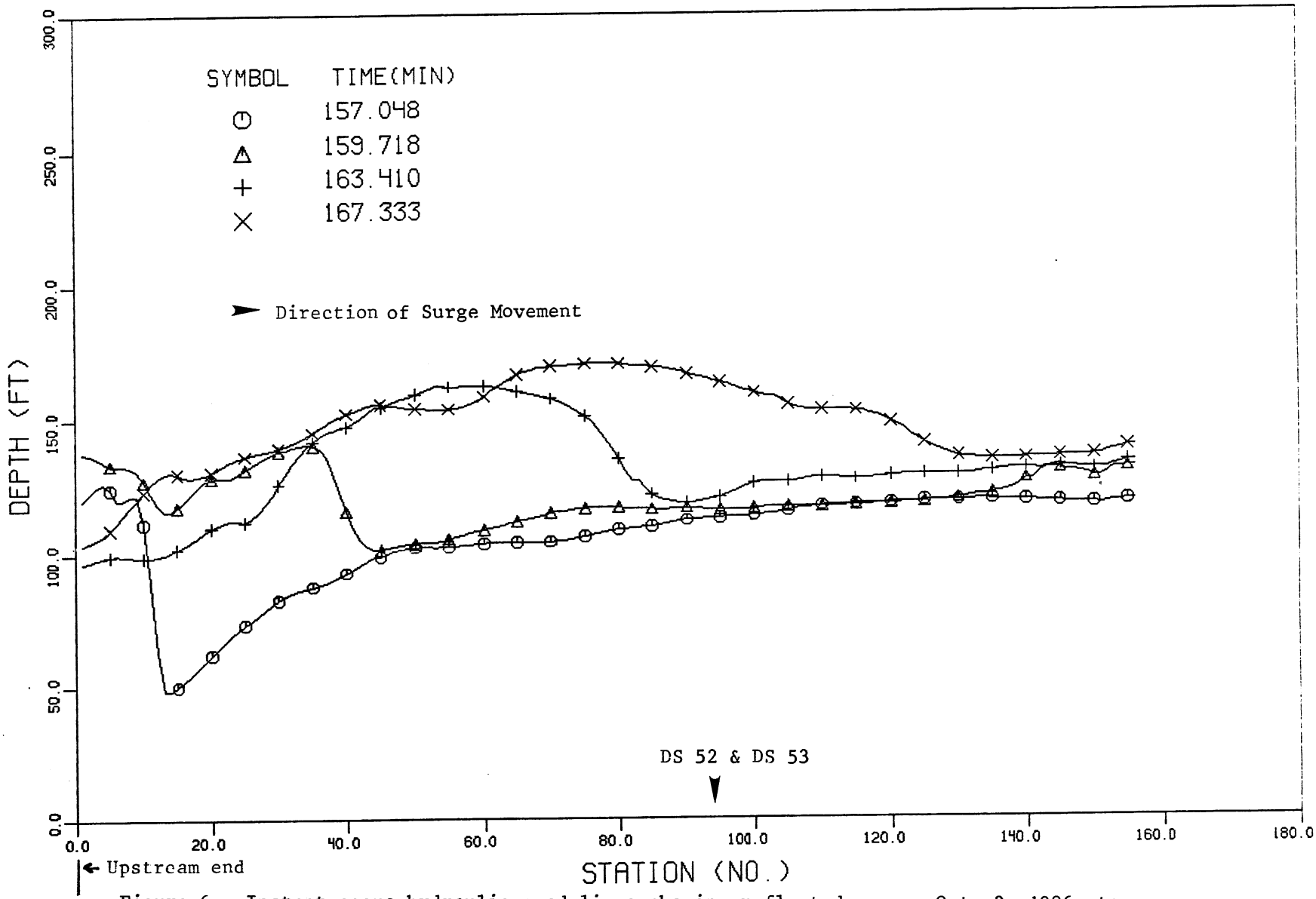

Figure 6. Instantaneous hydraulic gradelines showing reflected surge, Oct. 3, 1986 storm.

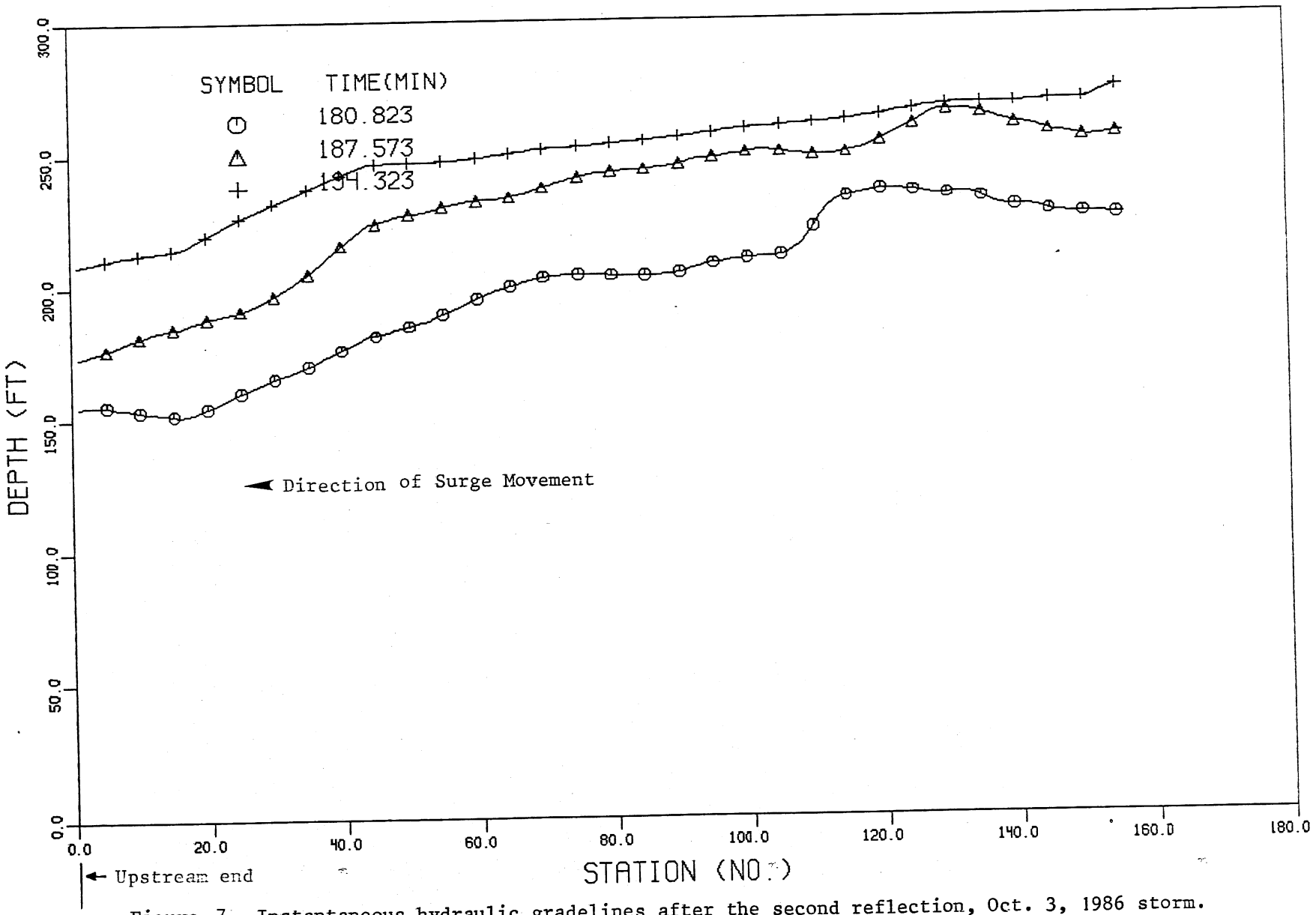

Figure 7. Instantaneous hydraulic gradelines after the second reflection, Oct. 3, 1986 storm.

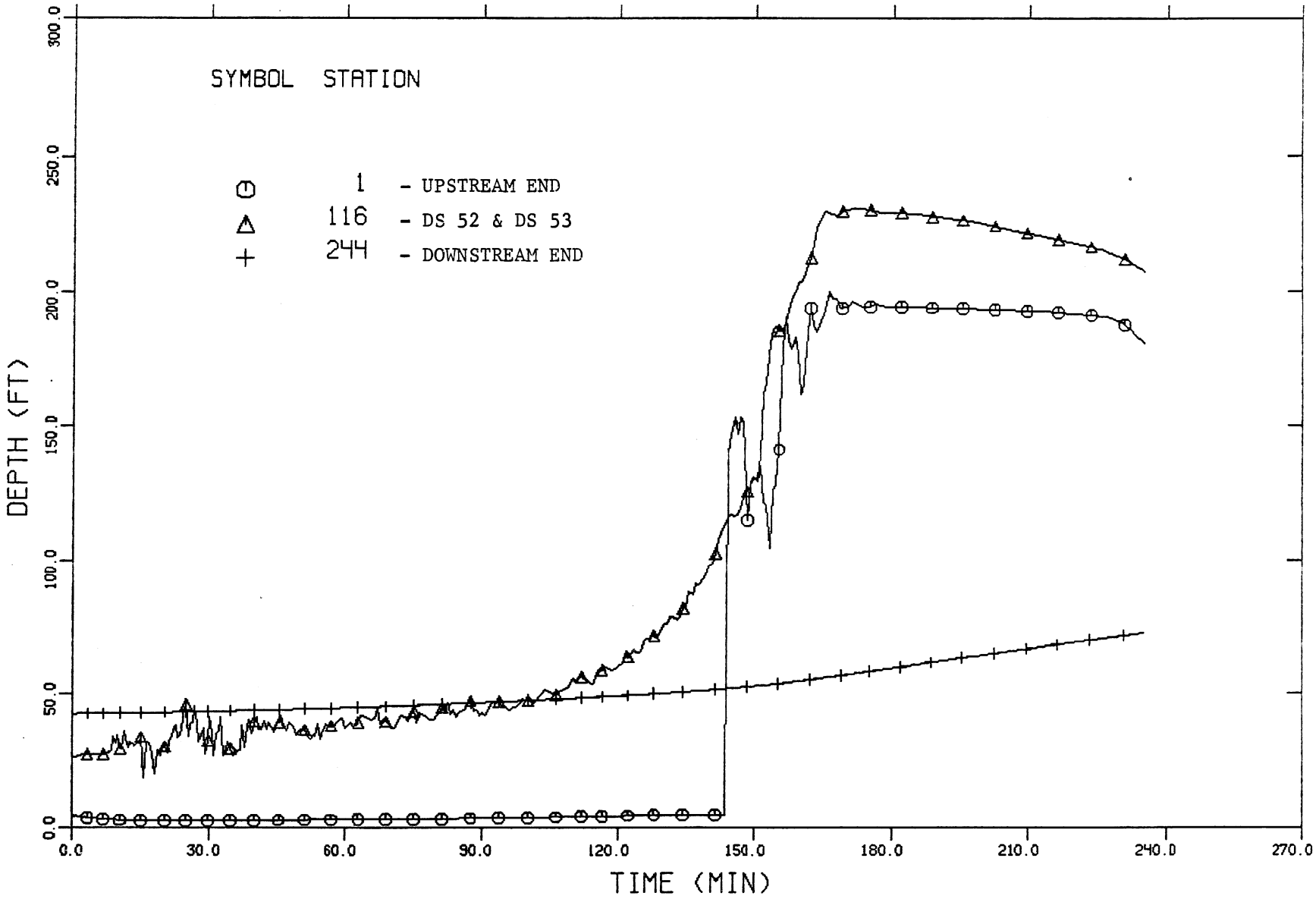

Figure 8. Water depth at three selected stations with reservoir, no inflow restriction, Oct. 3, 1986 storm.

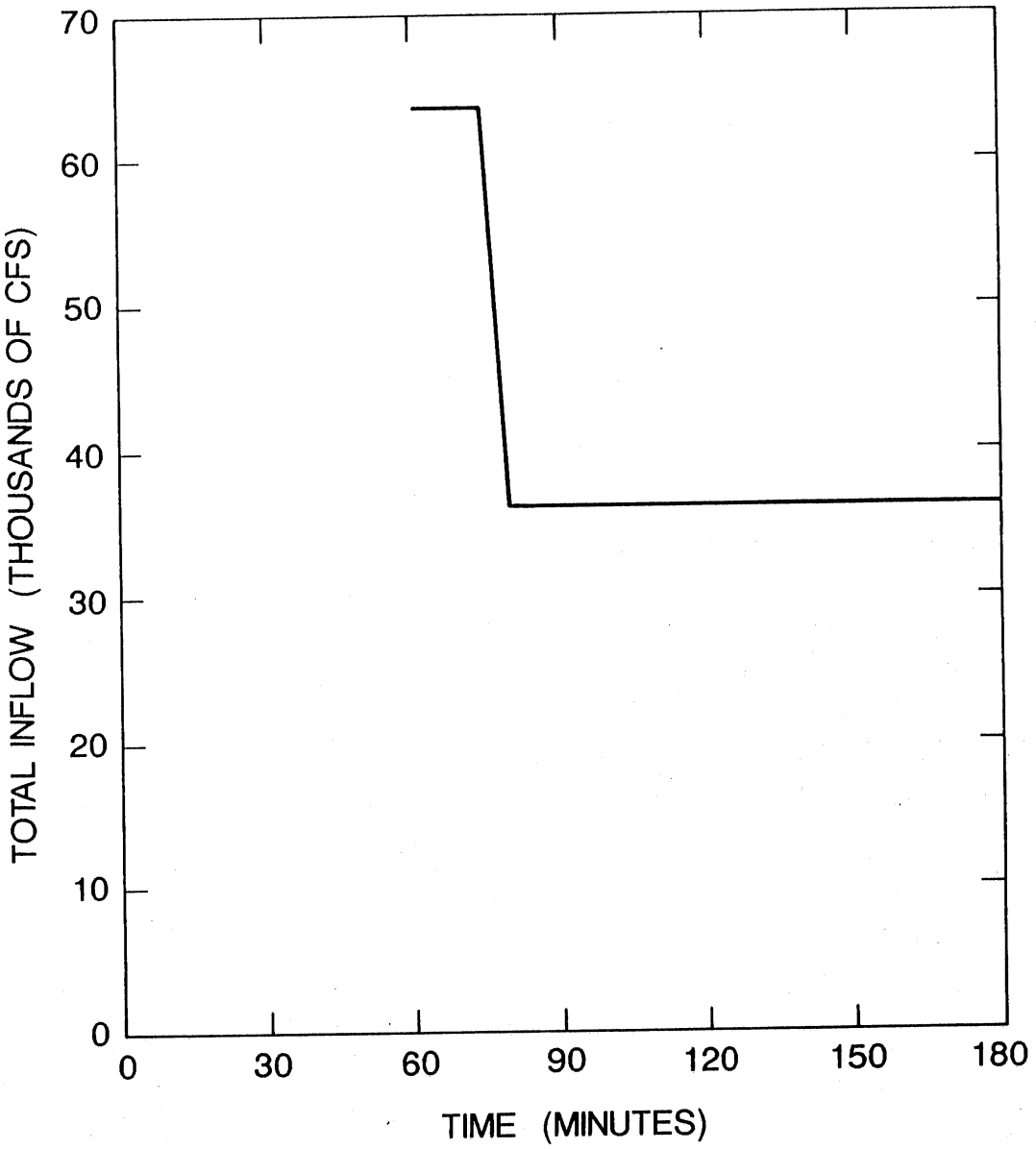

Fig. 9. Total inflow rate, maximum storm partially controlled.

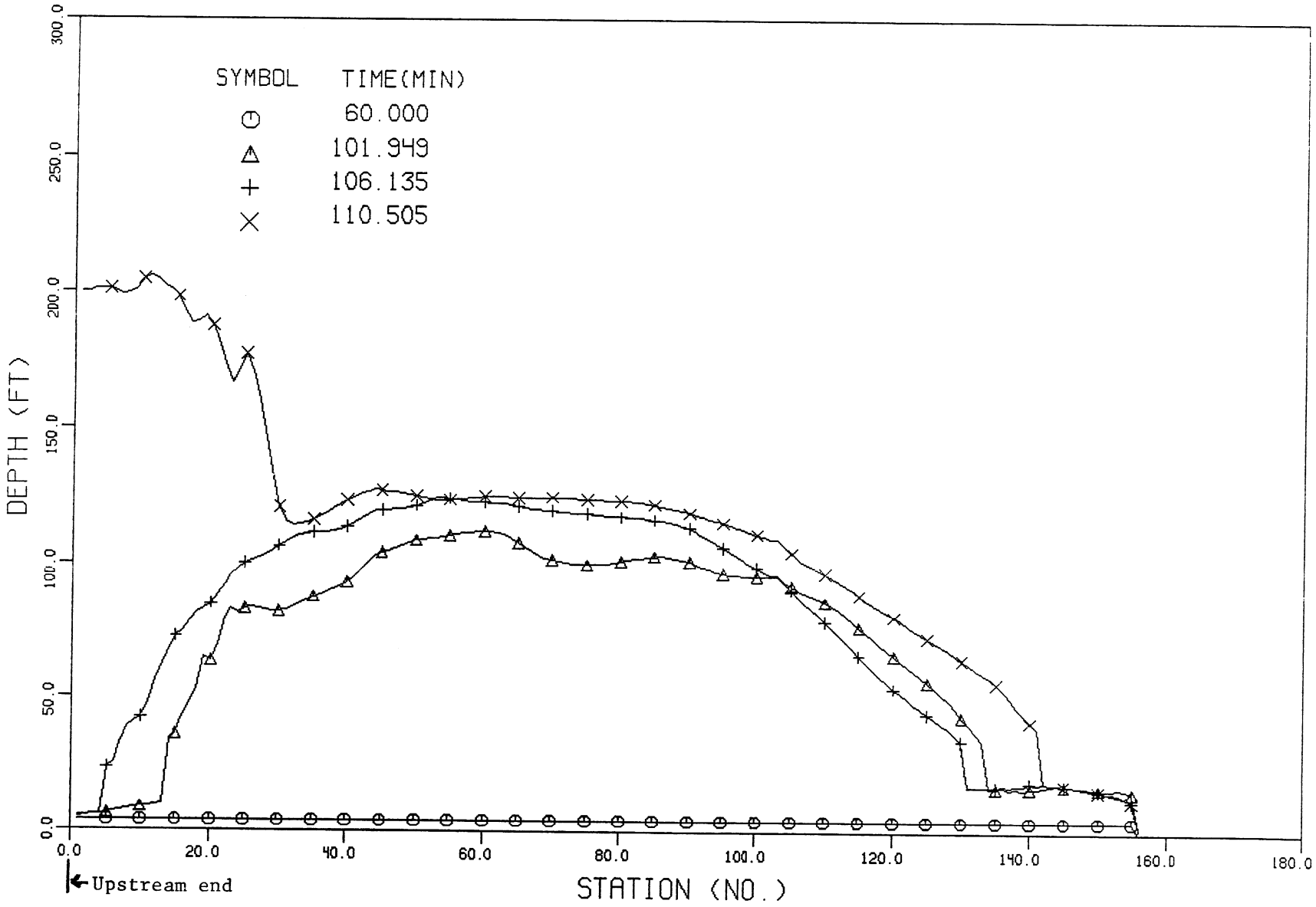

Fig. 10. Instantaneous hydraulic gradelines, reservoir initially empty.

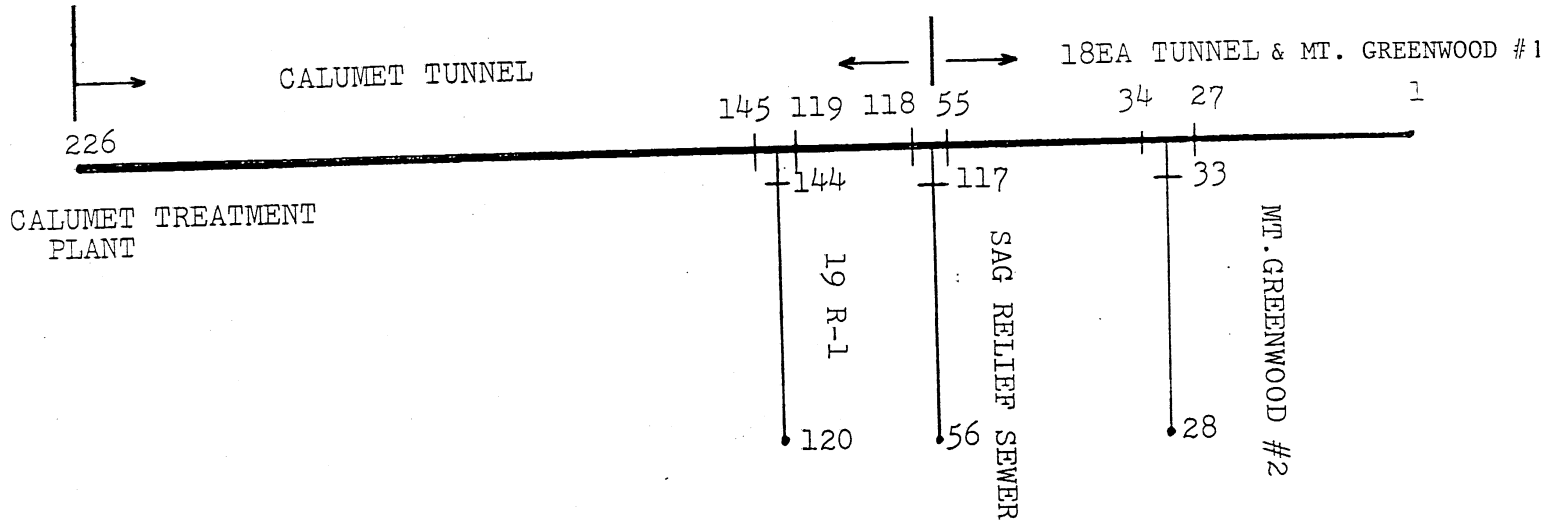

Fig. 11. Existing Calumet System configuration for modeling purposes.

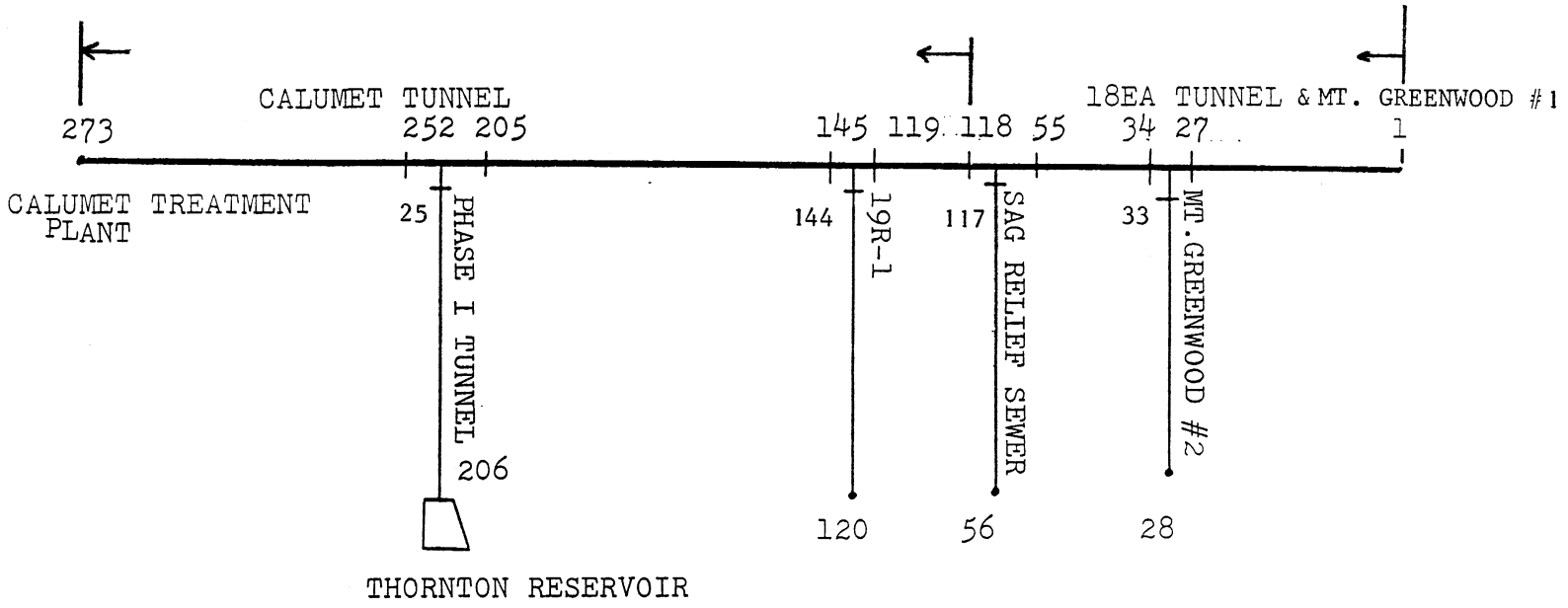

Fig. 12. Future Calumet System configuration for modeling purpose.

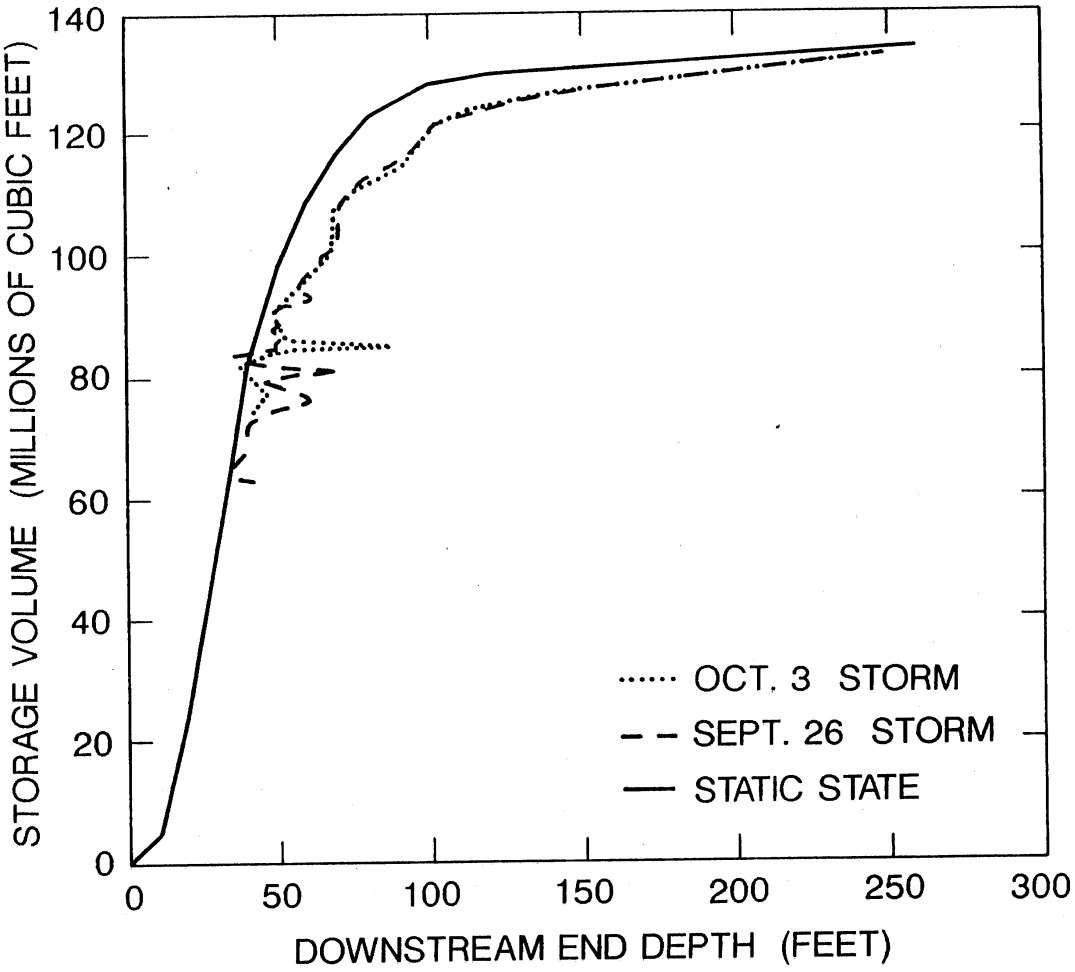

Fig. 13. Statically and dynamically determined correlation between volume and depth at downstream end, Mainstream System.

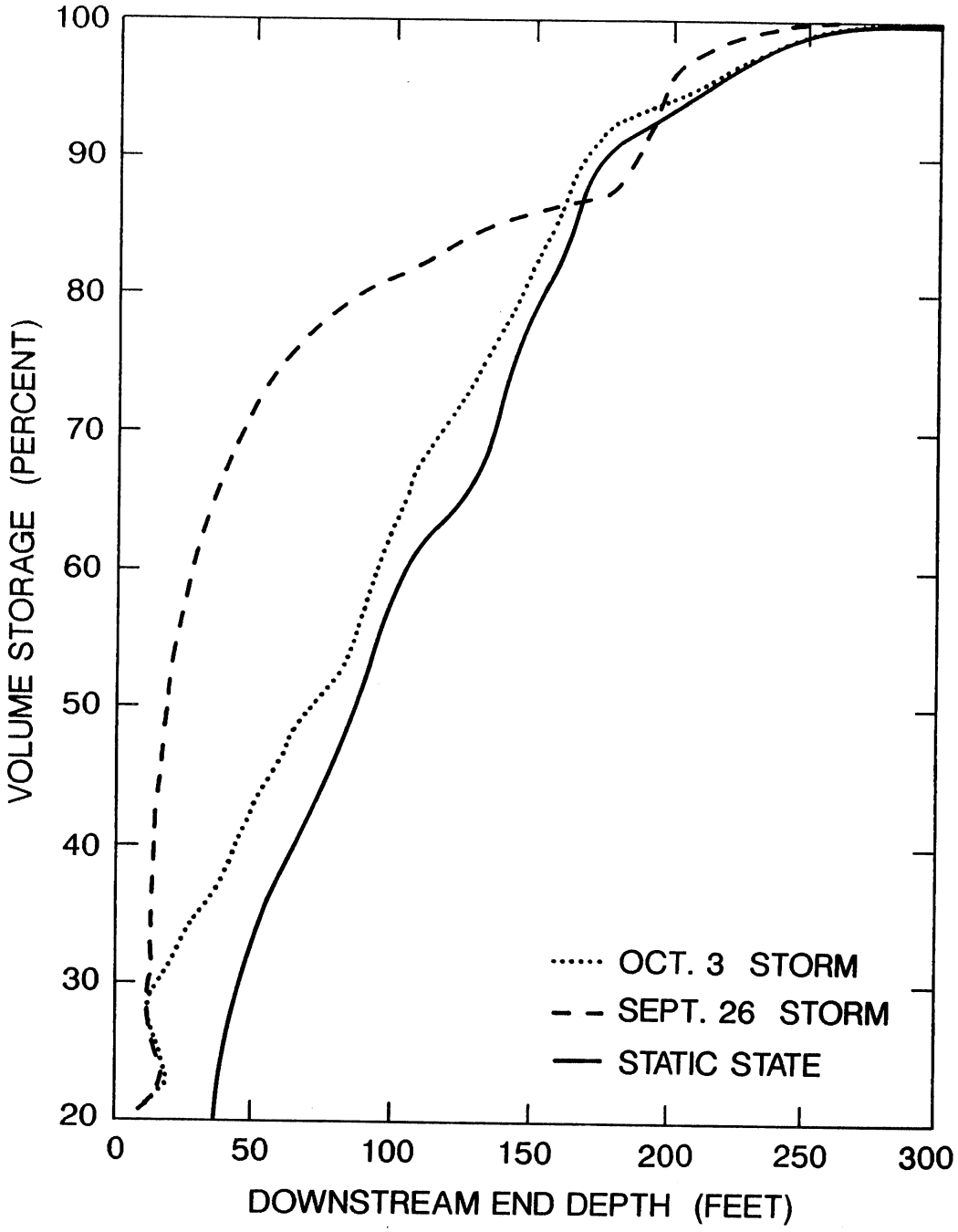

Fig. 14. Statically and dynamically determined correlation between storage volume and depth at downstream end, Calumet System.

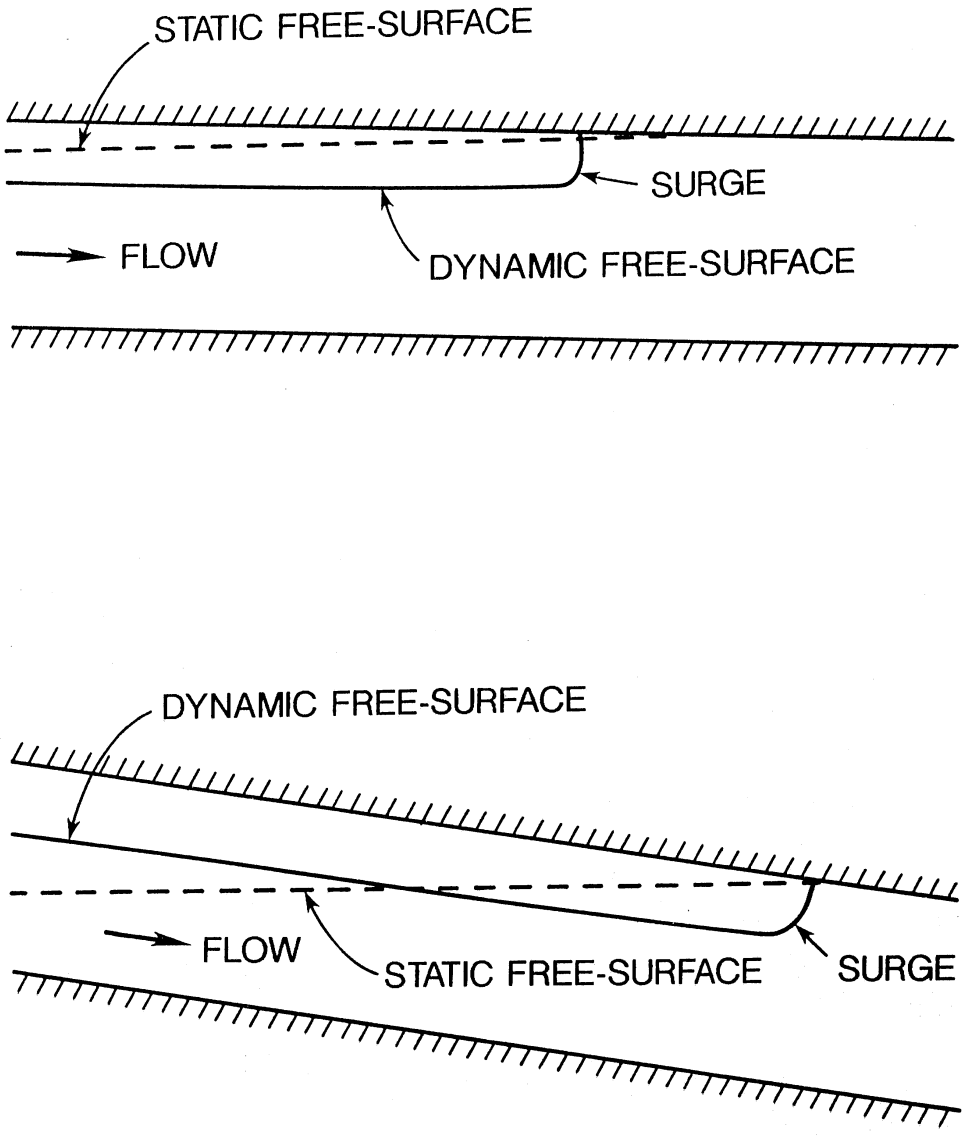

Fig. 15. Qualitative comparison of water surface profiles between static condition and dynamic condition.

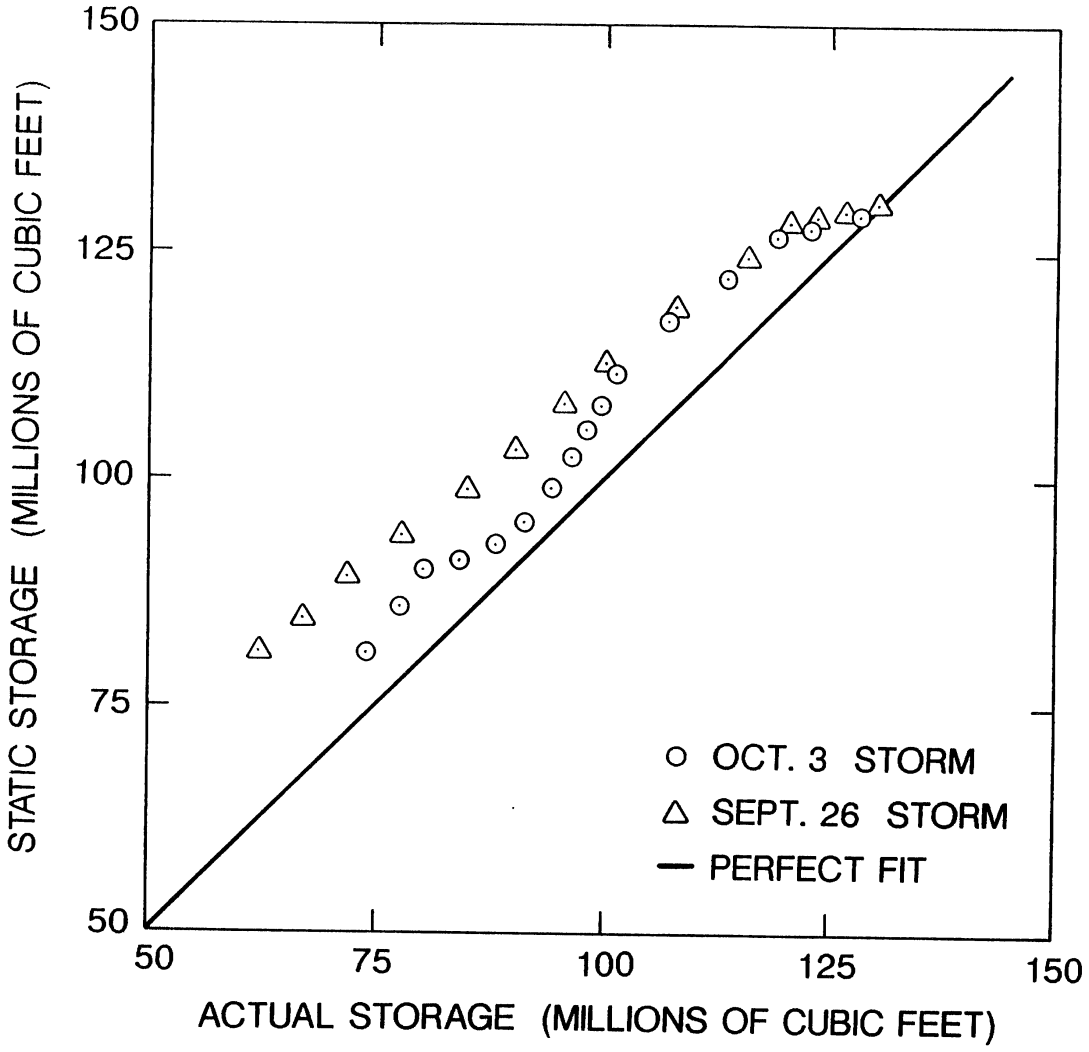

Fig. 16. Comparison of actual storage and static storage-Mainstream System.

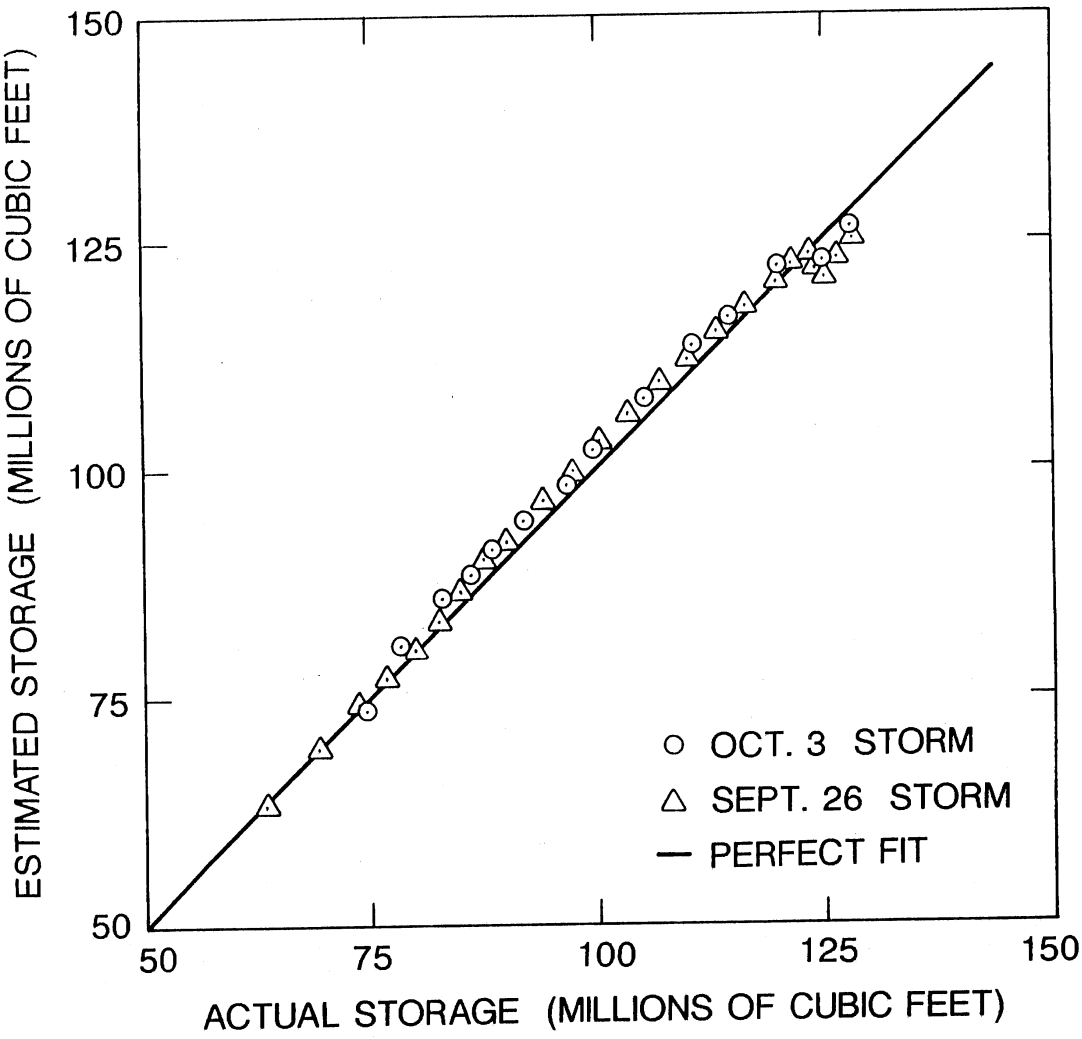

Fig. 17. Comparison of actual storage and estimated storage based on depth at two points - Mainstream System.

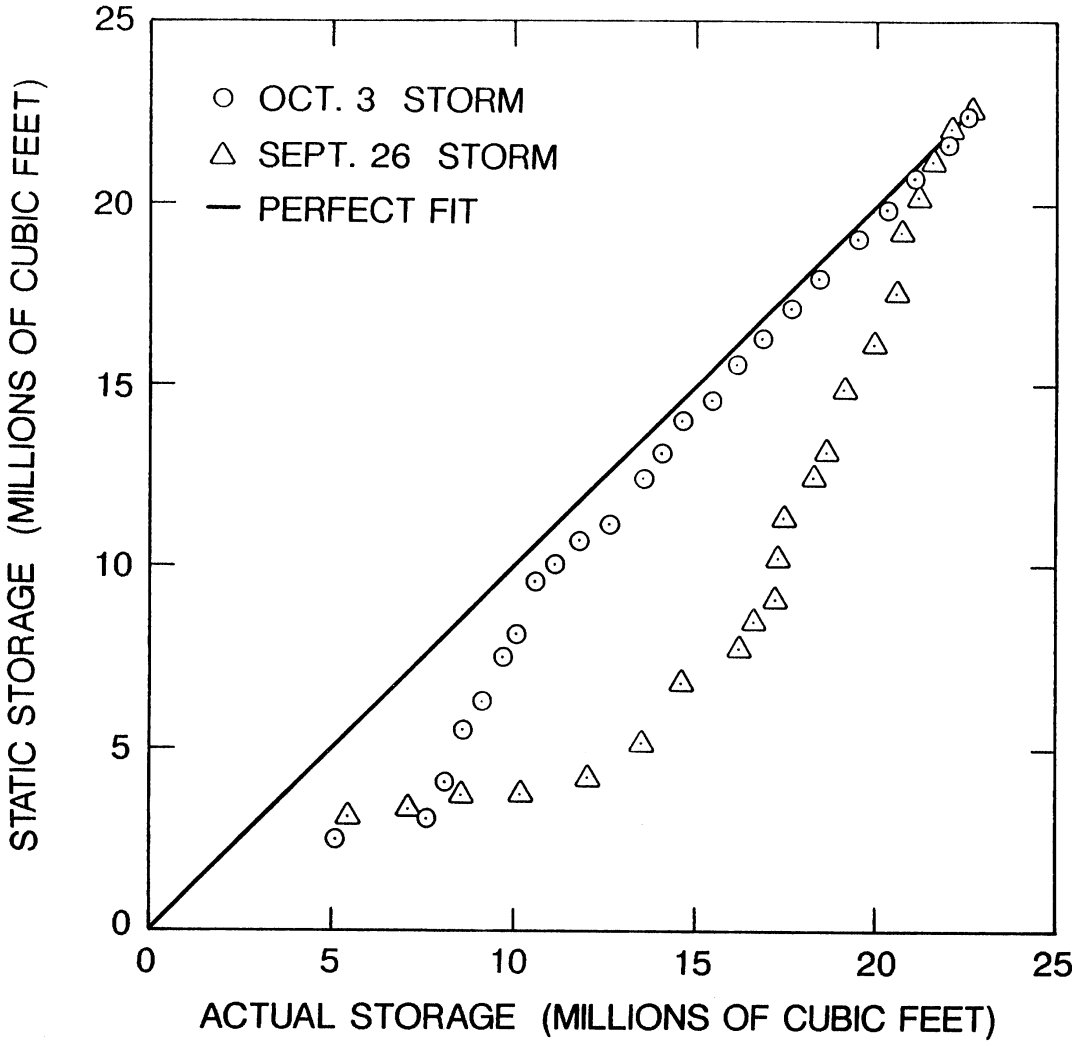

Fig. 18. Comparison of actual storage and static storage - Calumet System.

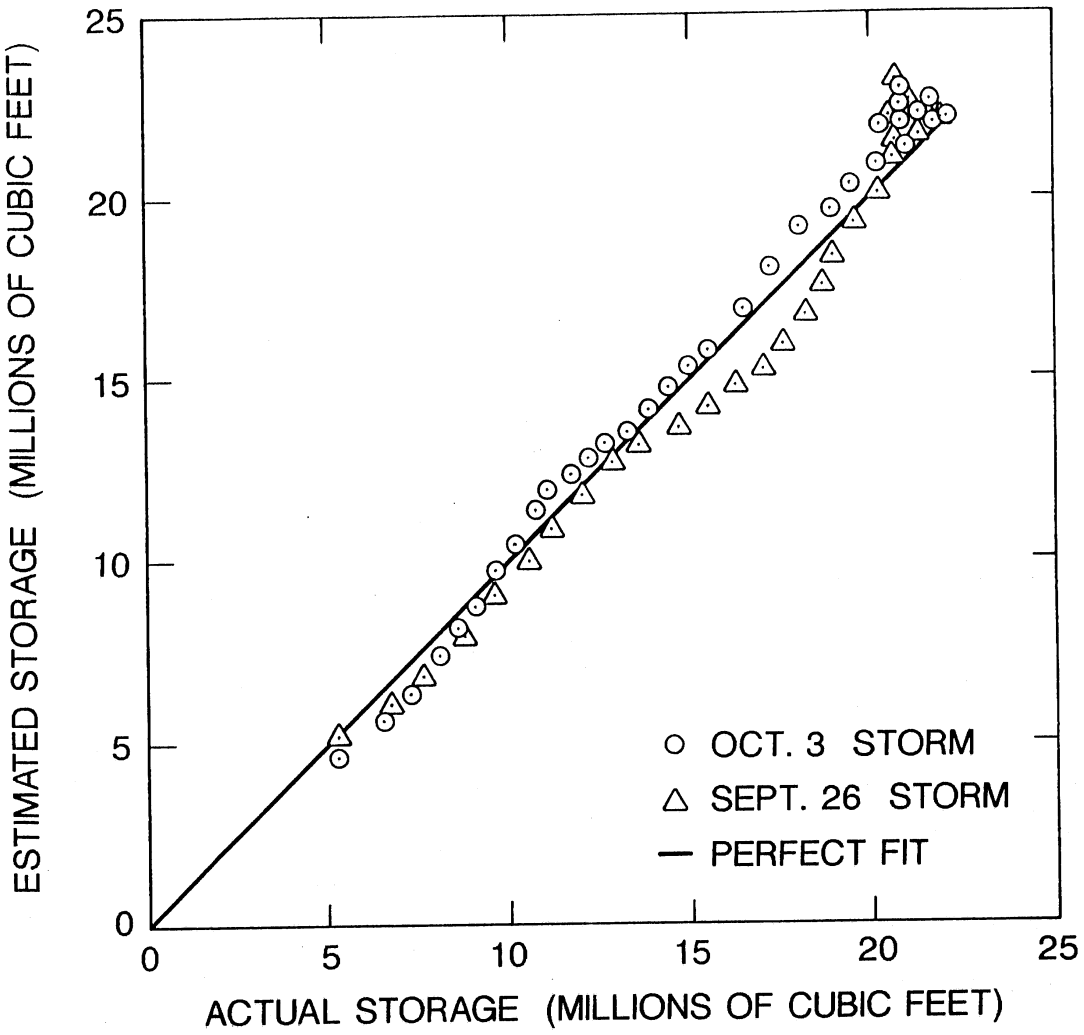

Fig. 19. Comparison of actual storage and estimated storage based on depth at two points - Calumet System.

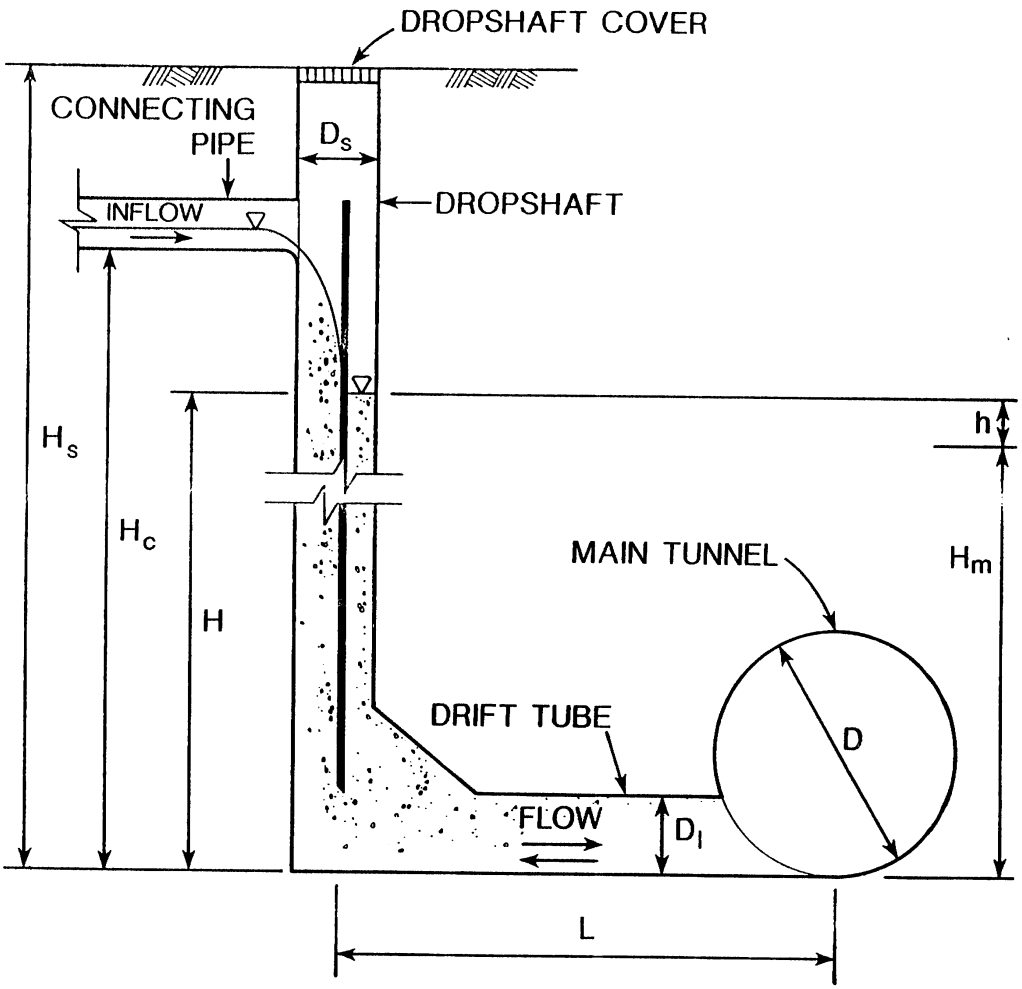

Fig. 20. A sketch of Dropshaft-Drift Tube System for geyser analysis.

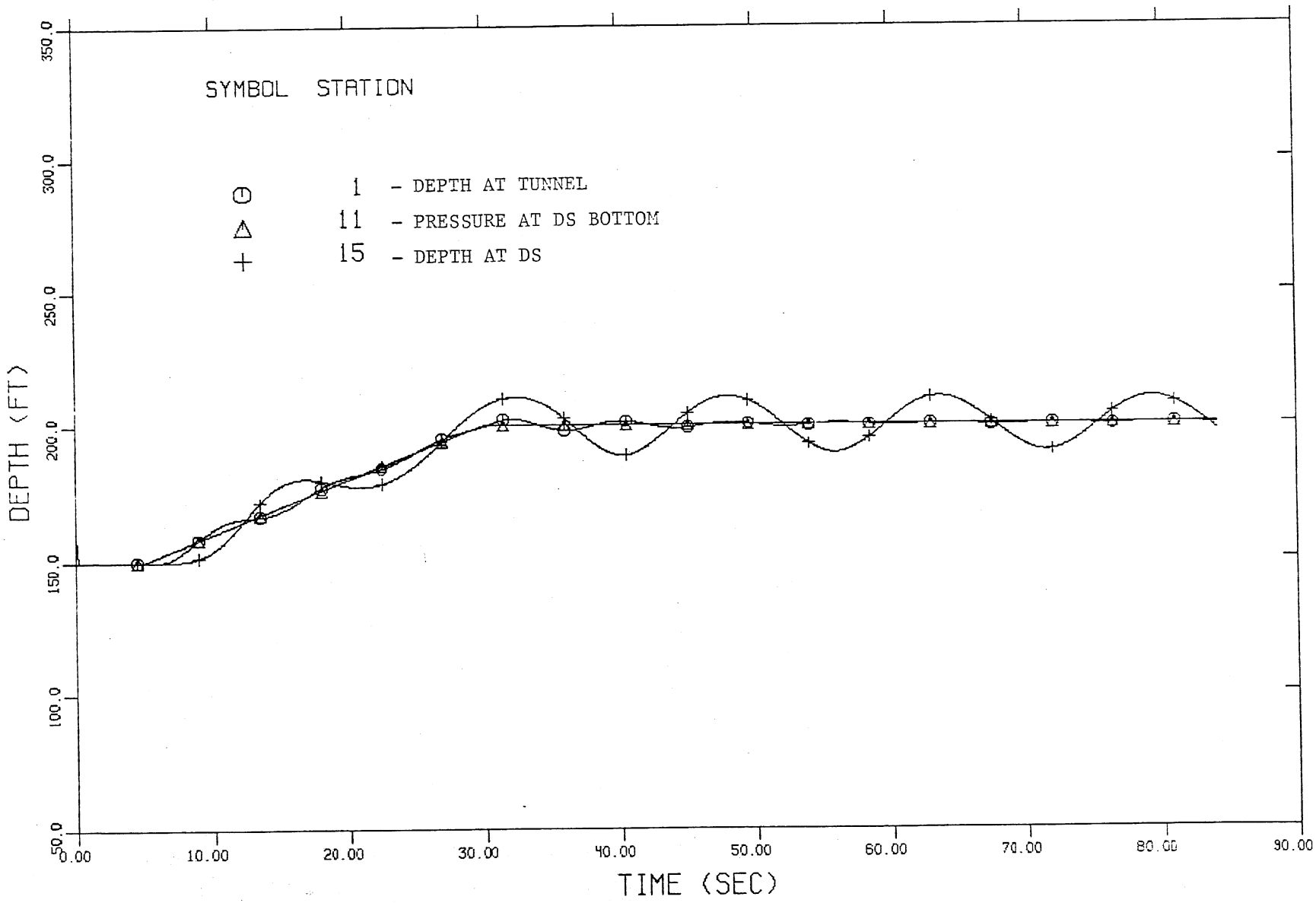

Fig. 21. Time variation of water depth in dropshaft due to slow rise in tunnel pressure, without resonance.

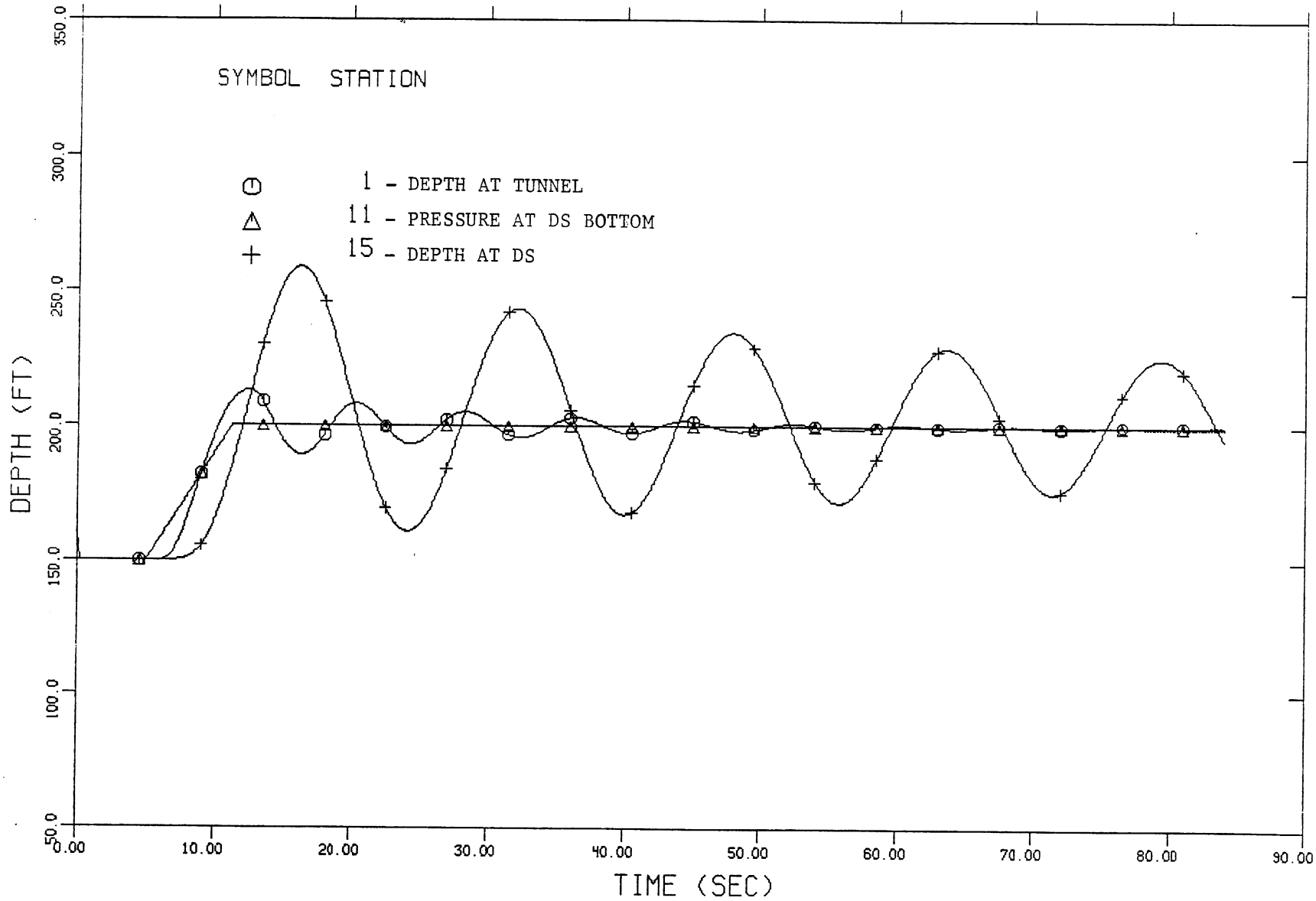

Fig. 22. Time variation of water depth in dropshaft due to rapid rise in tunnel pressure, without resonance.

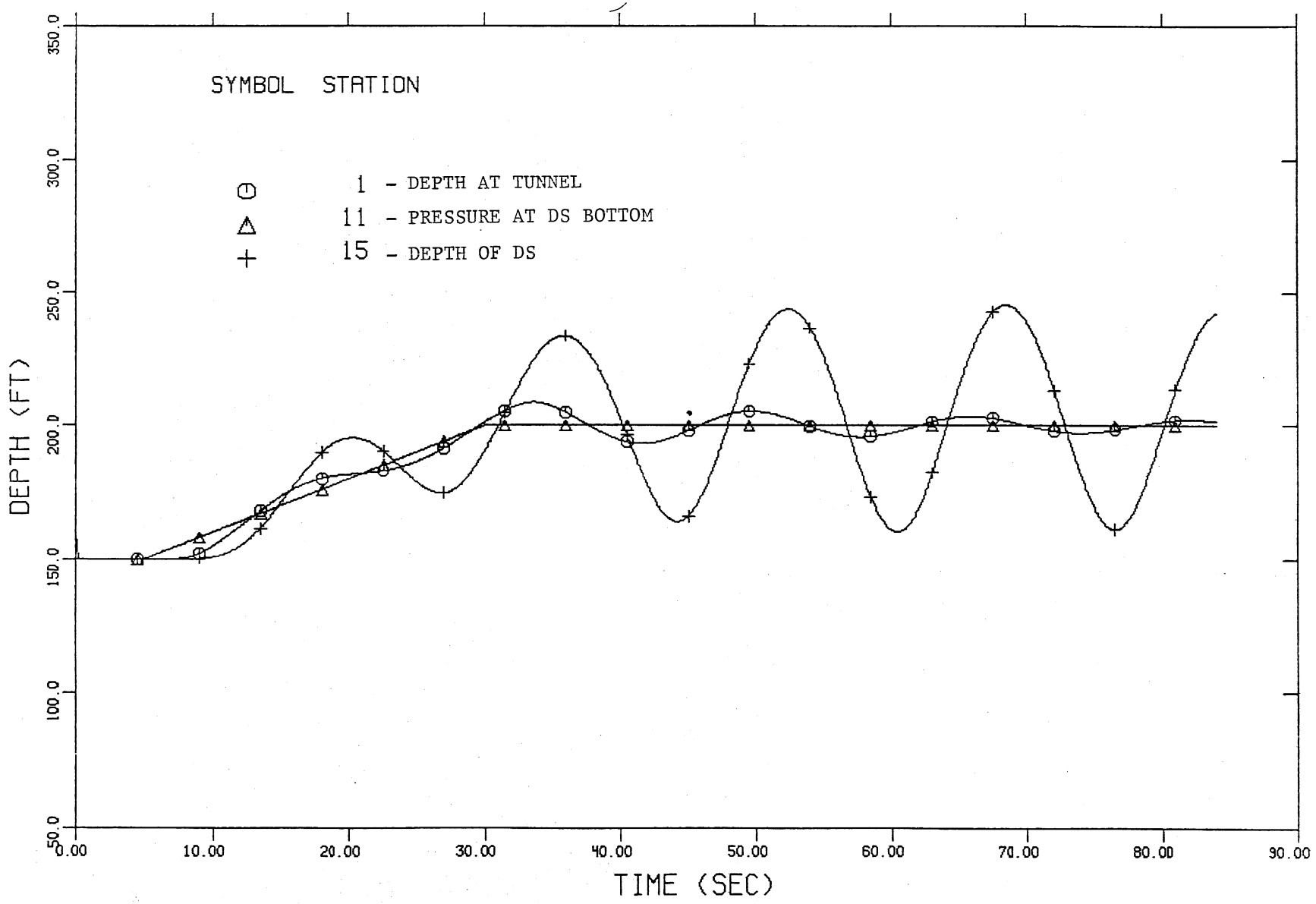

Fig. 23. Time variation of water depth in dropshaft due to slow rise in tunnel pressure, with resonance.

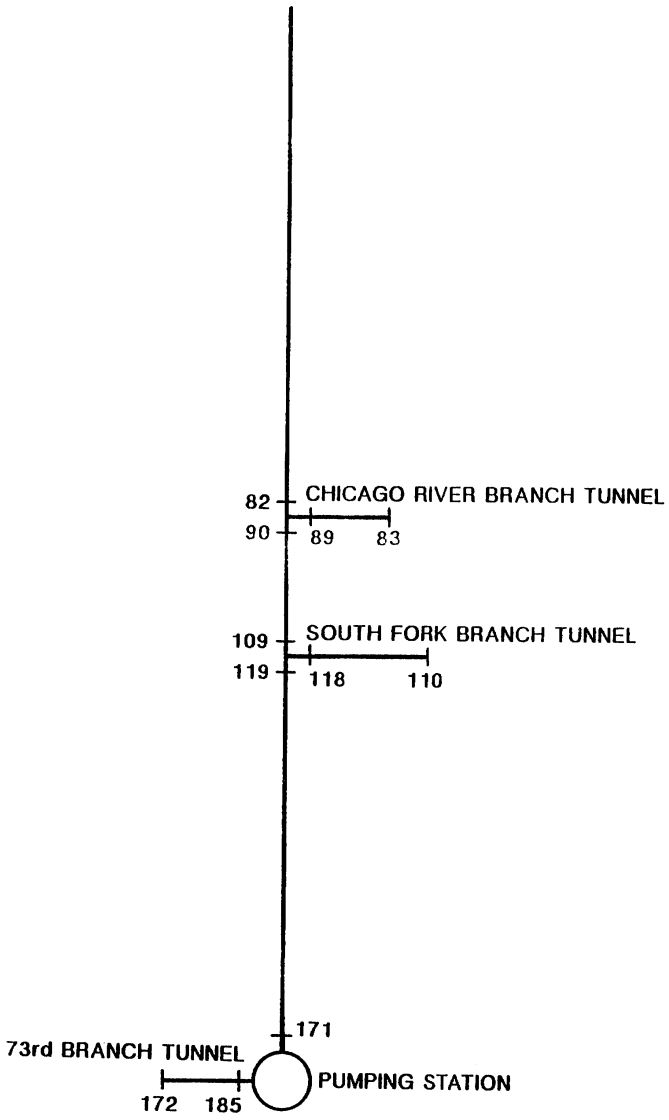

Fig. 24. Main stream System excluding the 13A, Nashville and Lawrence Ave. branch tunnels.

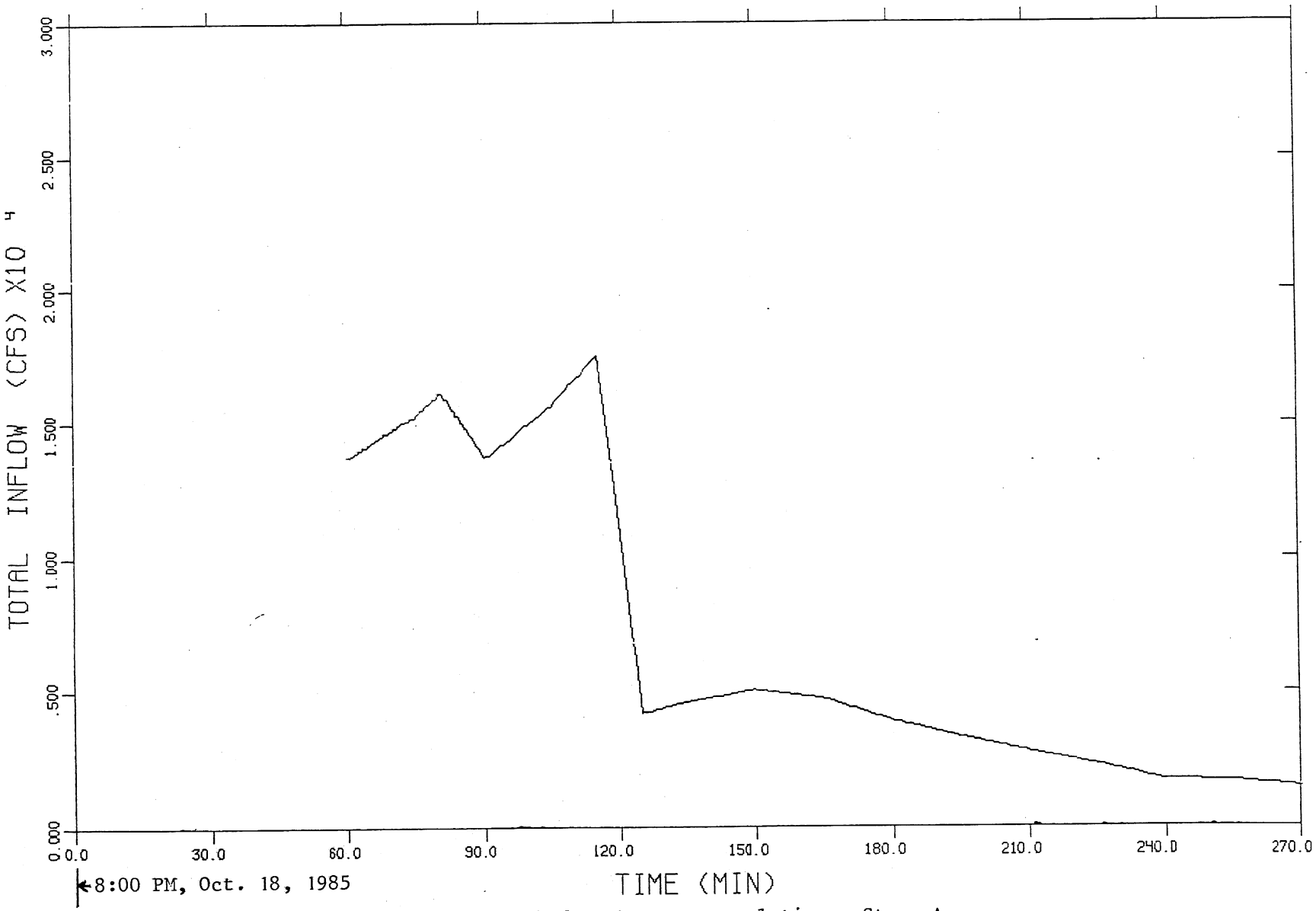

Fig. 25. Total inflow hydrograph for short term solutions, Storm A.

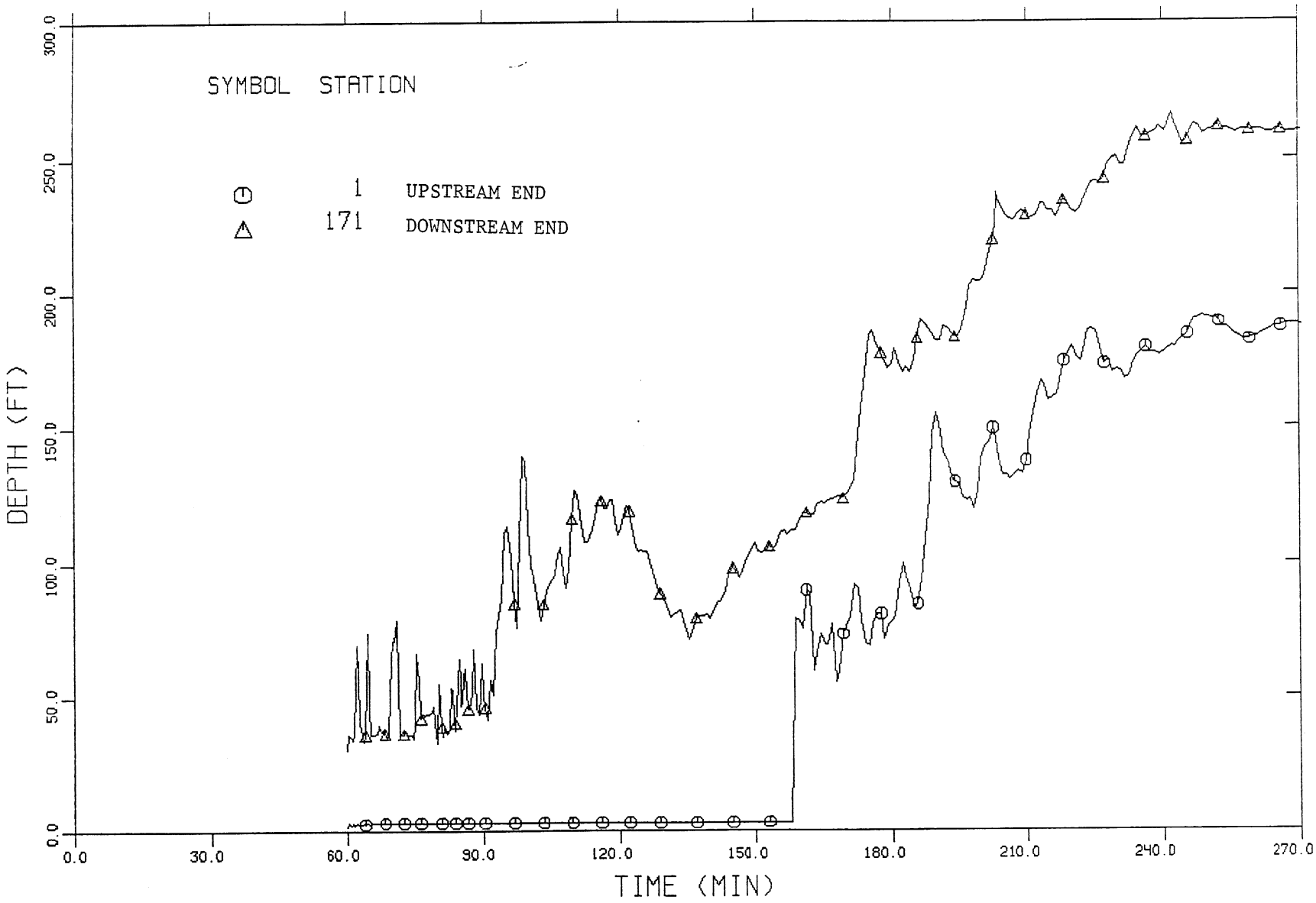

Fig. 26. Time variation of water depth at upstream and downstream ends, short-term solution, Storm A.

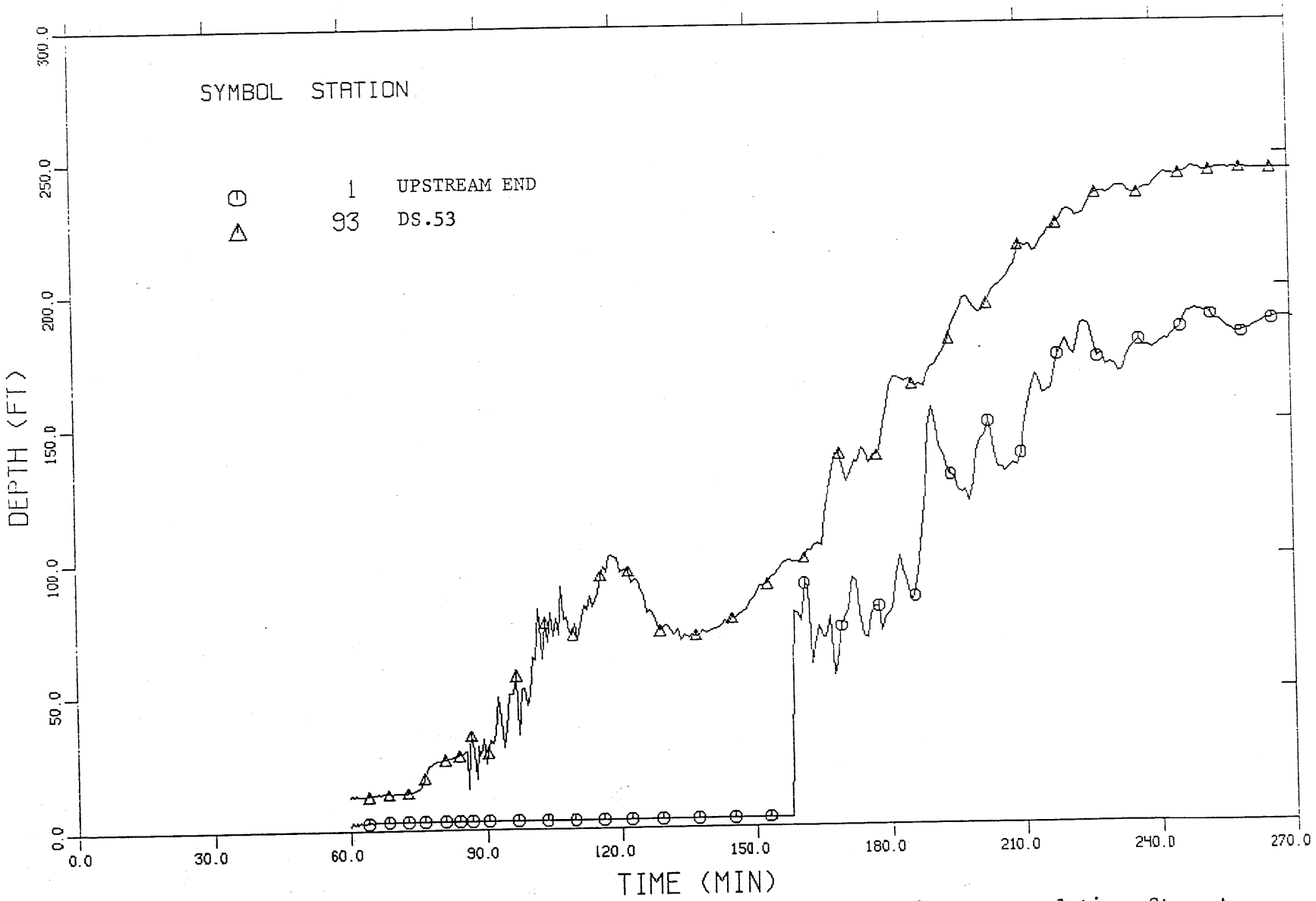

Fig. 27. Time variation of water depth at DS-53 and the upstream end, short-term solution, Storm A.

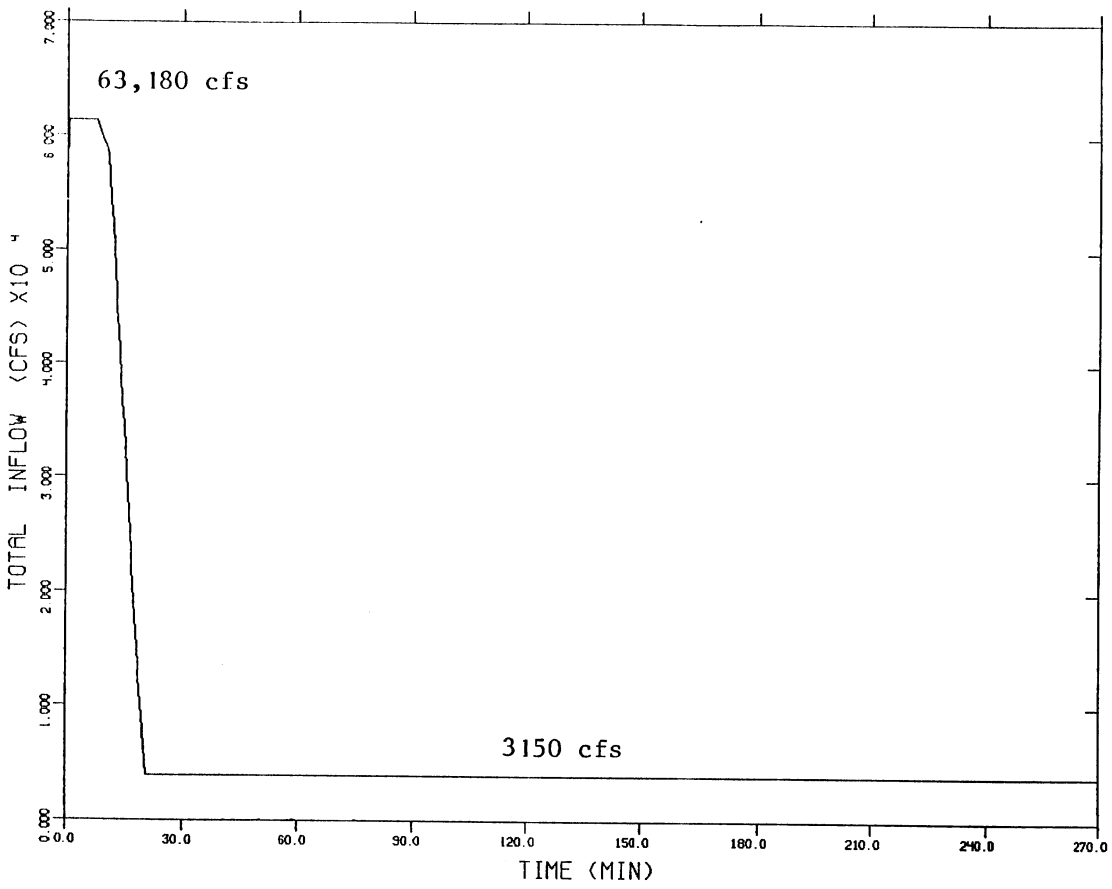

Fig. 28. Total inflow hydrograph for short-term solution, Storm B.

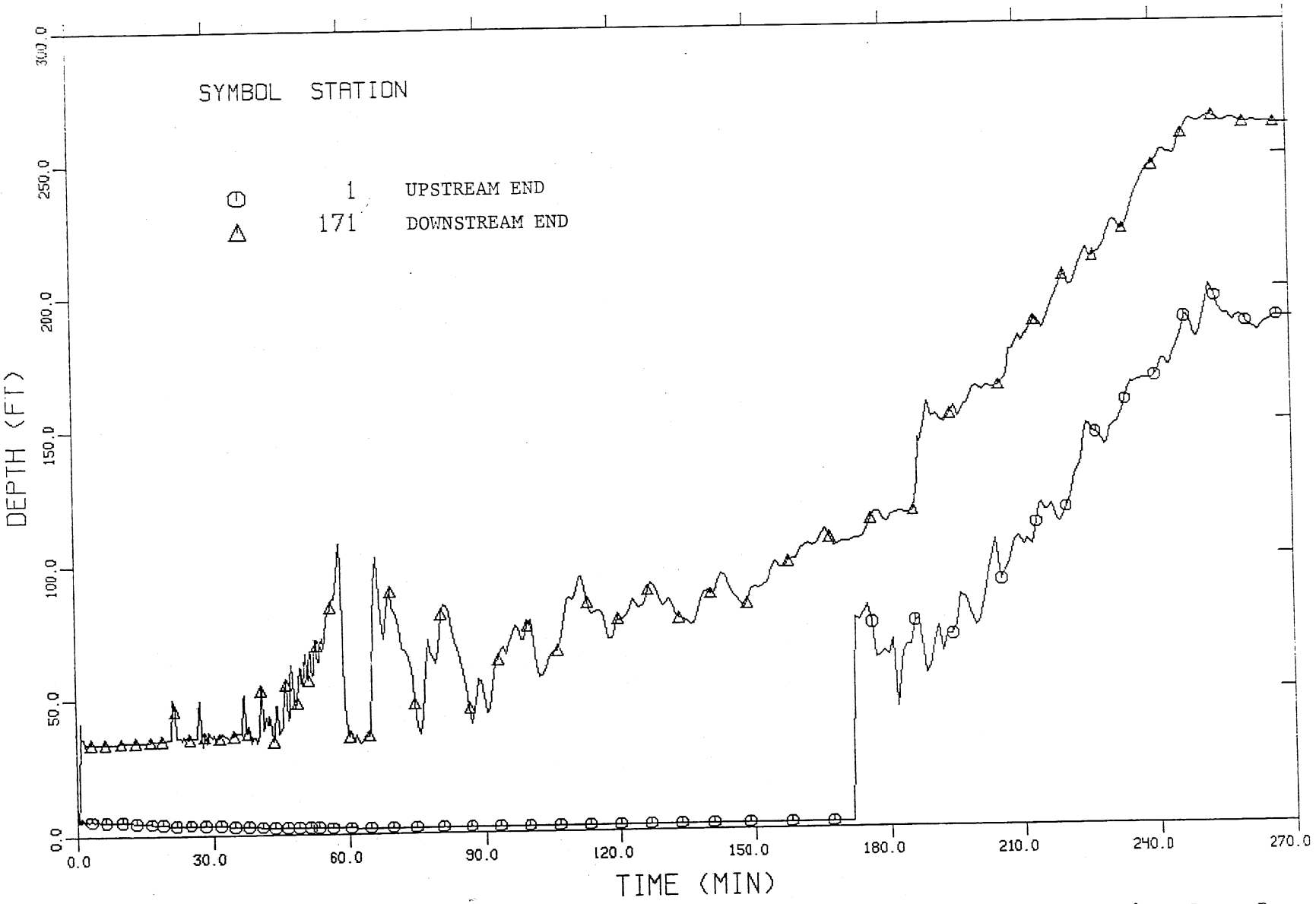

Fig. 29. Time variation of water depth at upstream and downstream ends, short-term solution, Storm B.

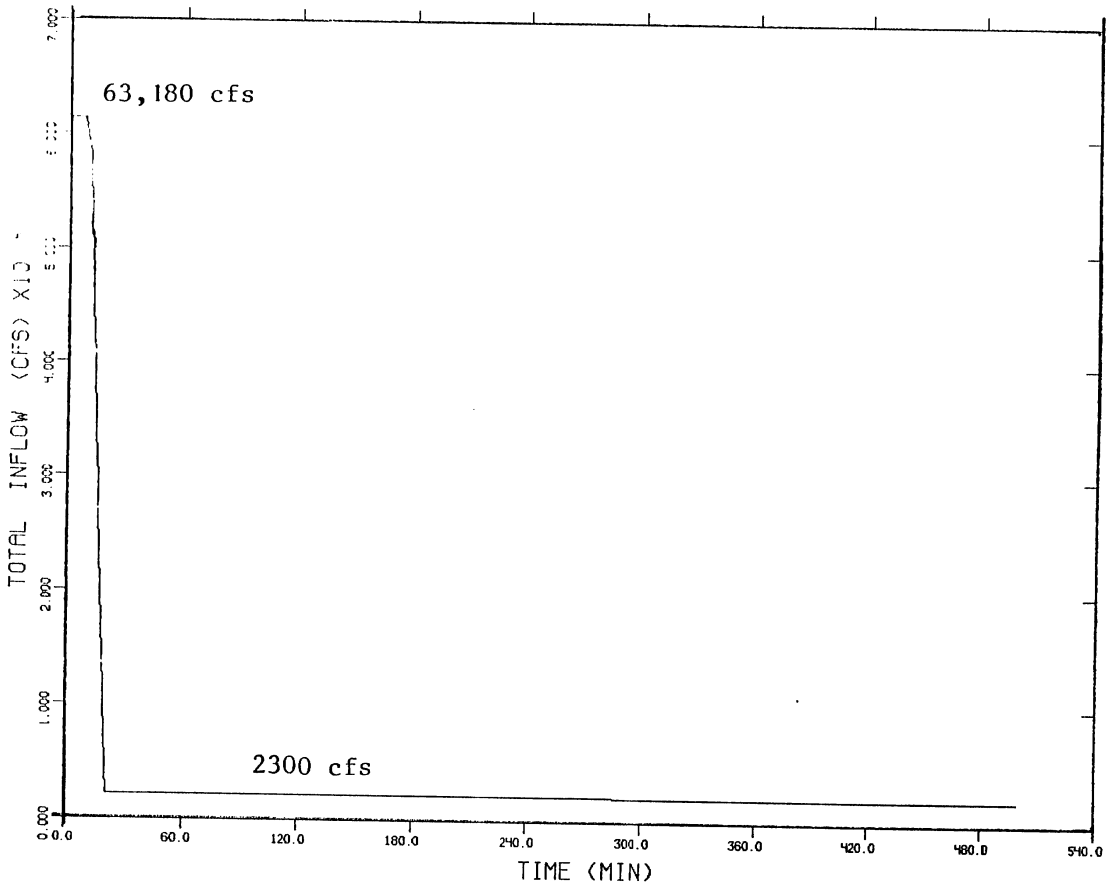

Fig. 30. Total inflow hydrograph for short-term solution, Storm C.

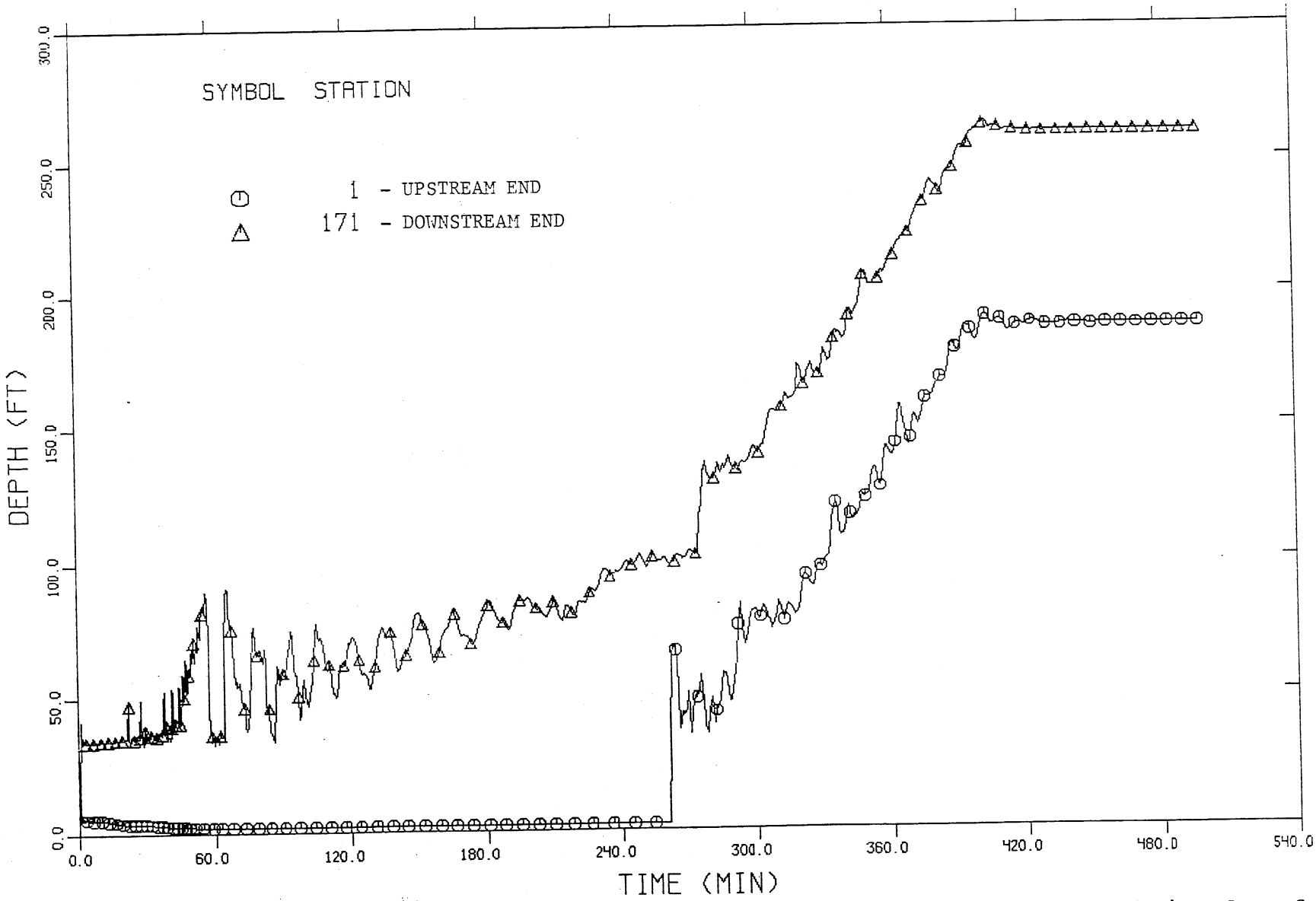

Fig. 31. Time variation of water depth at upstream and downstream ends, short-term solution, Storm C.

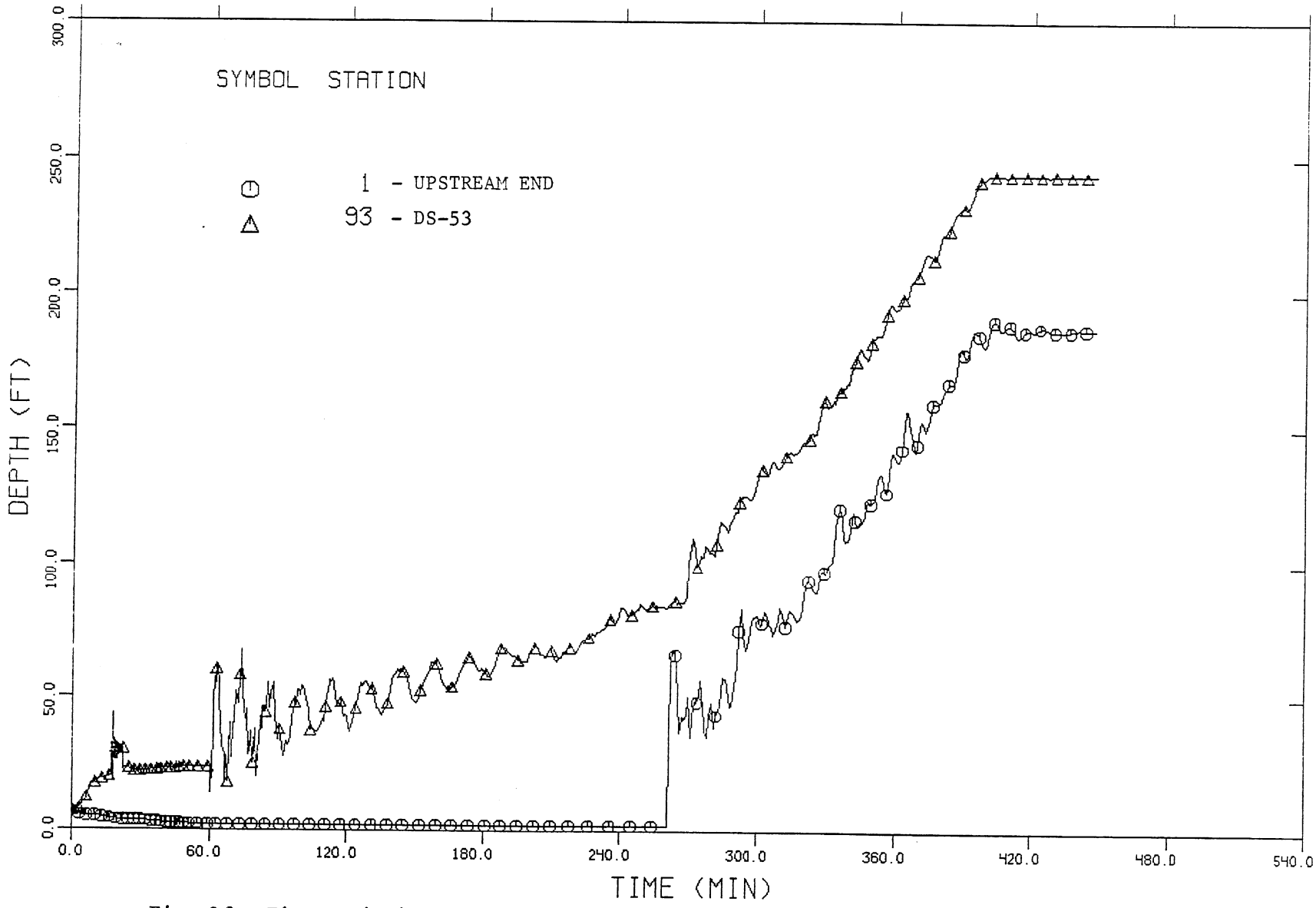

Fig. 32. Time variation of water depth at DS-53 and upstream end, short-term solution, Storm C.

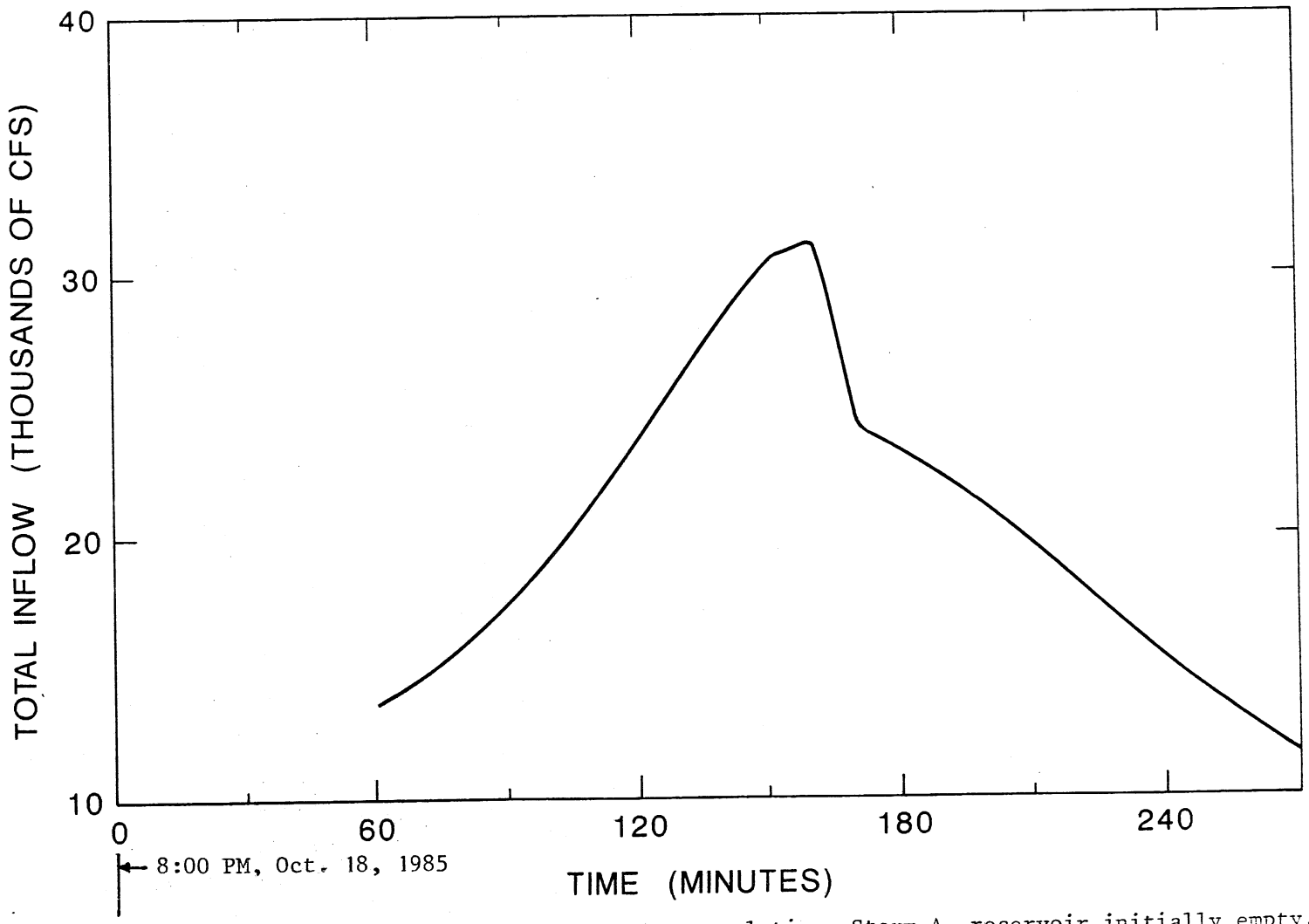

Fig. 33. Total inflow hydrograph, long-term solution, Storm A, reservoir initially empty.

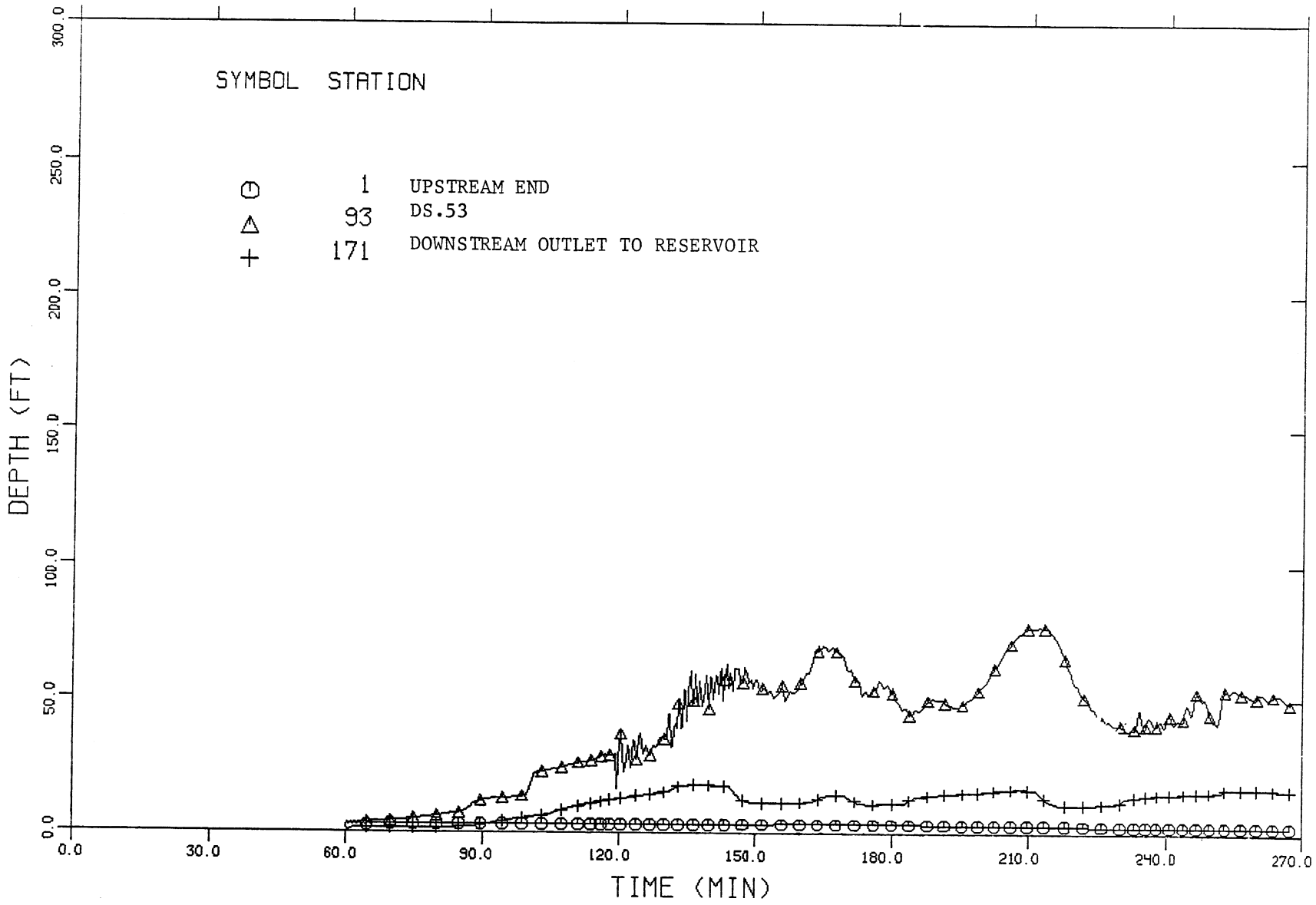

Fig. 34. Time variation of water depth at three stations, long-term solution, Storm A, reservoir initially empty.

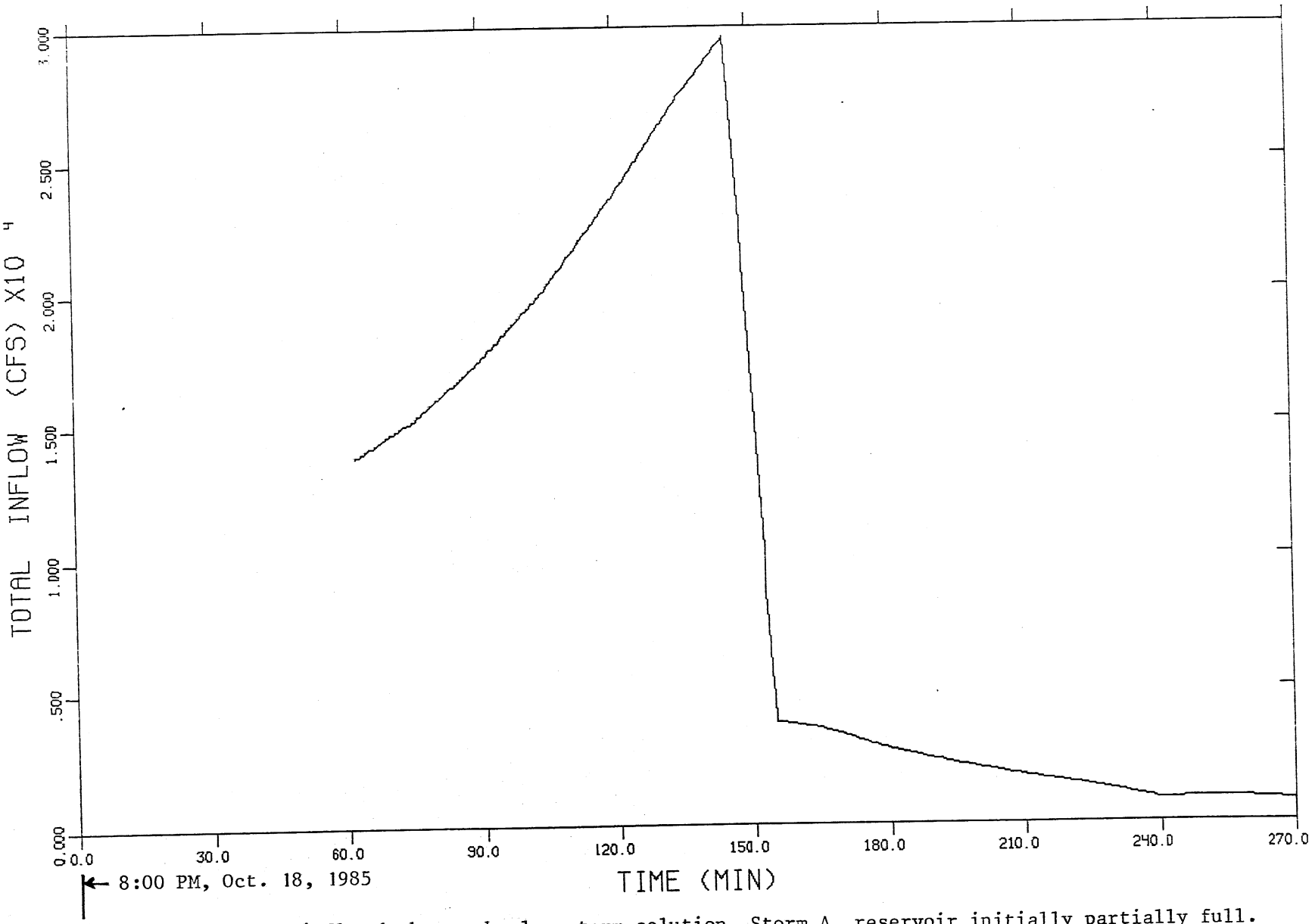

Fig. 35. Total inflow hydrograph, long-term solution, Storm A, reservoir initially partially full.

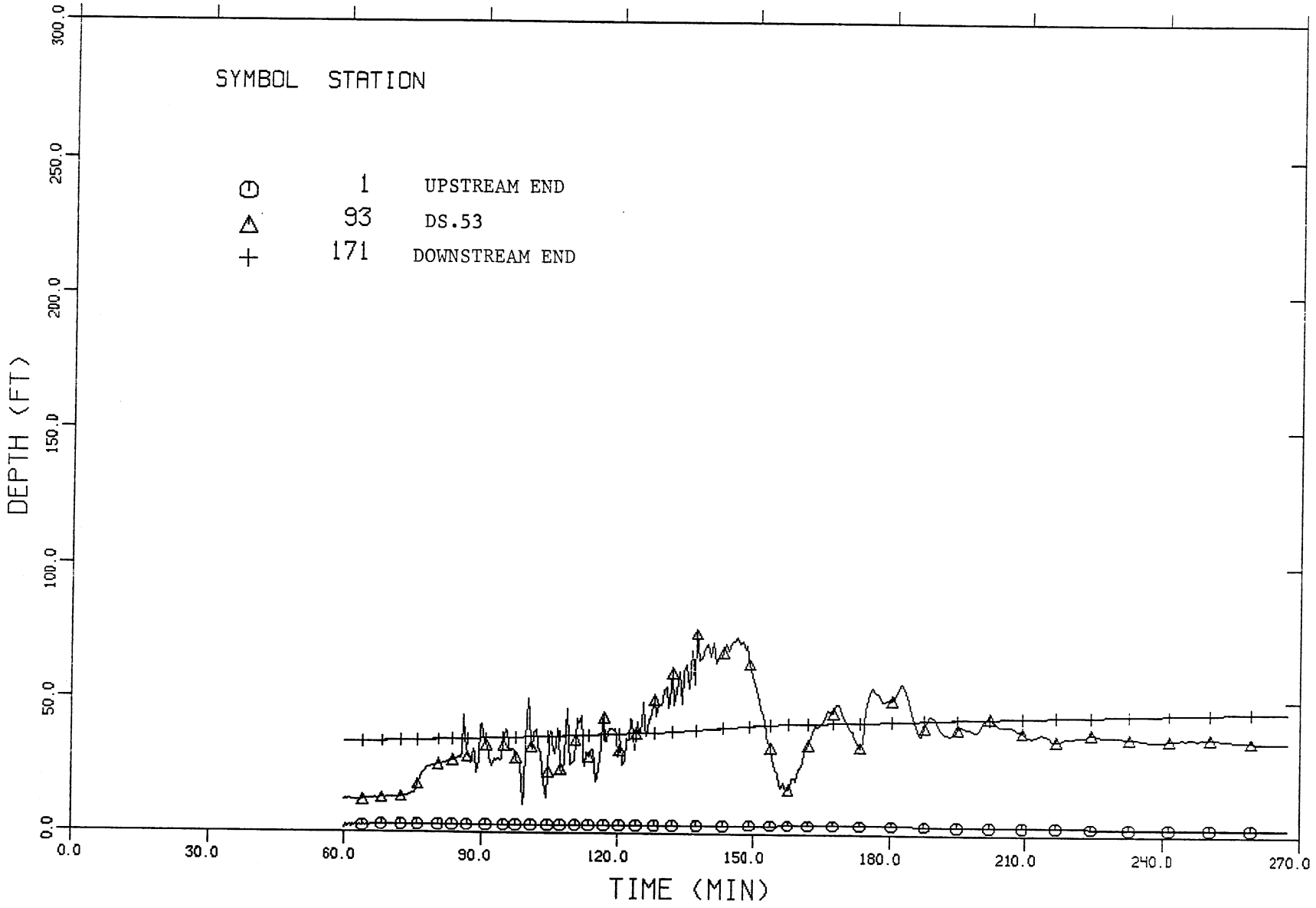

Fig. 36. Time variation of water depth at three key station, long-term solution, Storm A, reservoir initially partially full.

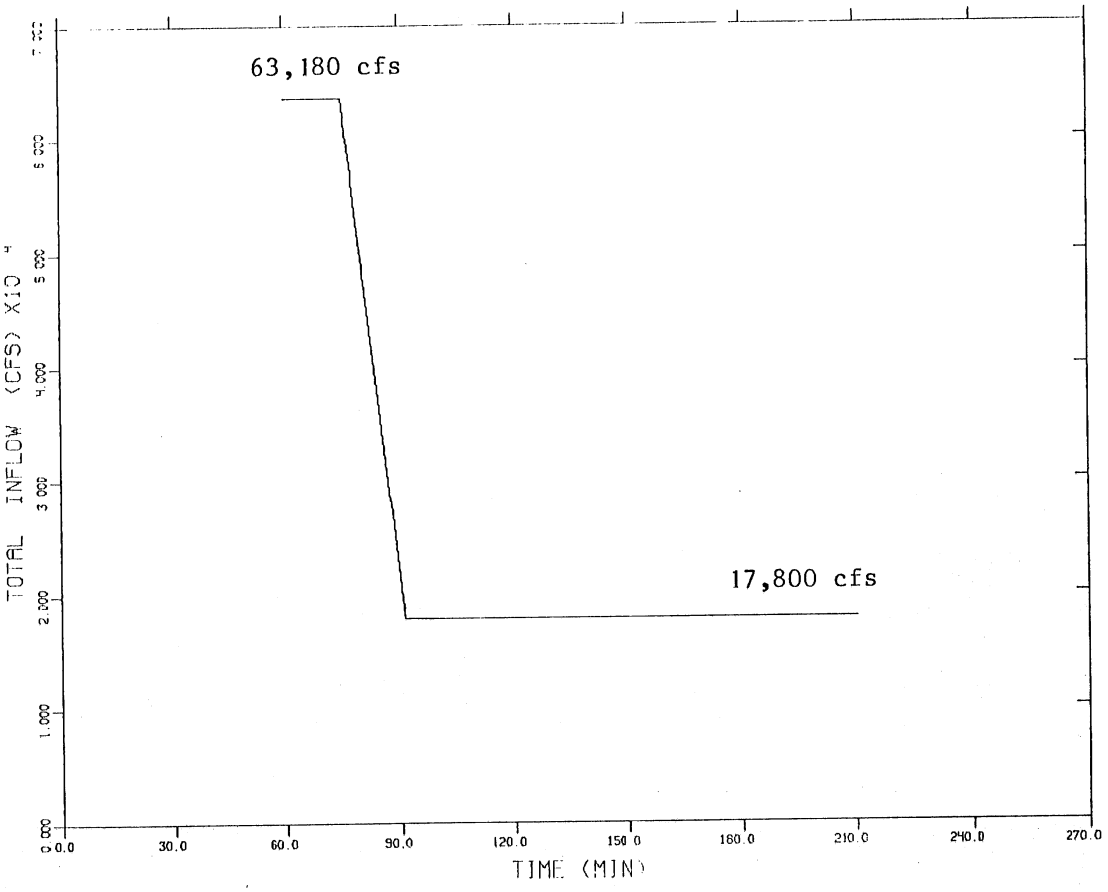

Fig. 37. Total inflow hydrograph, long-term solution, Storm B and C, reservoir initially empty.

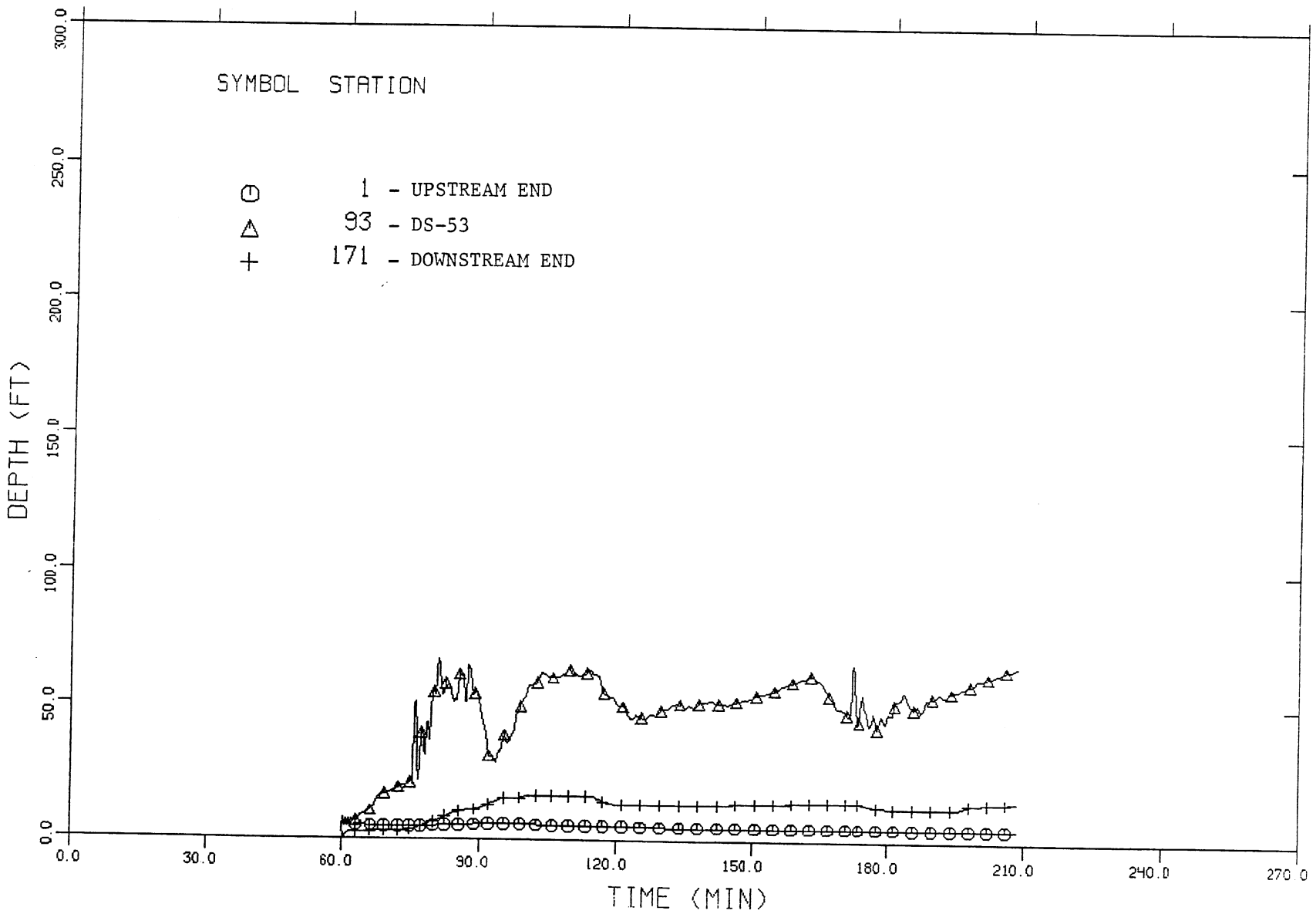

Fig. 38. Time variation of water depth at three key stations, long-term solution, Storm B and C, reservoir initially empty.

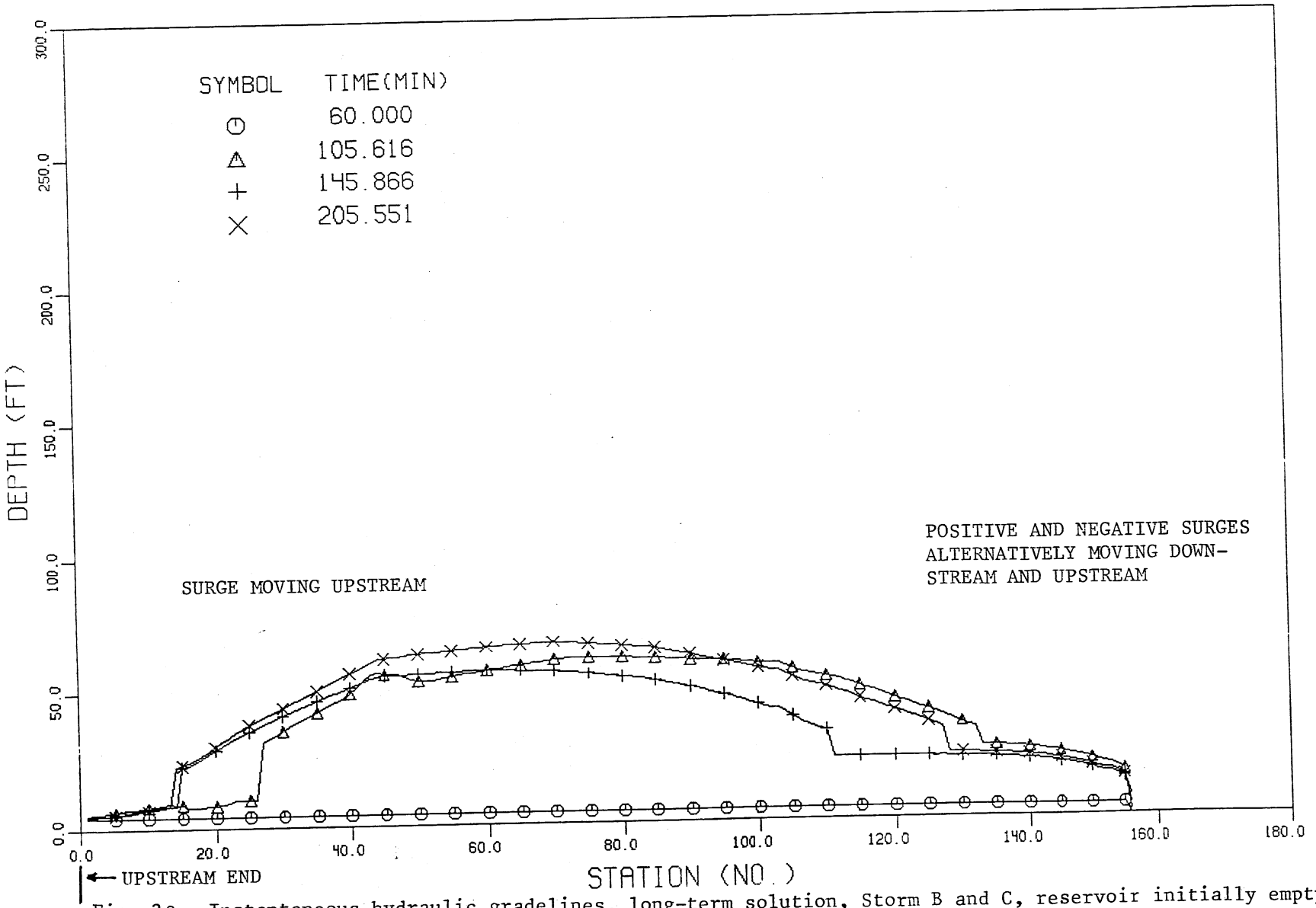

Fig. 39. Instantaneous hydraulic gradelines, long-term solution, Storm B and C, reservoir initially empty.

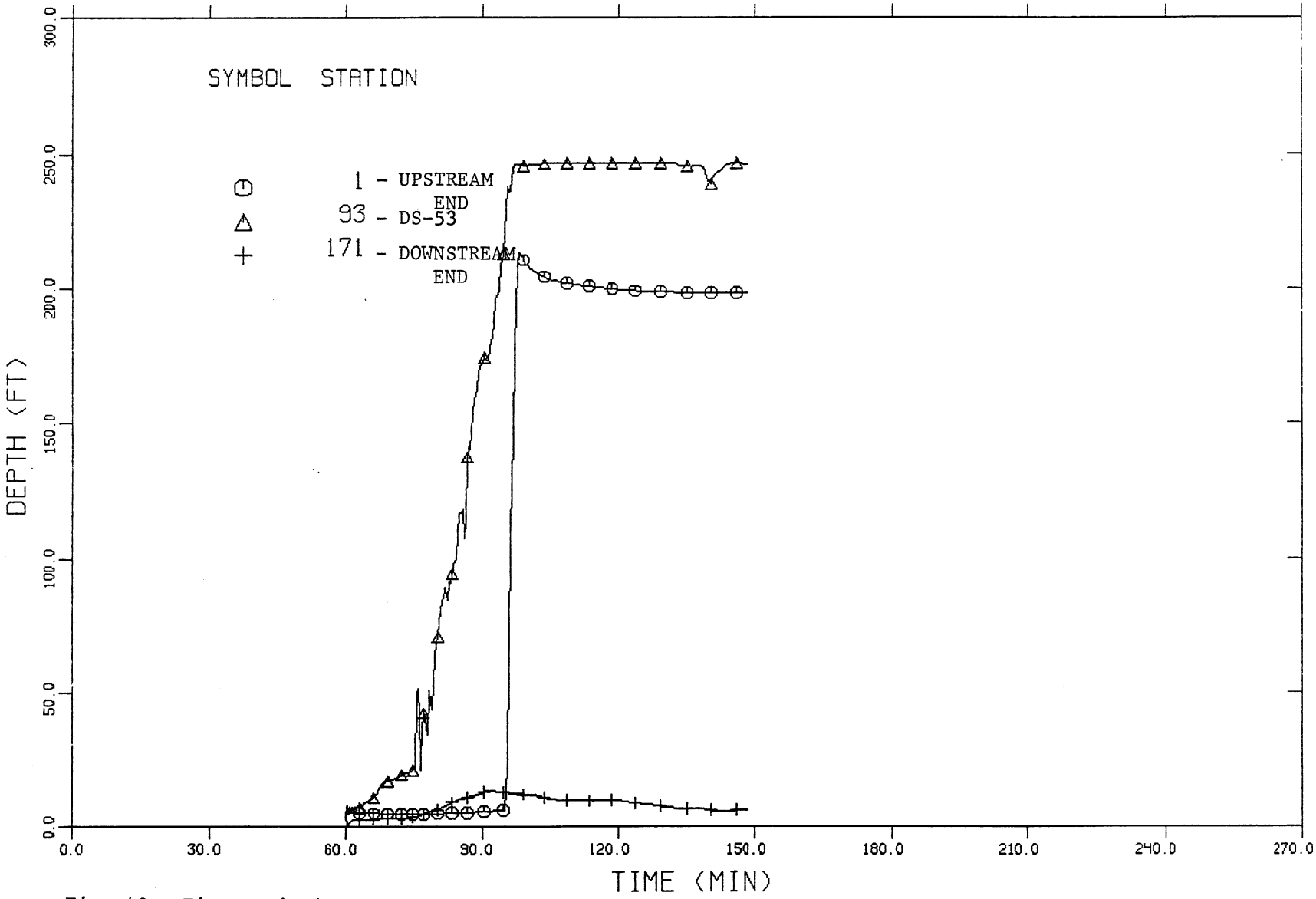

Fig. 40. Time variation of water depth at three key stations, long-term structural solution, Storm C, reservoir initially empty.

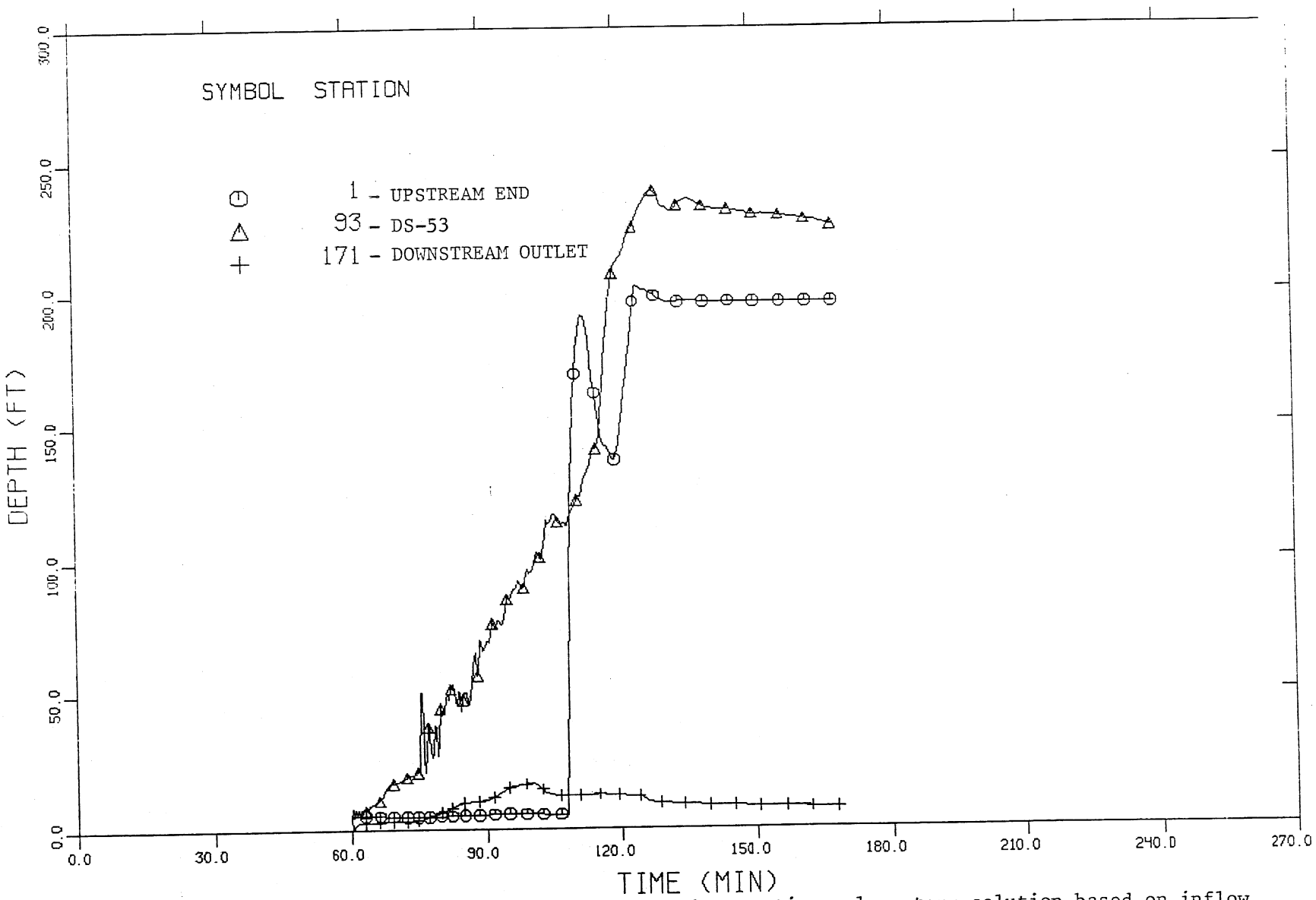

Fig. 41. Time variation of water depth at three key stations, long-term solution based on inflow control and surge structure, Storm C, reservoir initially empty.

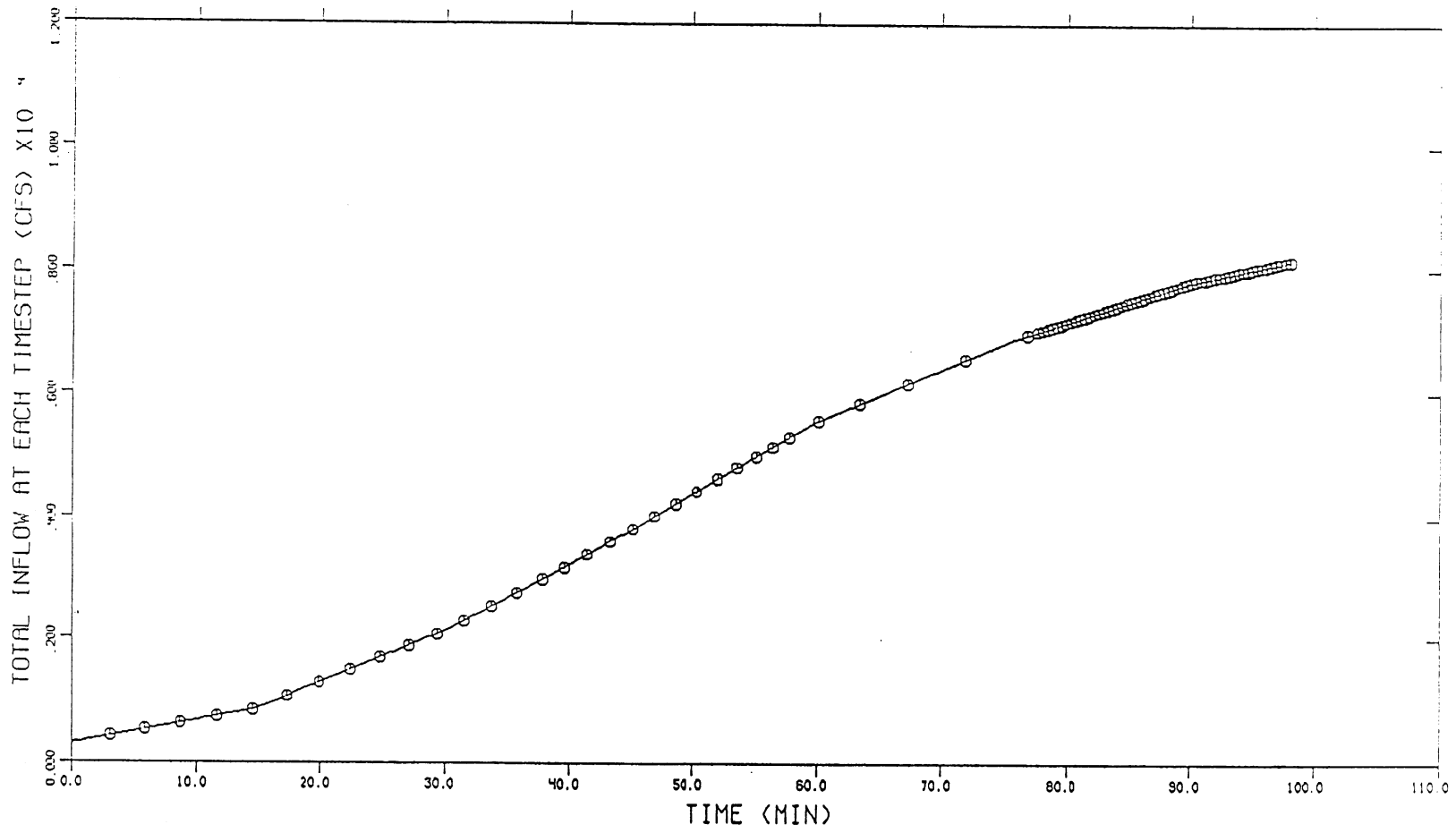

Fig. 42. Total inflow hydrograph for Calumet System due to September 26, 1986, storm.

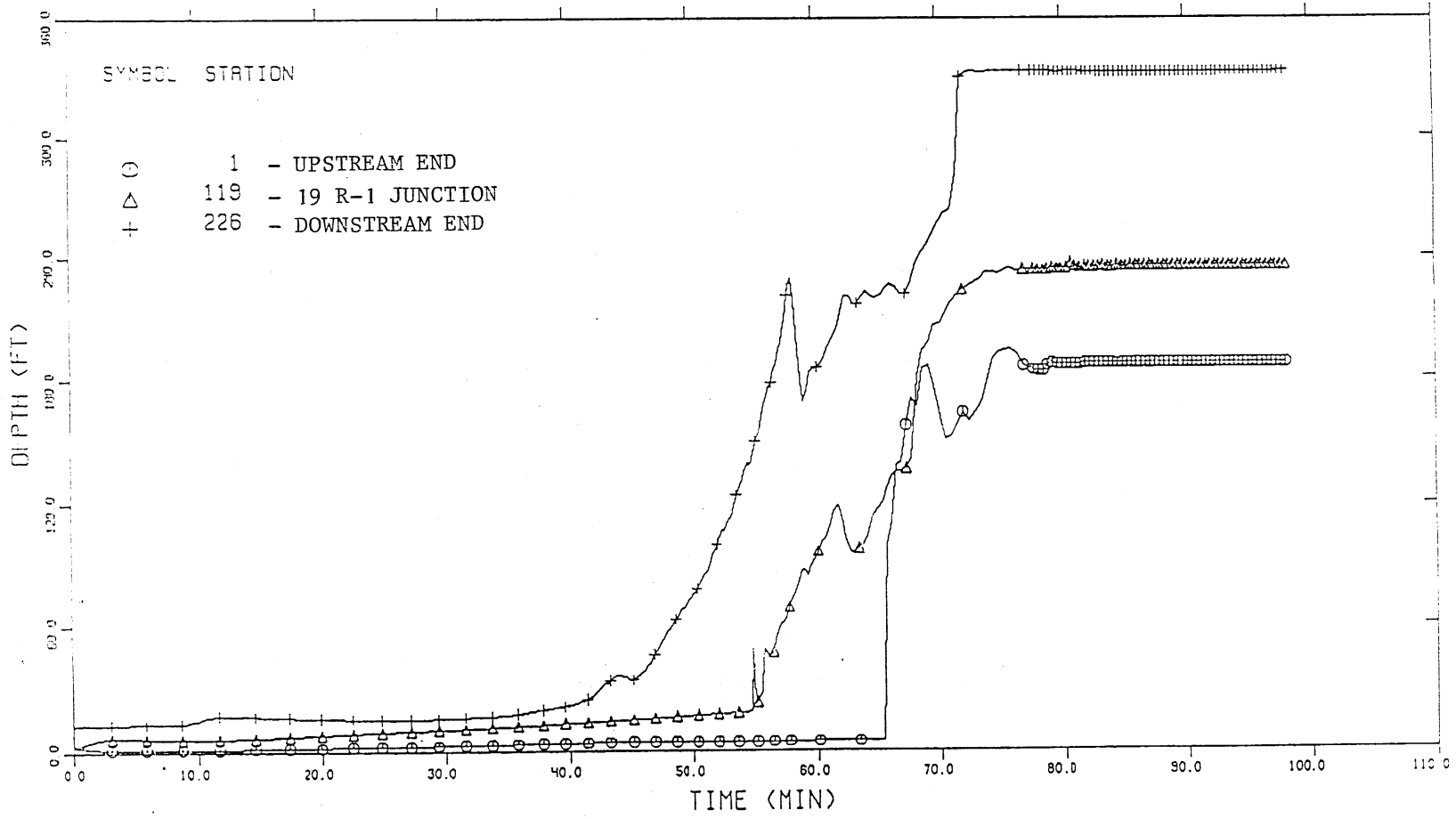

Figure 43. Time variation of water depth at three key stations.

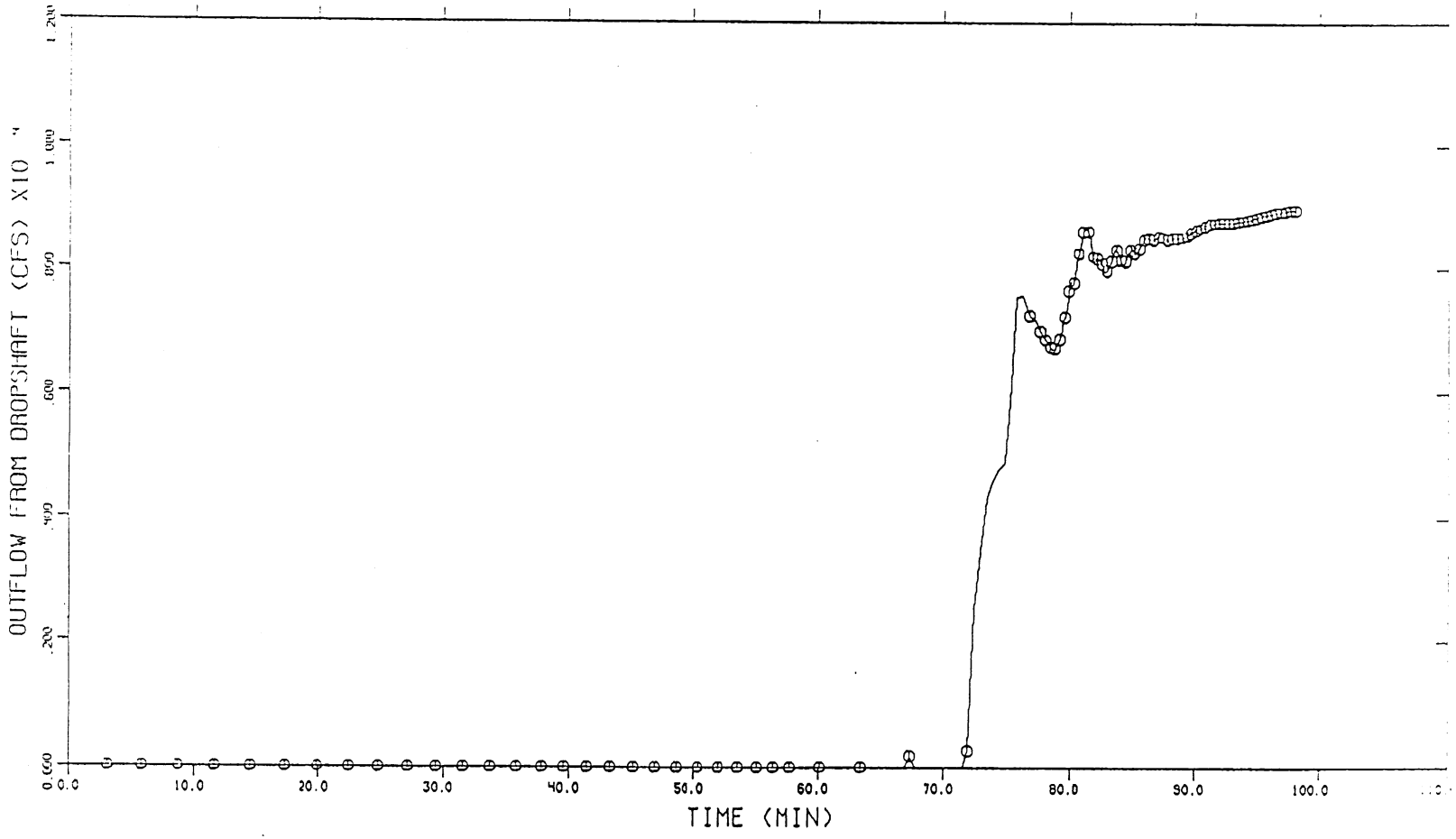

Fig. 44. Total overflow hydrograph.

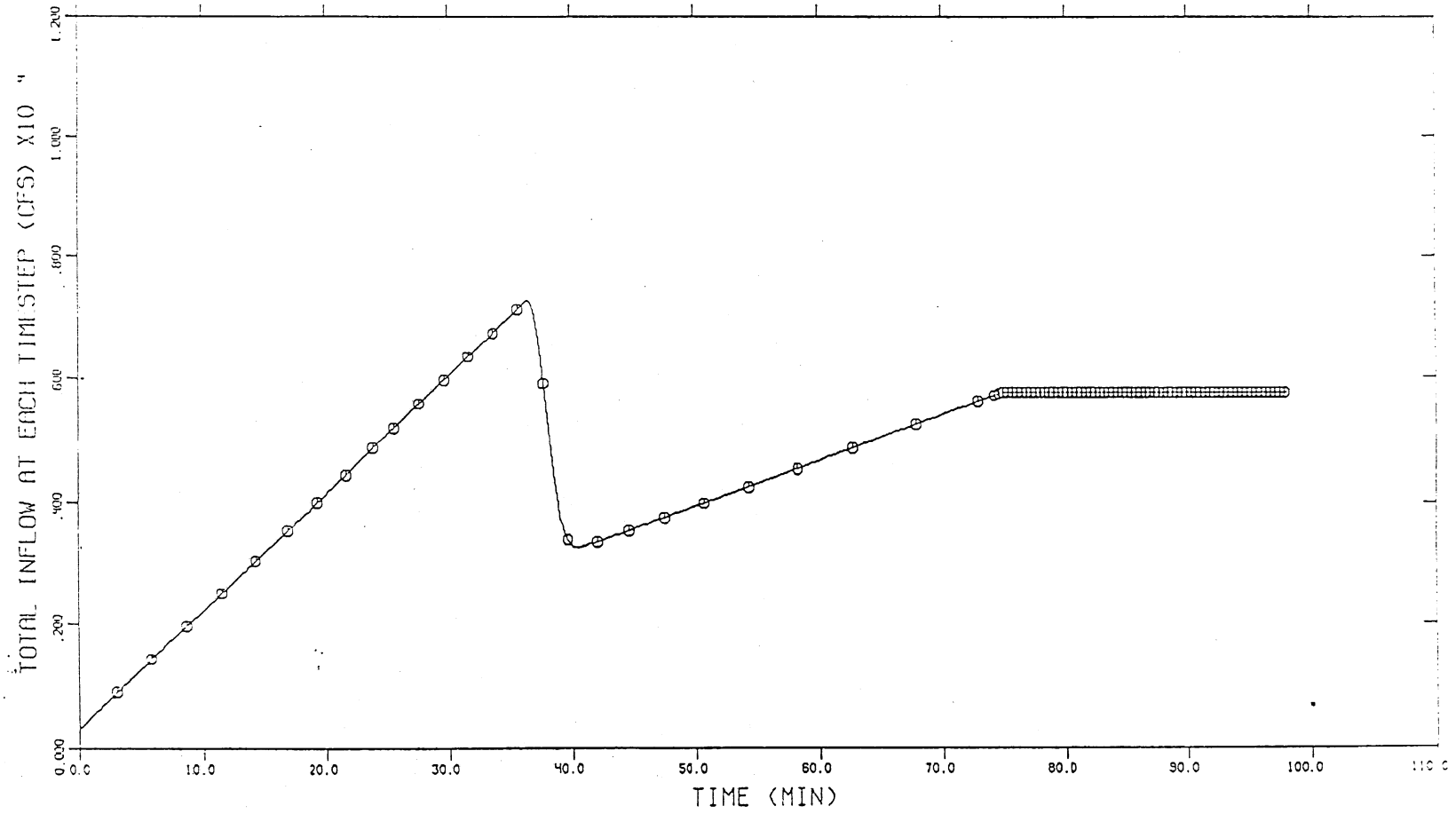

Fig. 45. Total inflow hydrograph, short term solution, maximum design flow.

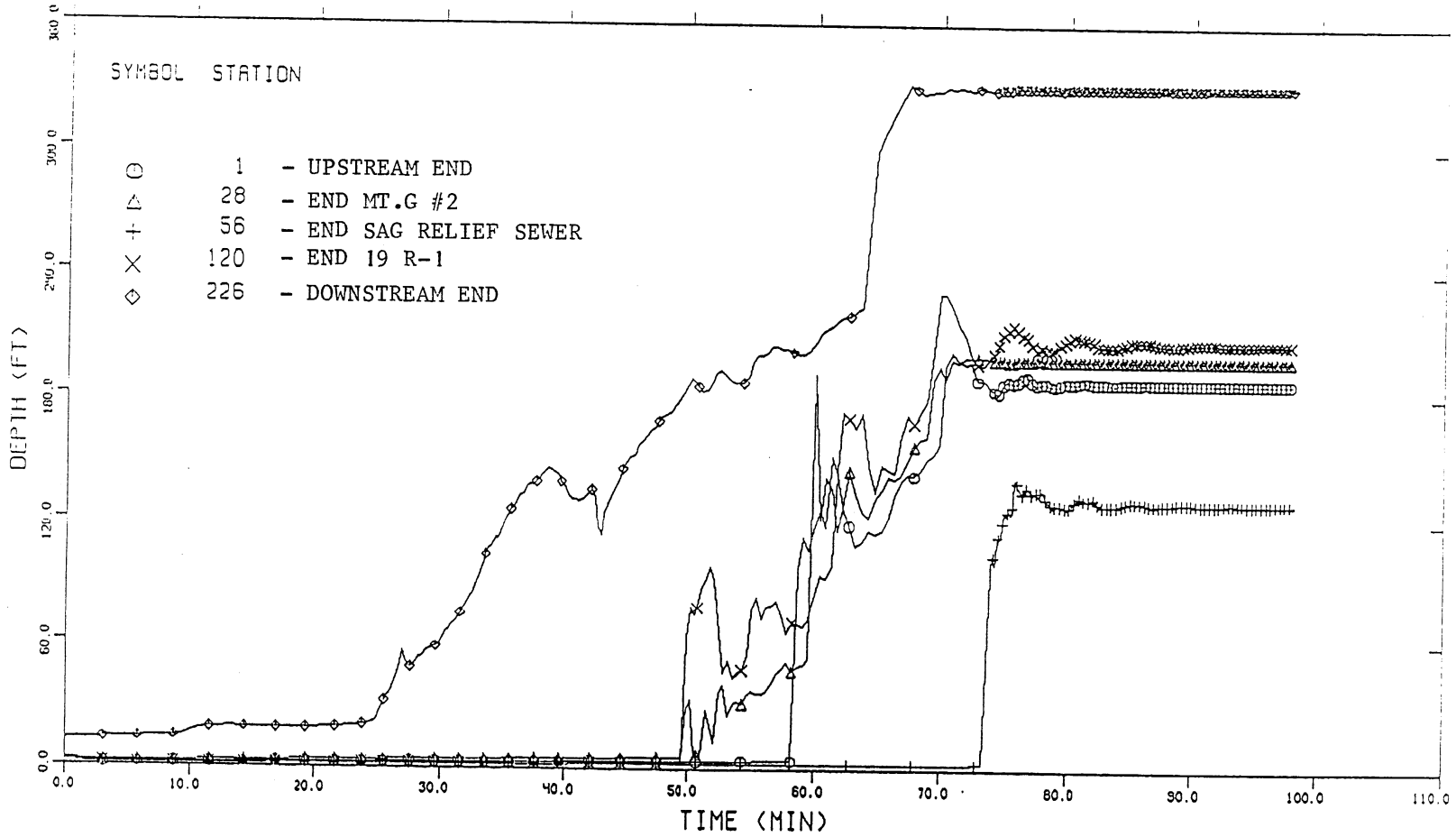

Fig. 46. Time variation of water depth at five key stations, short term solution, maximum design flow.

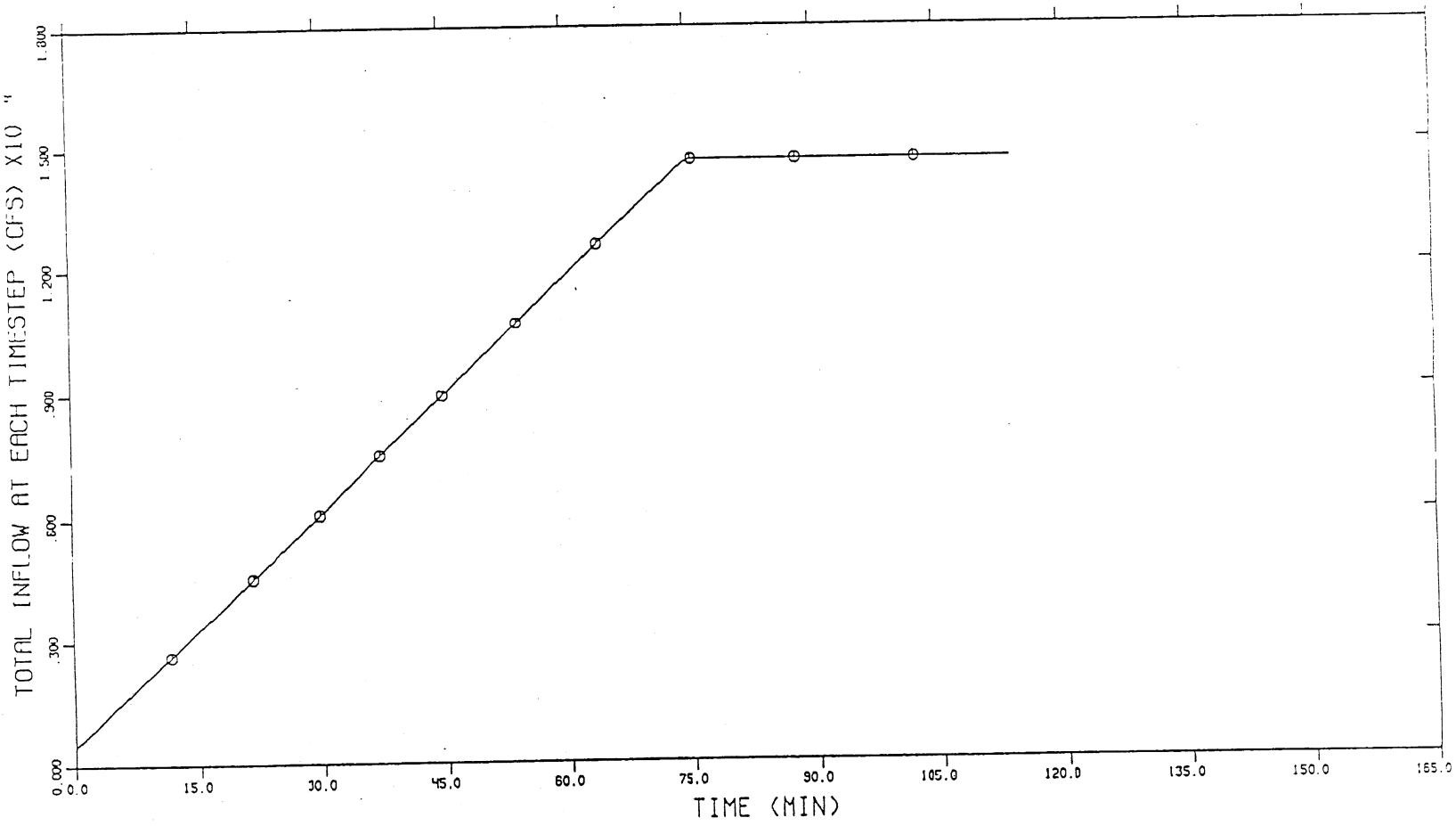

Fig. 47. Total inflow hydrograph, maximum design flow A.

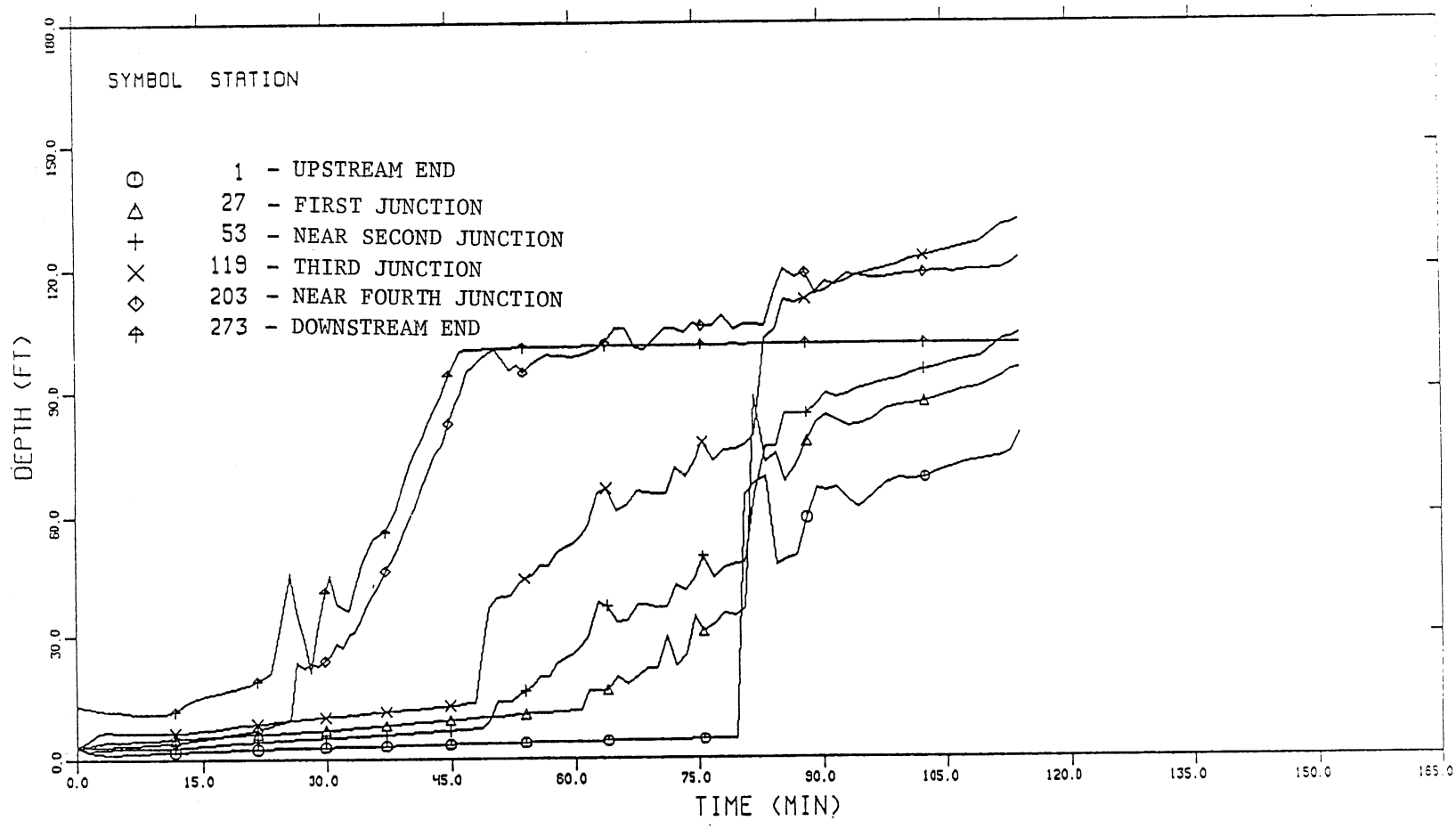

Fig. 48. Time variation of water depth at six key stations, maximum design flow.

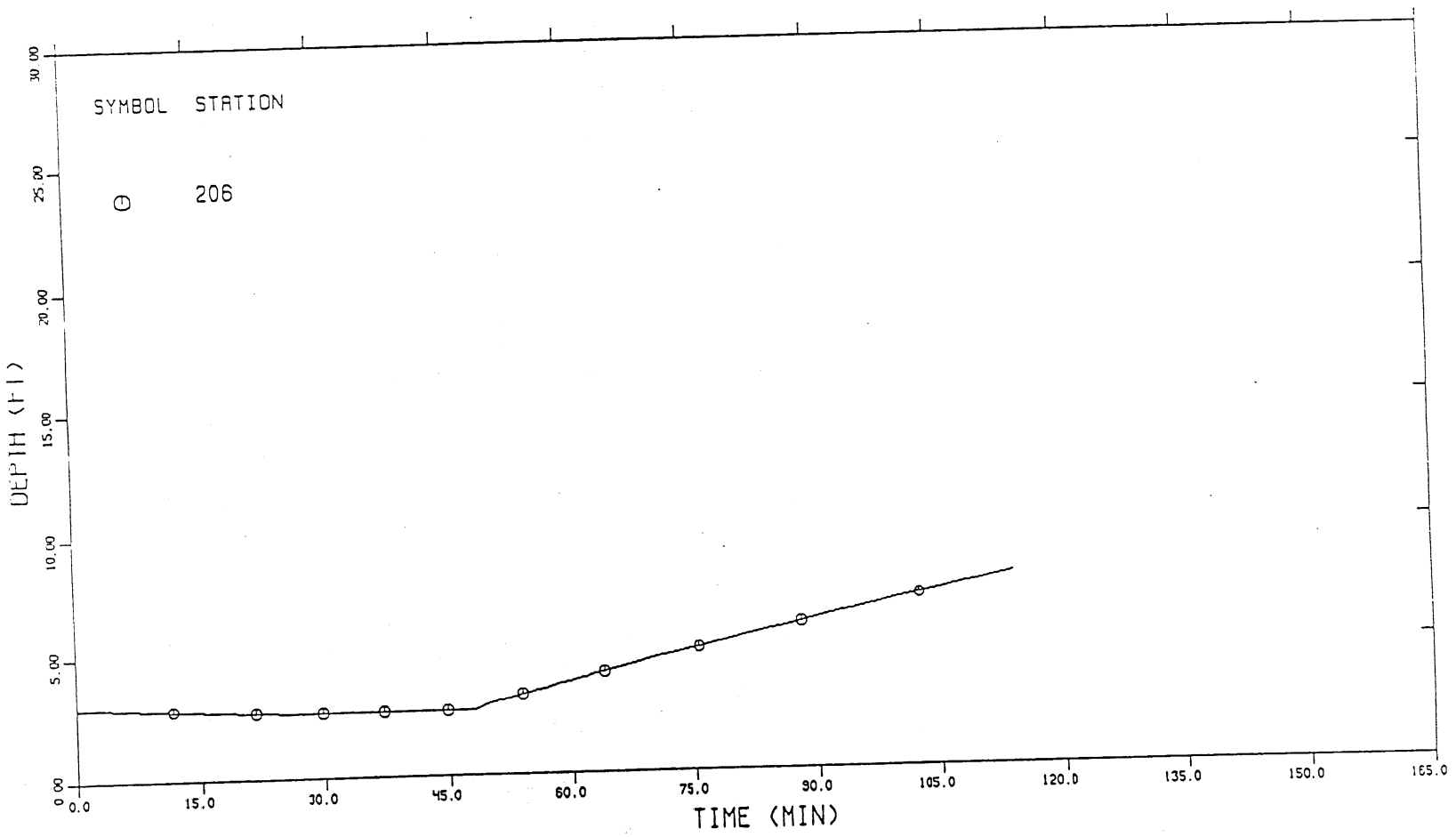

Fig. 49. Time variation of water depth at reservoir, maximum design flow.

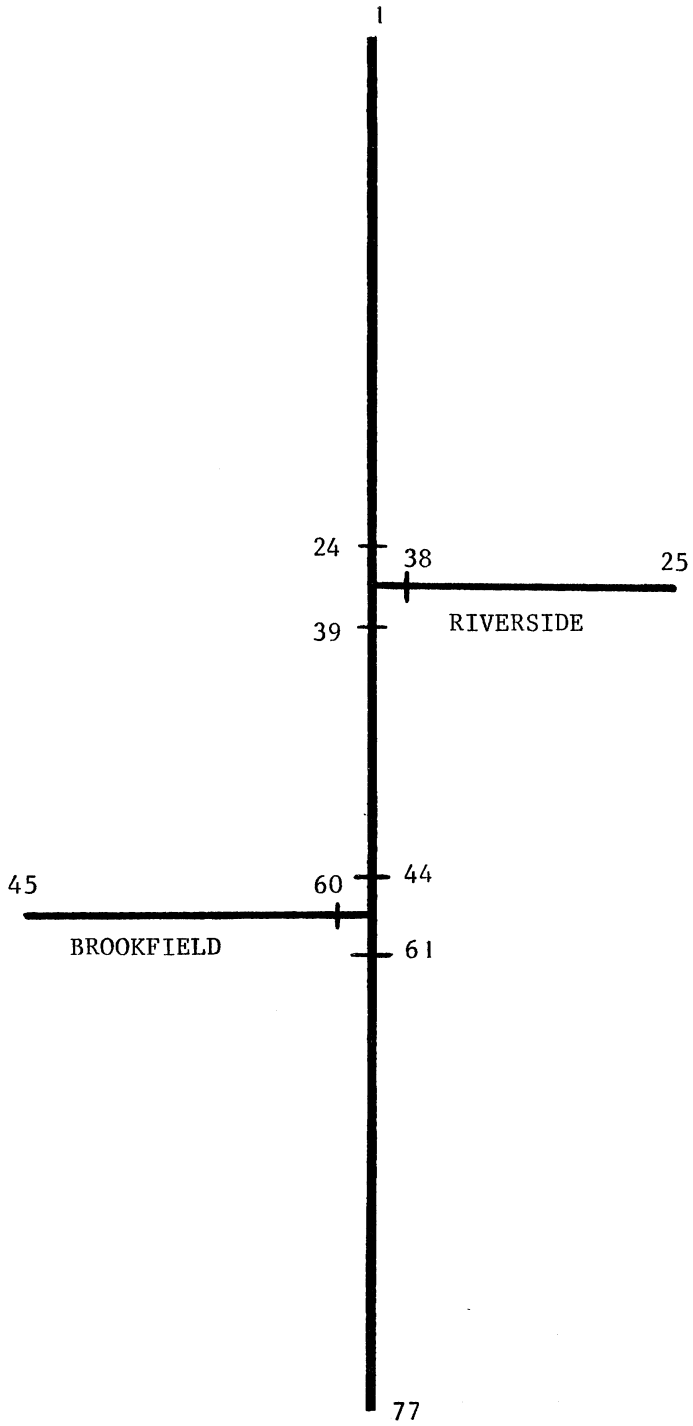

Fig. 50. Des Plaines South System configuration for modeling purpose.

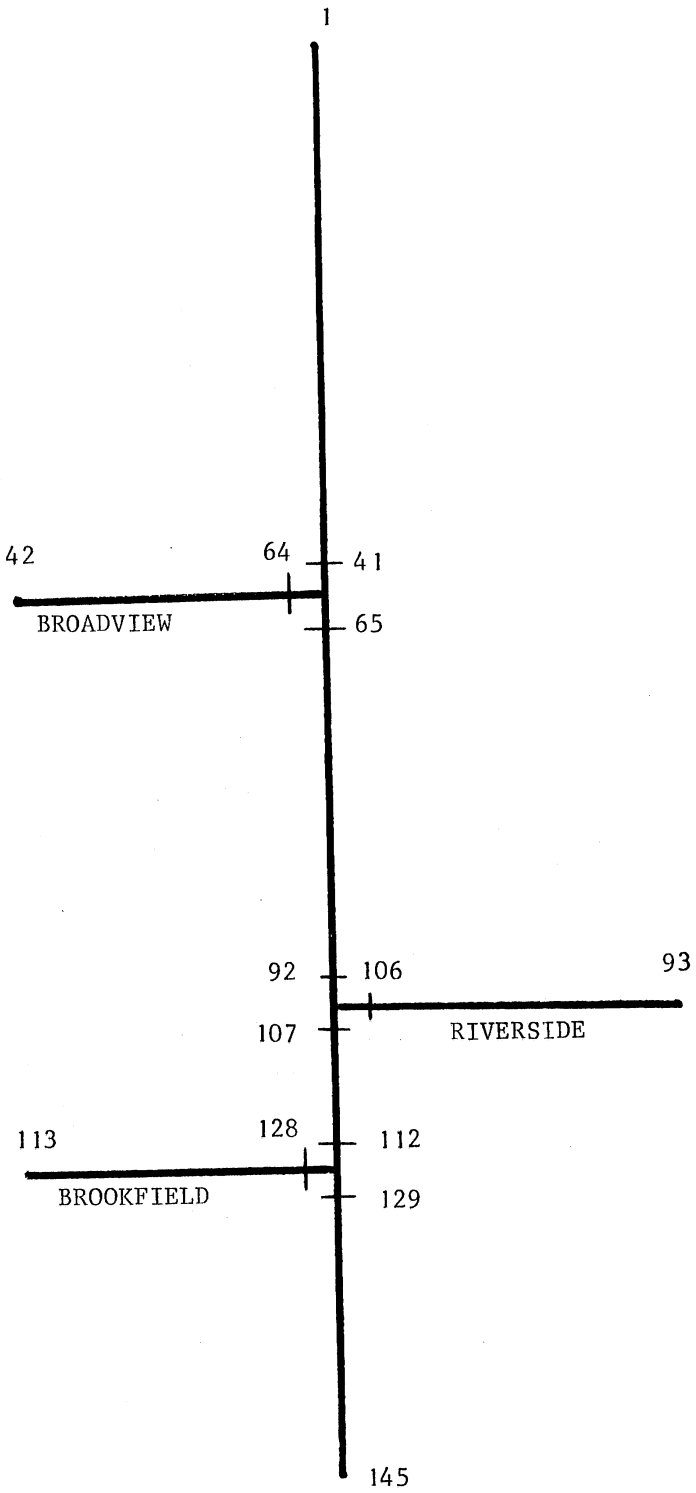

Fig. 51. Des Plaines South-Middle System configuration for modeling purpose.

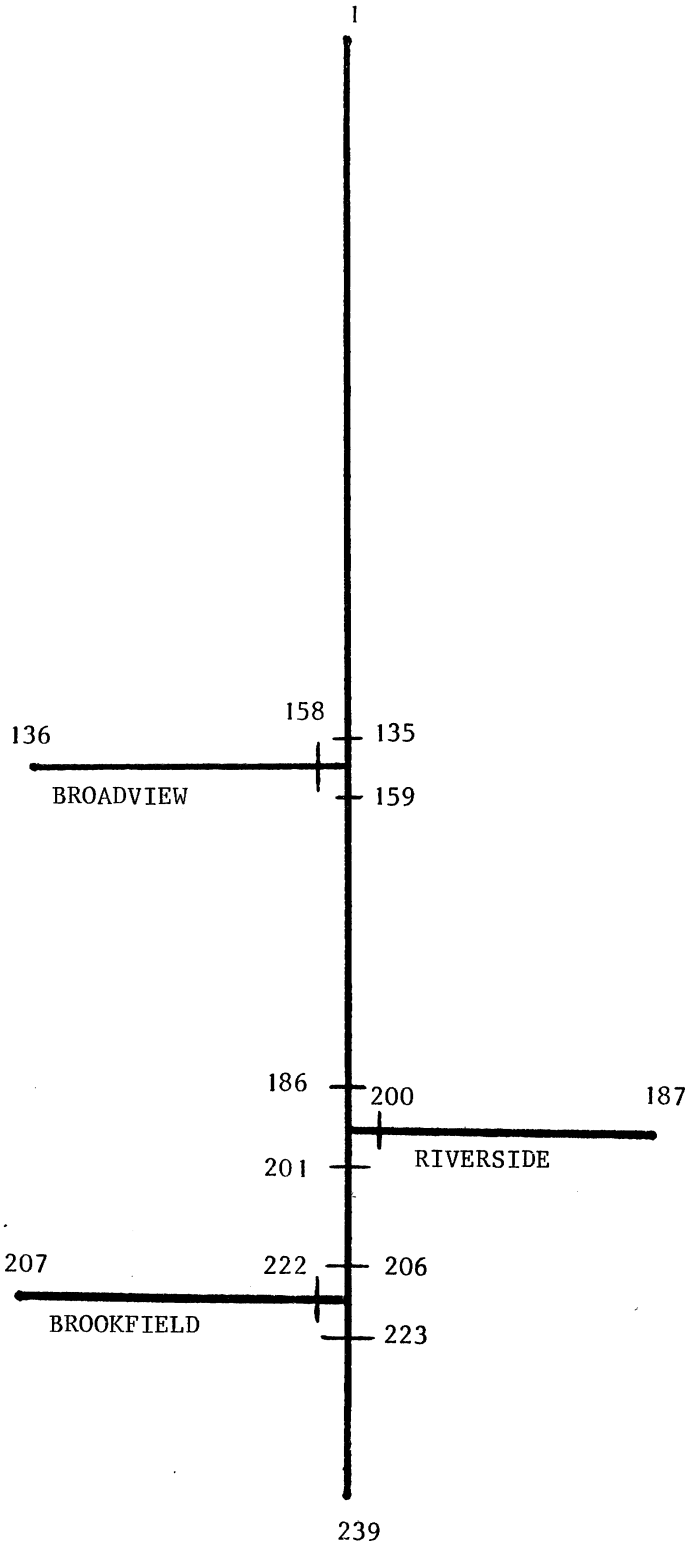

Fig. 52. Des Plaines complete system configuration for modeling purpose.

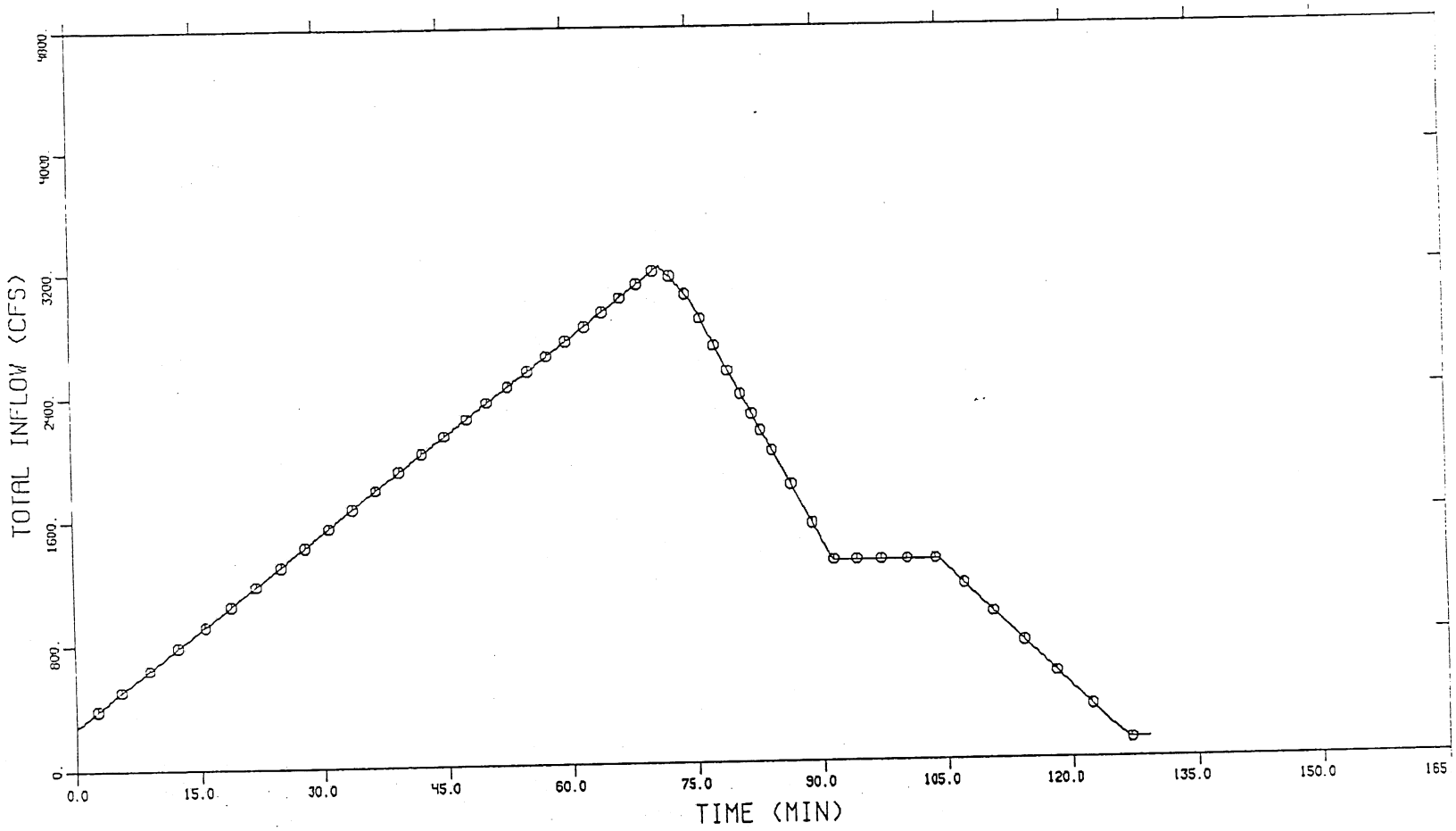

Fig. 53. Total controlled inflow hydrograph, South Desplain System.

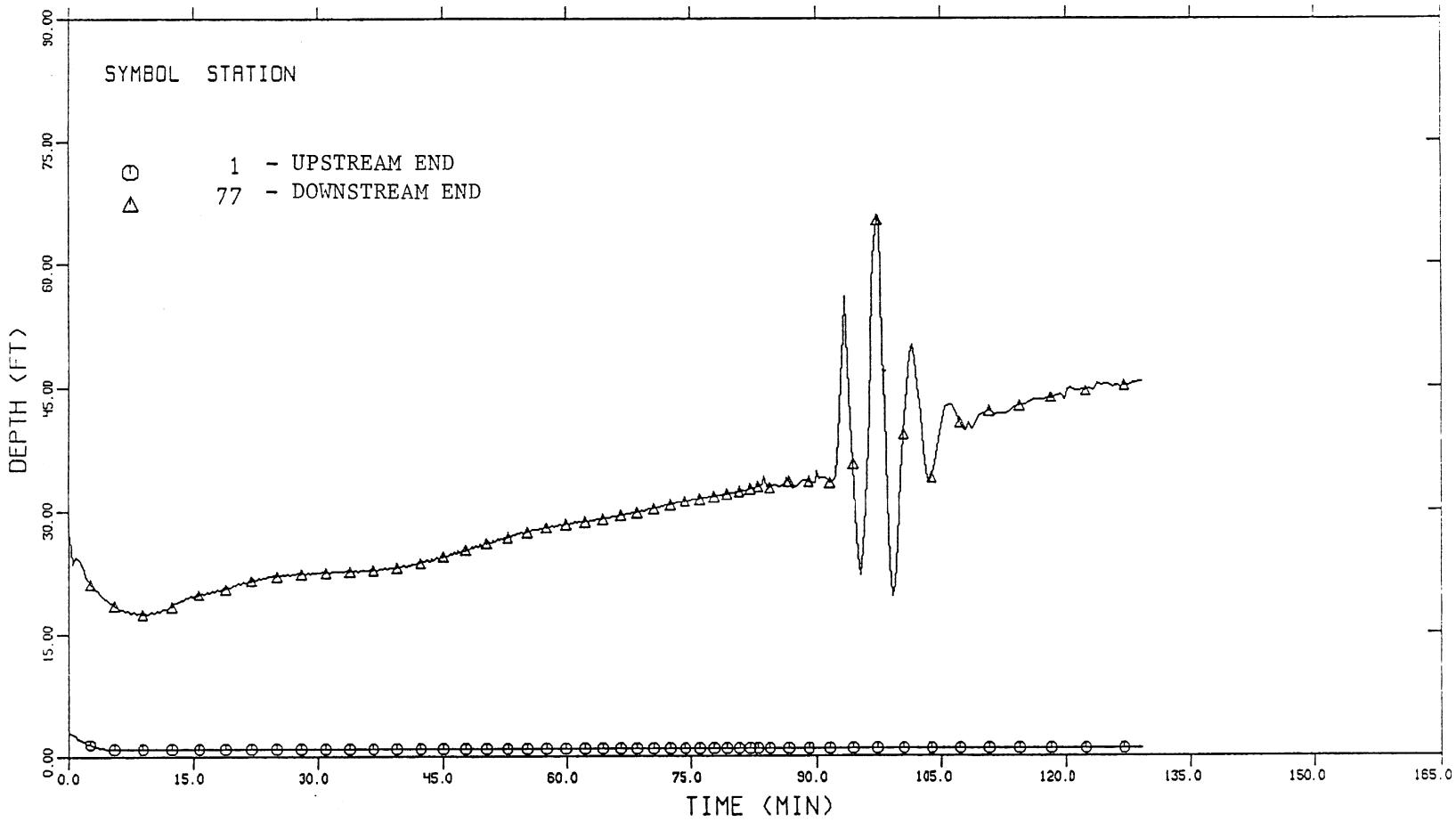

Fig. 54. Time variation of water depth, South Des Plaines System.

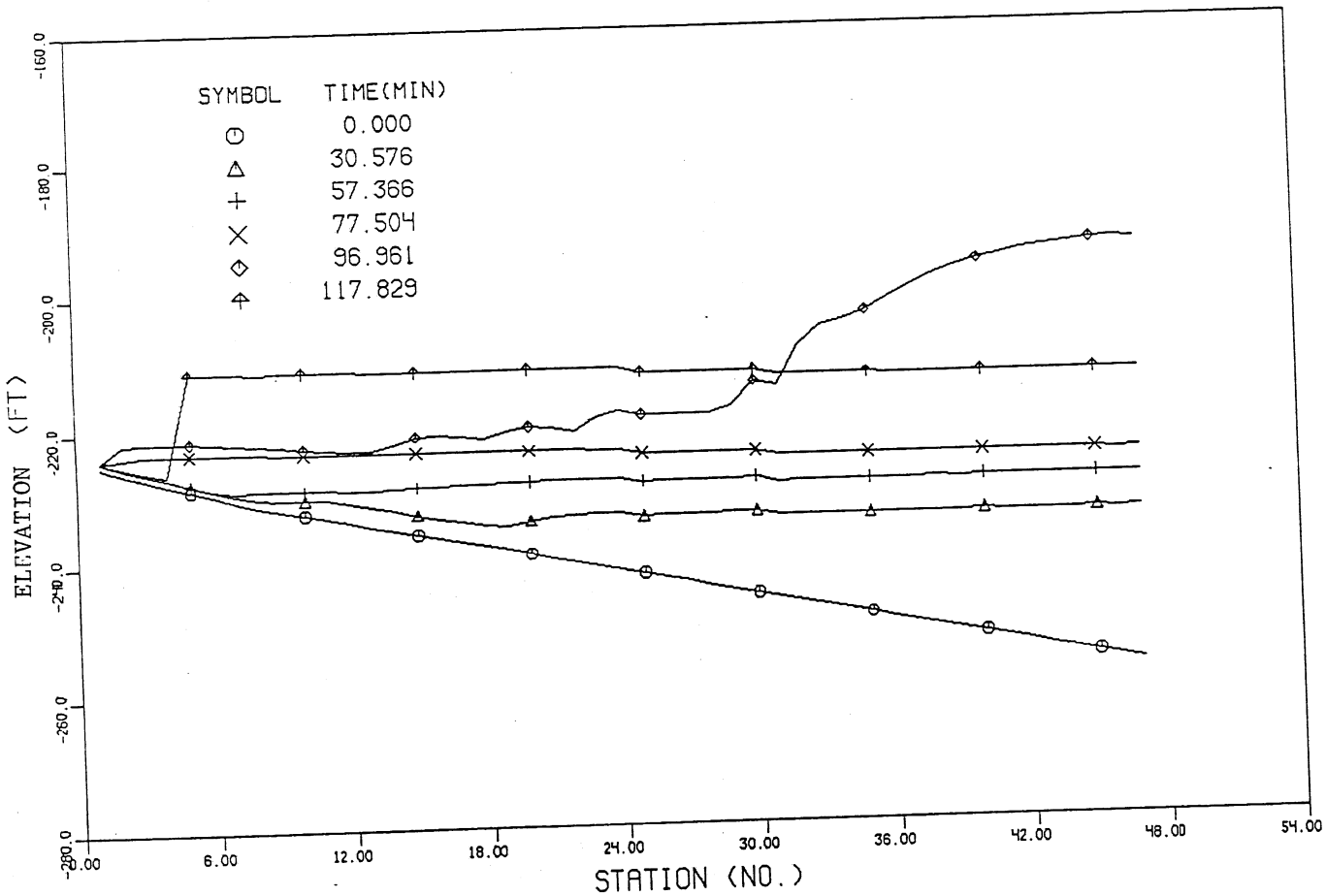

Fig. 55. Instantaneous hydraulic gradelines, South Des Plaines System.

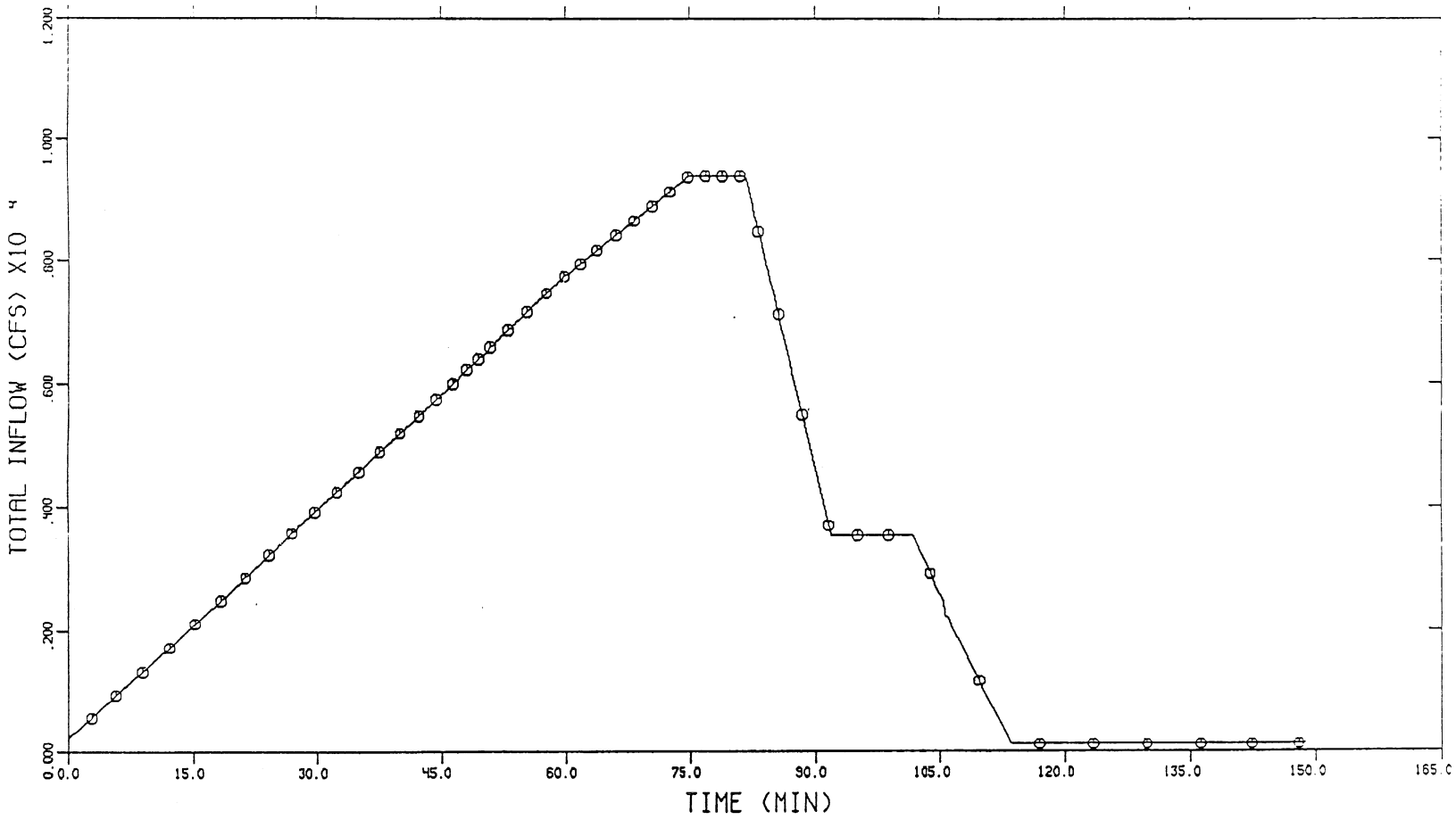

Fig. 56. Total inflow hydrograph - South-Middle System.

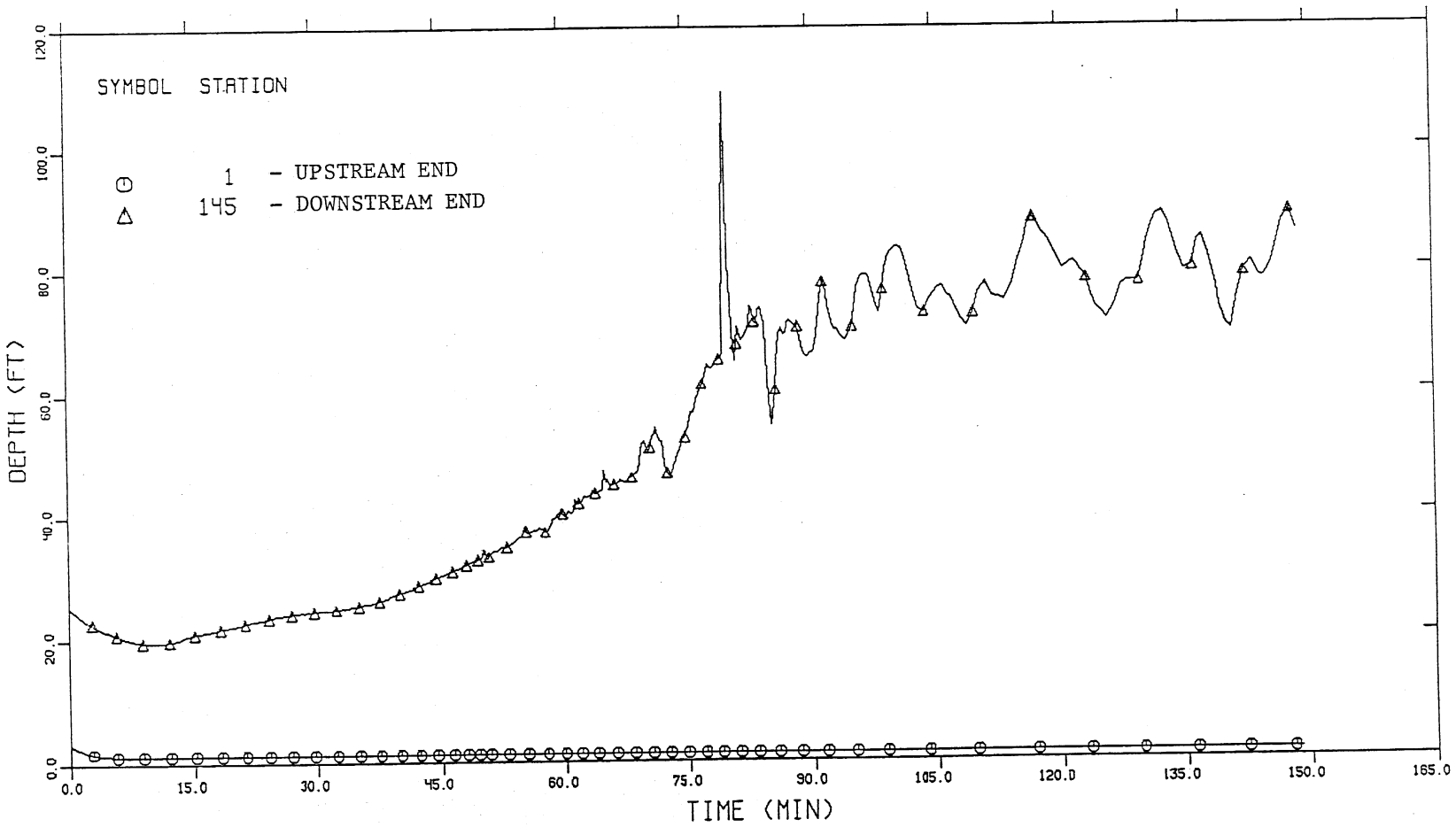

Fig. 57. Time variation of water depth at the ends of main tunnel, South-Middle System.

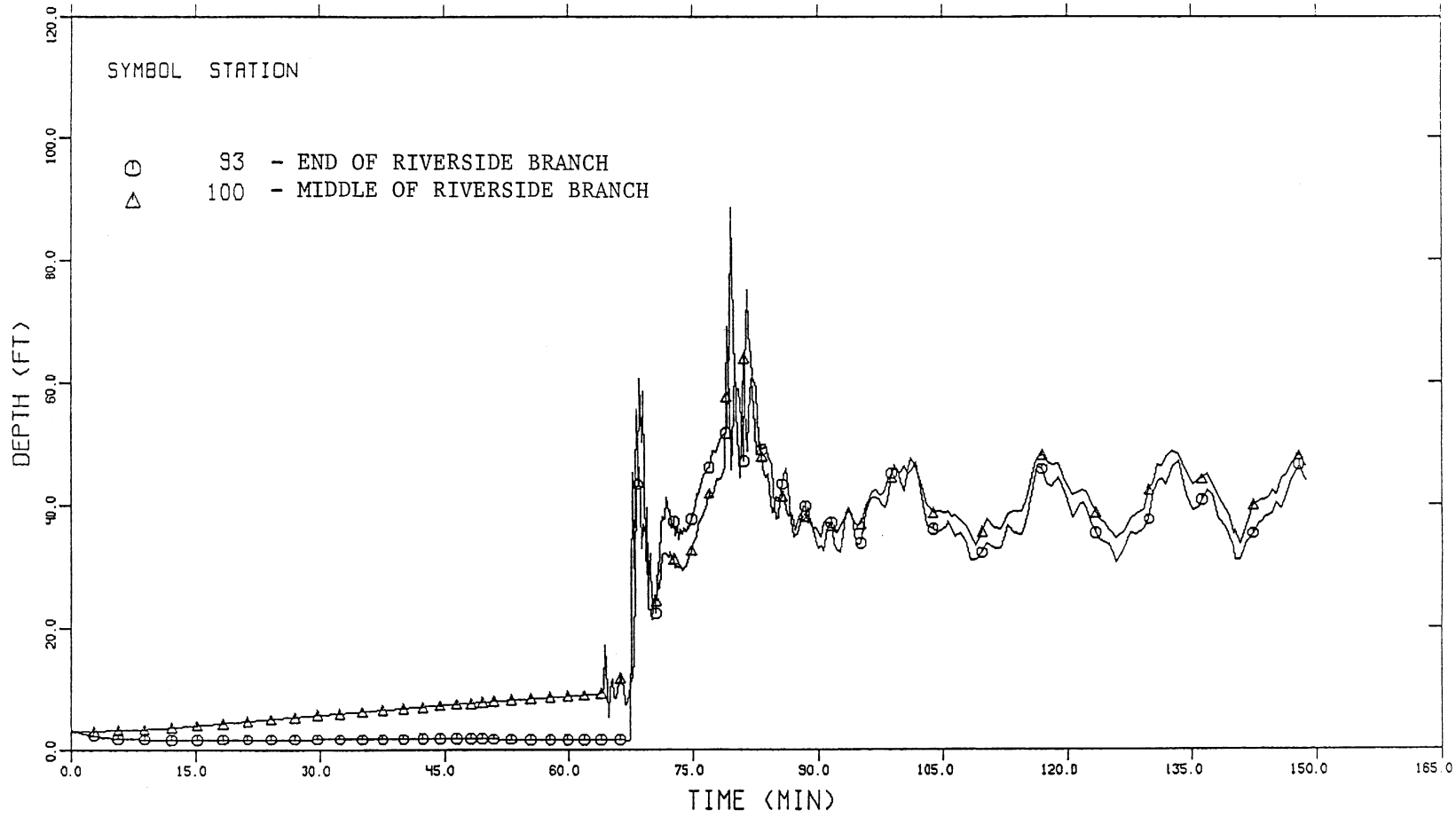

Fig. 58. Time variation of water depth in Riverside Branch, South-Middle System.

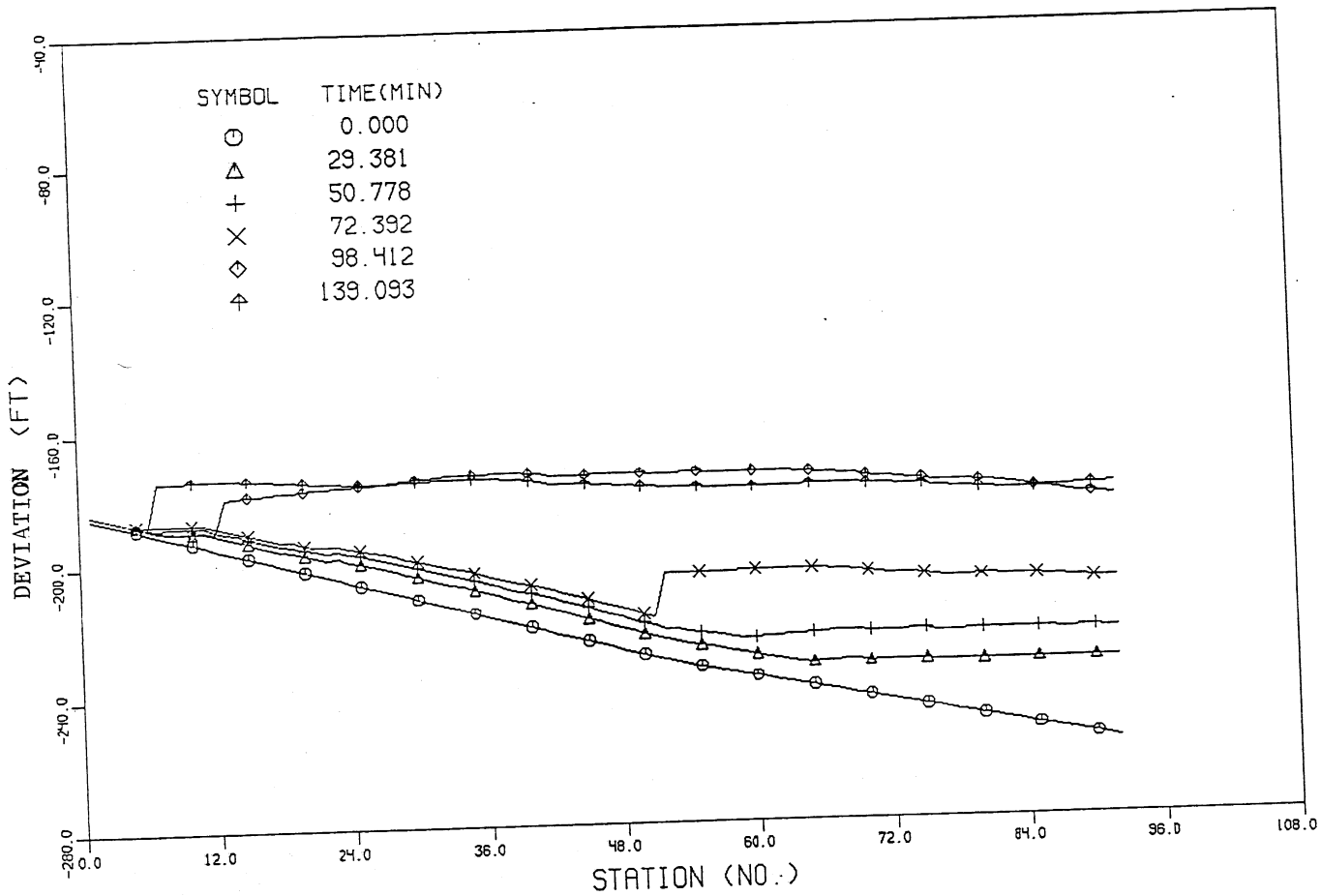

Fig. 59. Instantaneous hydraulic gradelines.

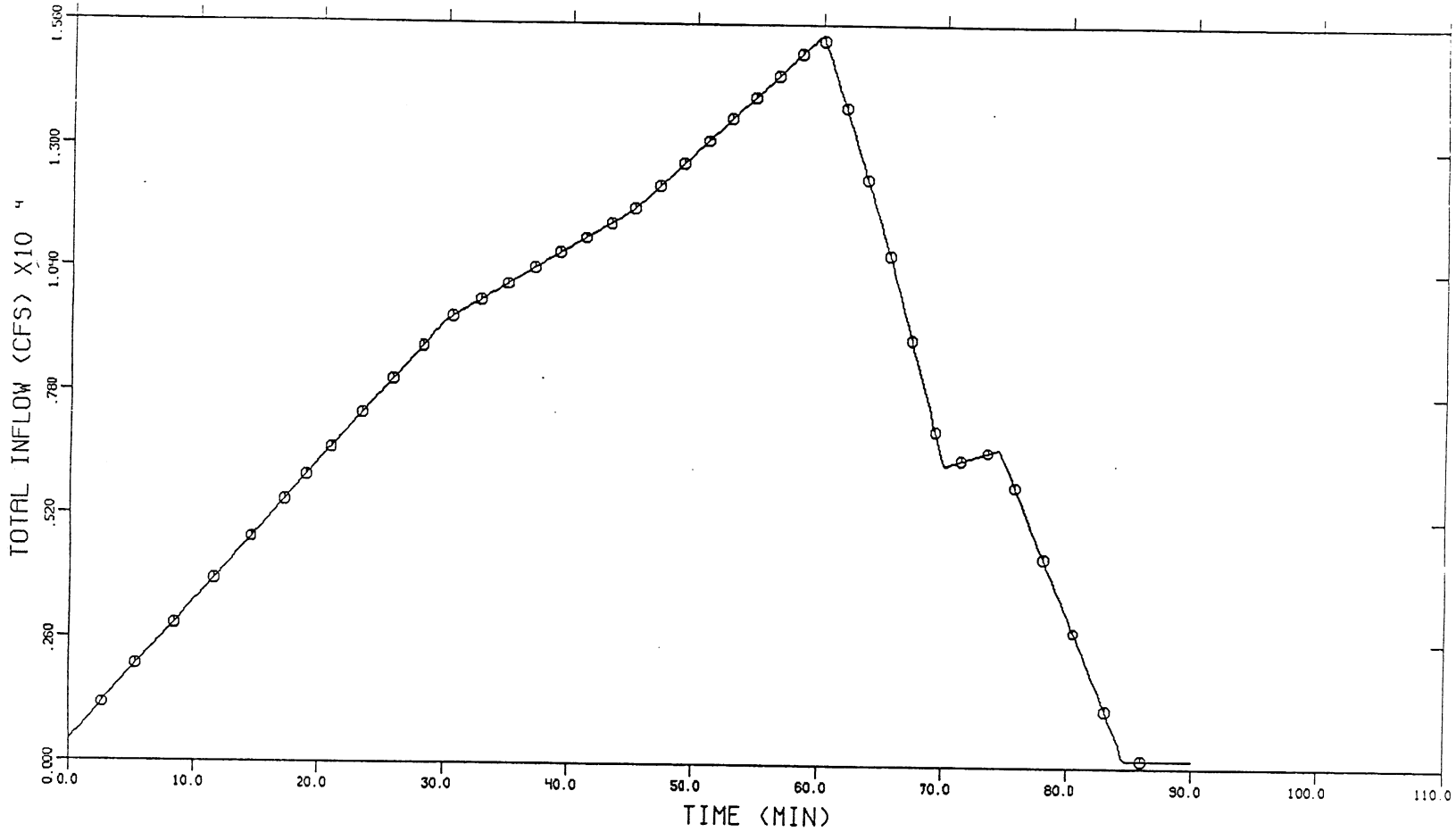

Fig. 60. Total inflow hydrograph - Complete Desplain System.

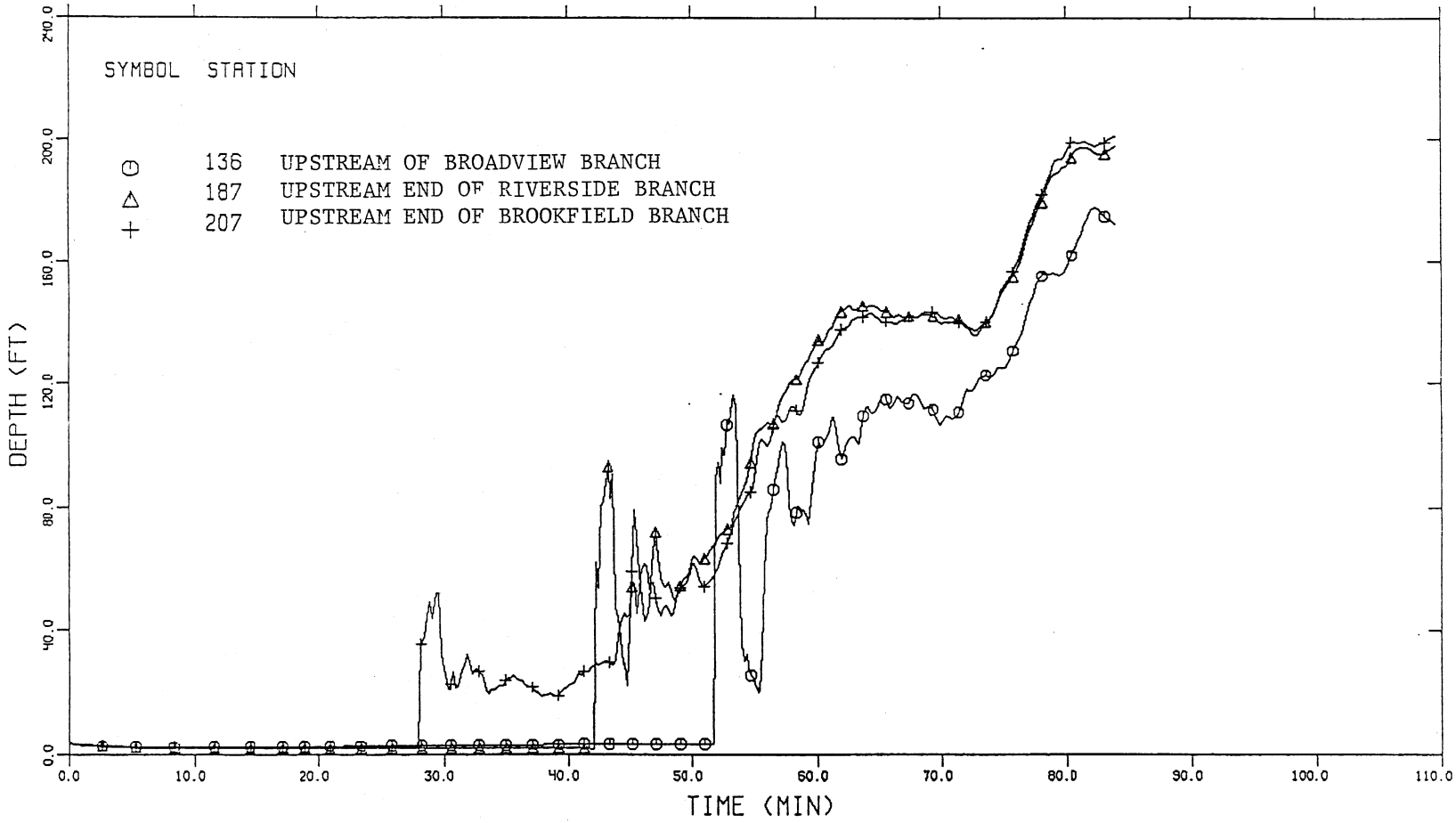

Fig. 61. Time variation of water depth at upstream ends of branch tunnels - complete Des Plaines System.

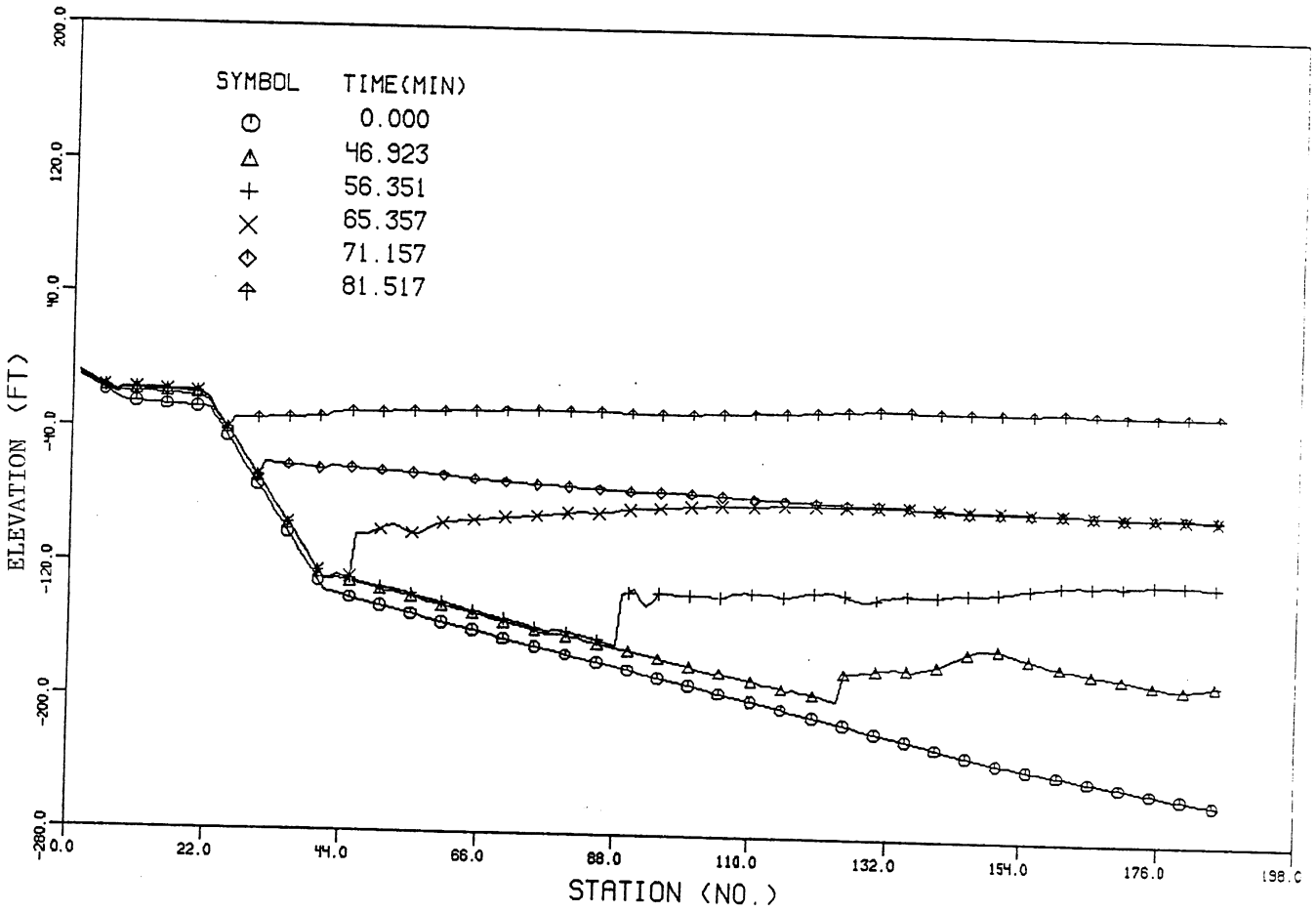

Fig. 62. Instantaneous hydraulic gradelines.

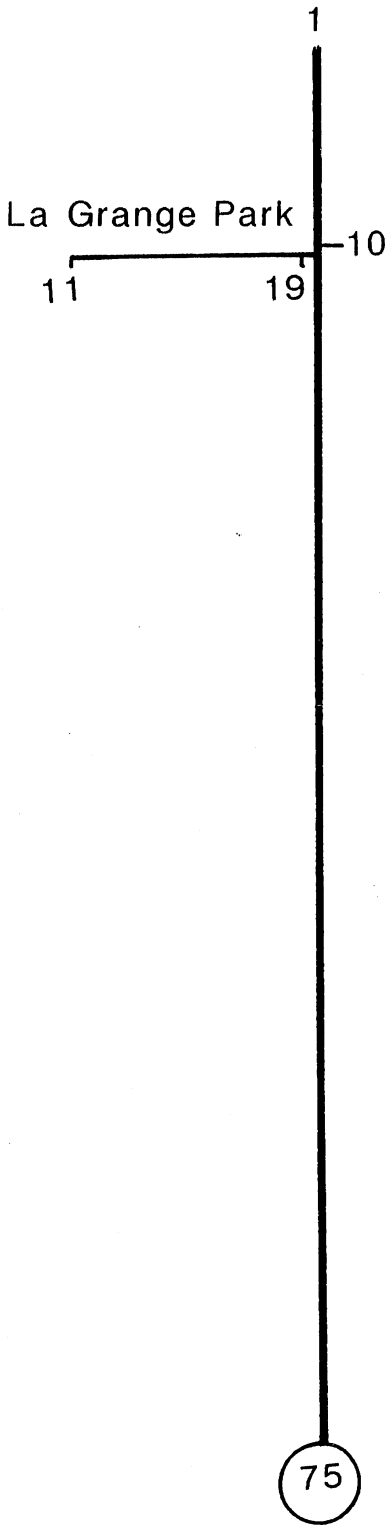

Fig. 63. 13A tunnel model system configuration.

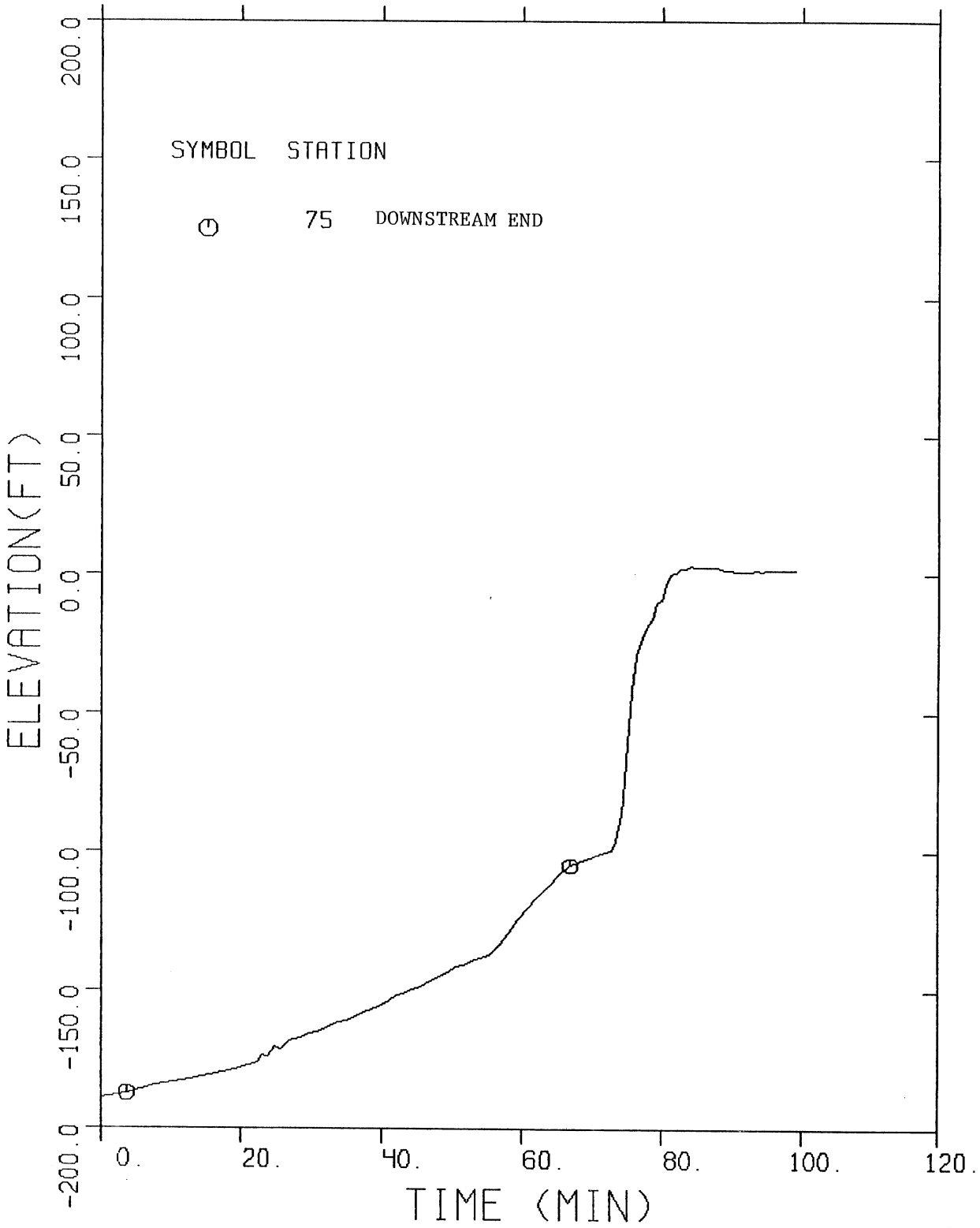

Fig. 6 4. Time variation of water surface elevation at downstream end, existing peak flow.

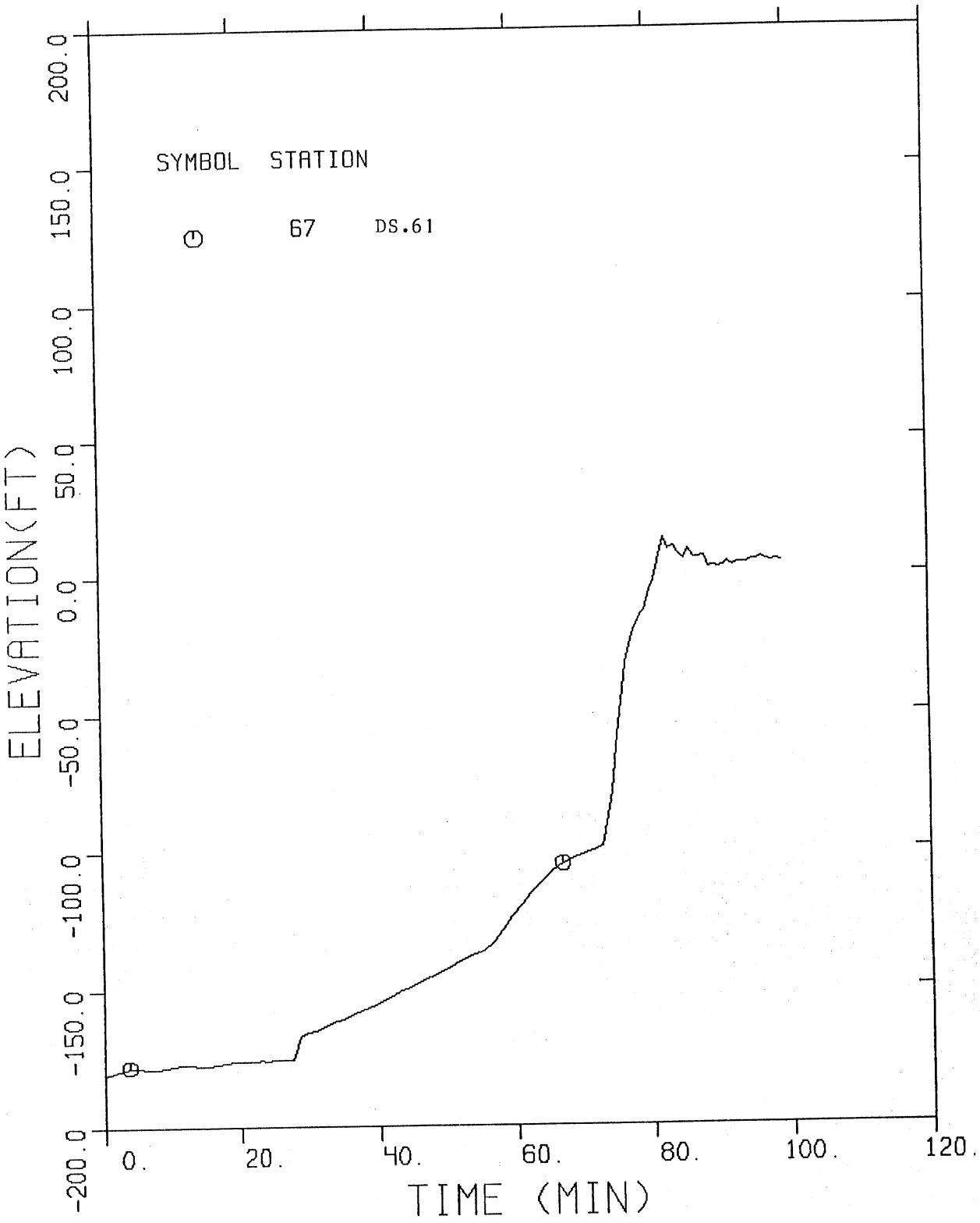

Fig. 65. Time variation of water surface elevation at DS.61, existing peak flow.

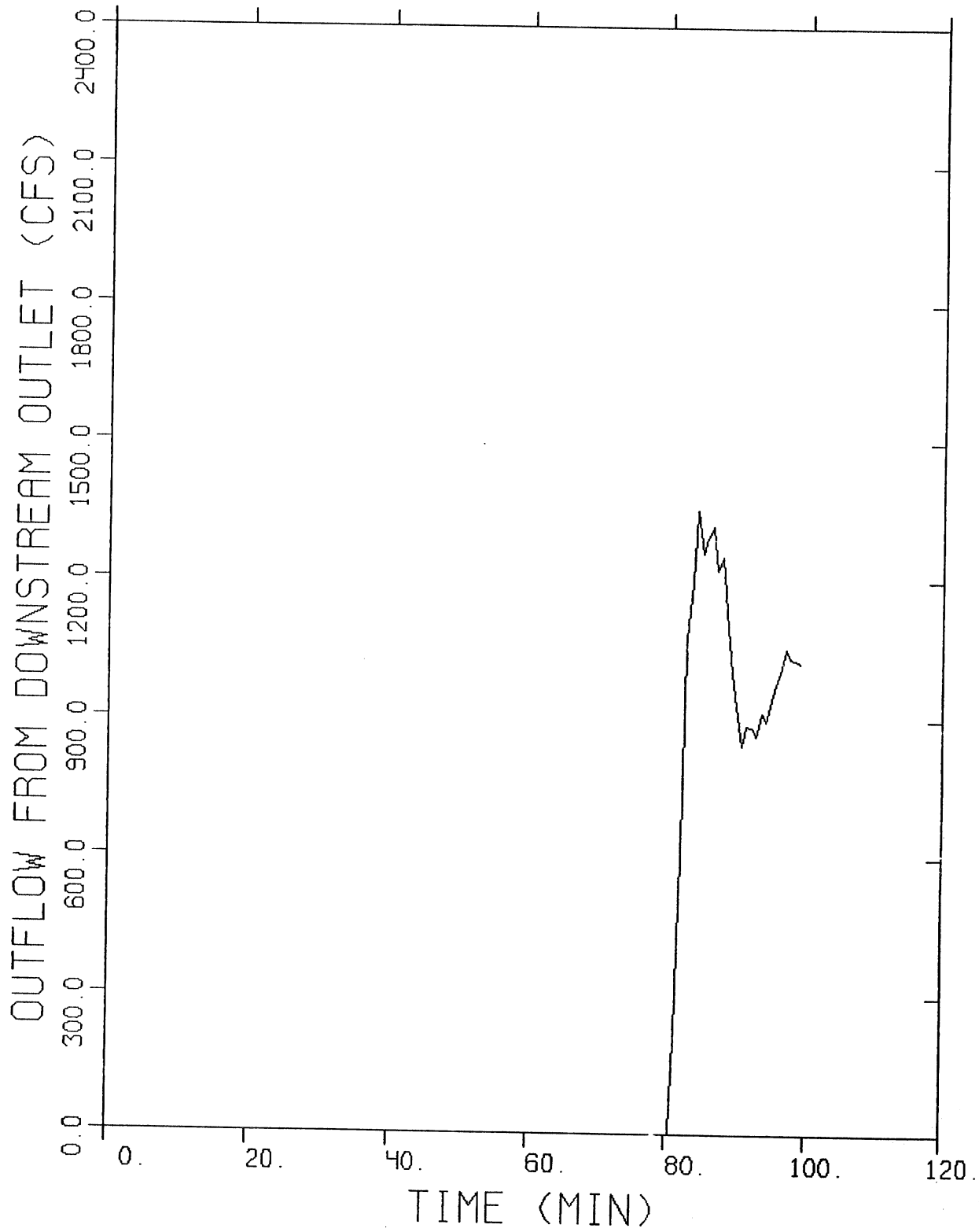

Fig. 66. Overflow hydrograph from 13A tunnel, existing peak flow.

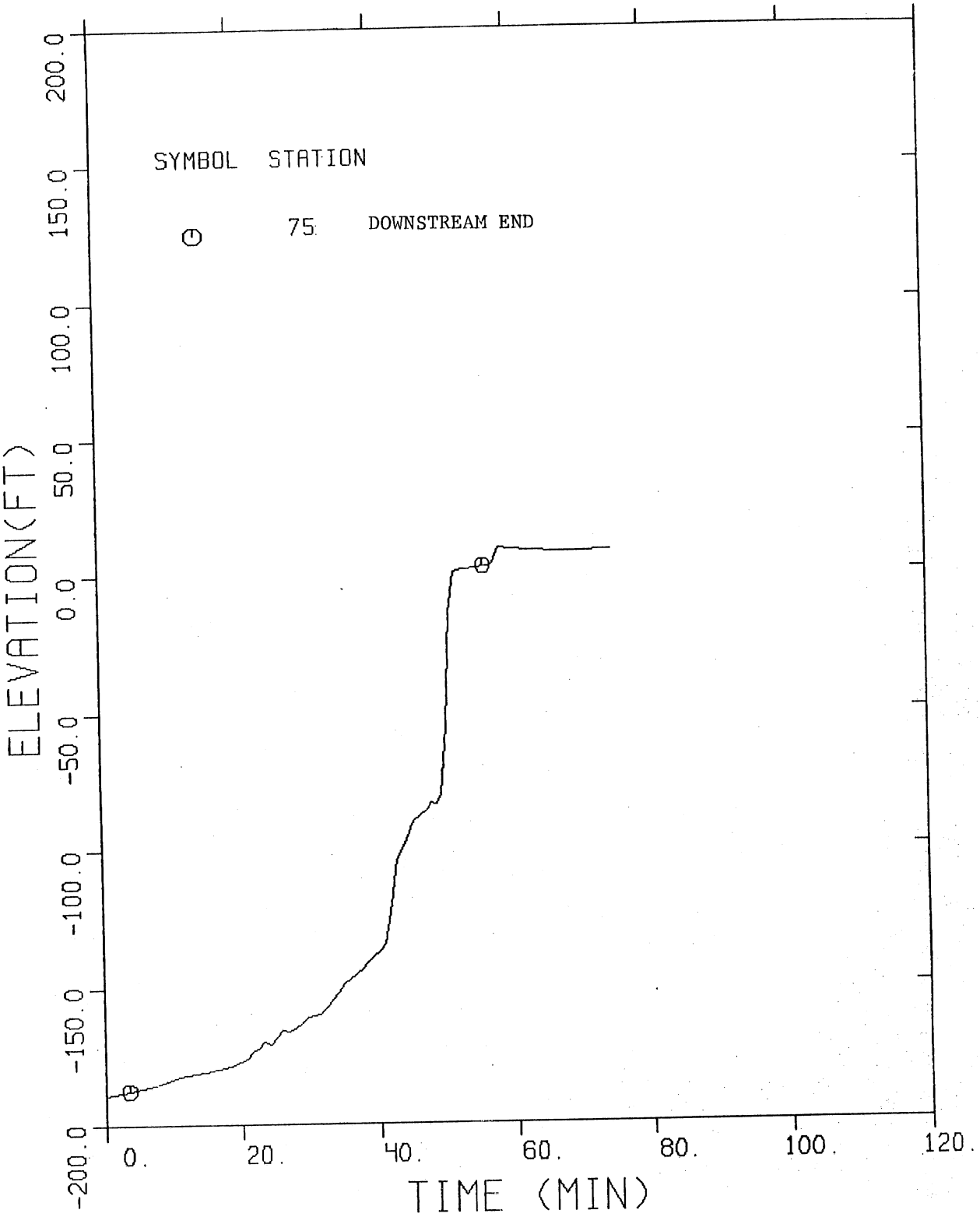

Fig. 67. Time variation of water surface elevation at downstream end, future peak flow.

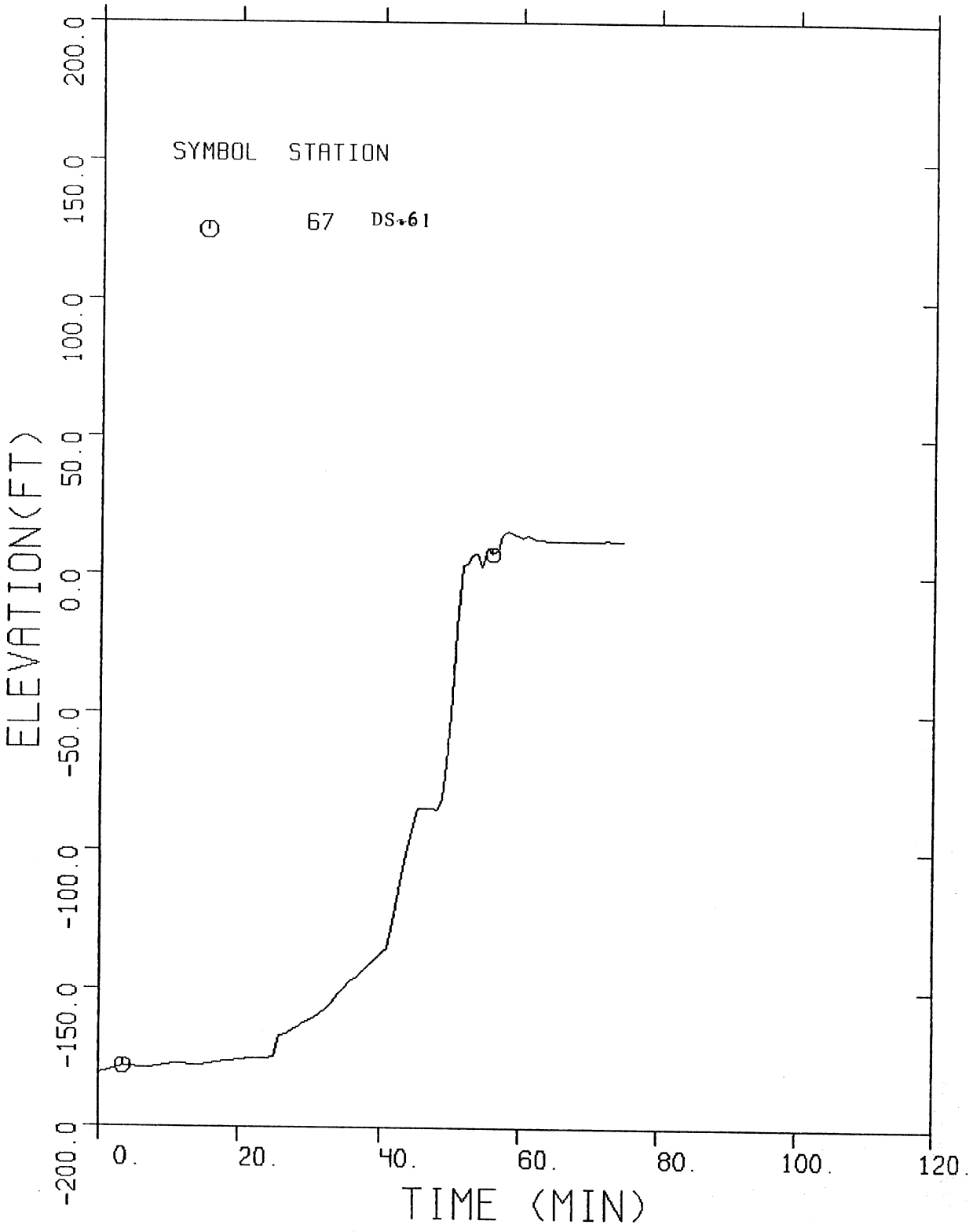

Fig. 68. Time variation of water surface elevation at DS.61, future peak flow.

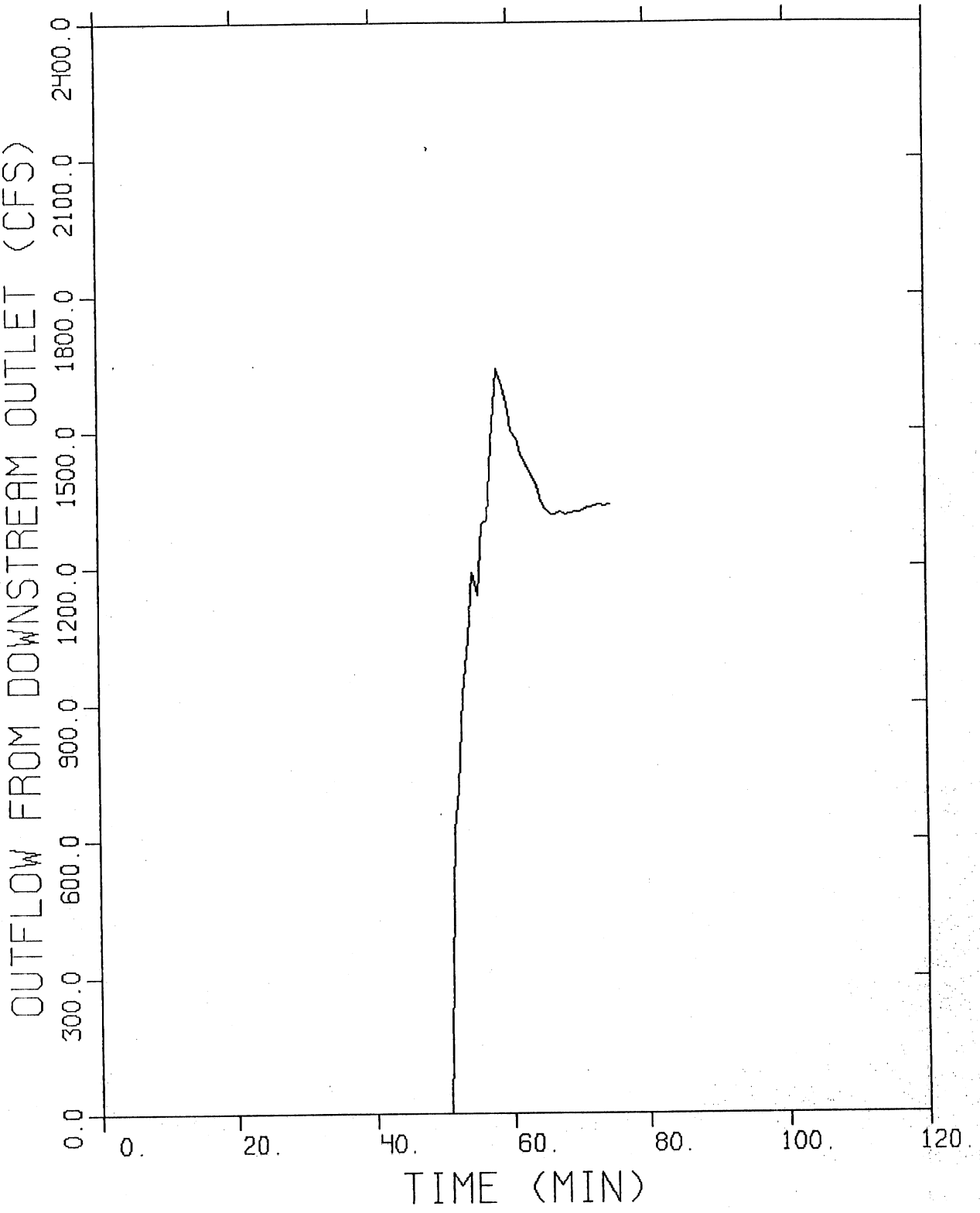

Fig. 69. Overflow hydrograph from 13A tunnel, future peak flow.

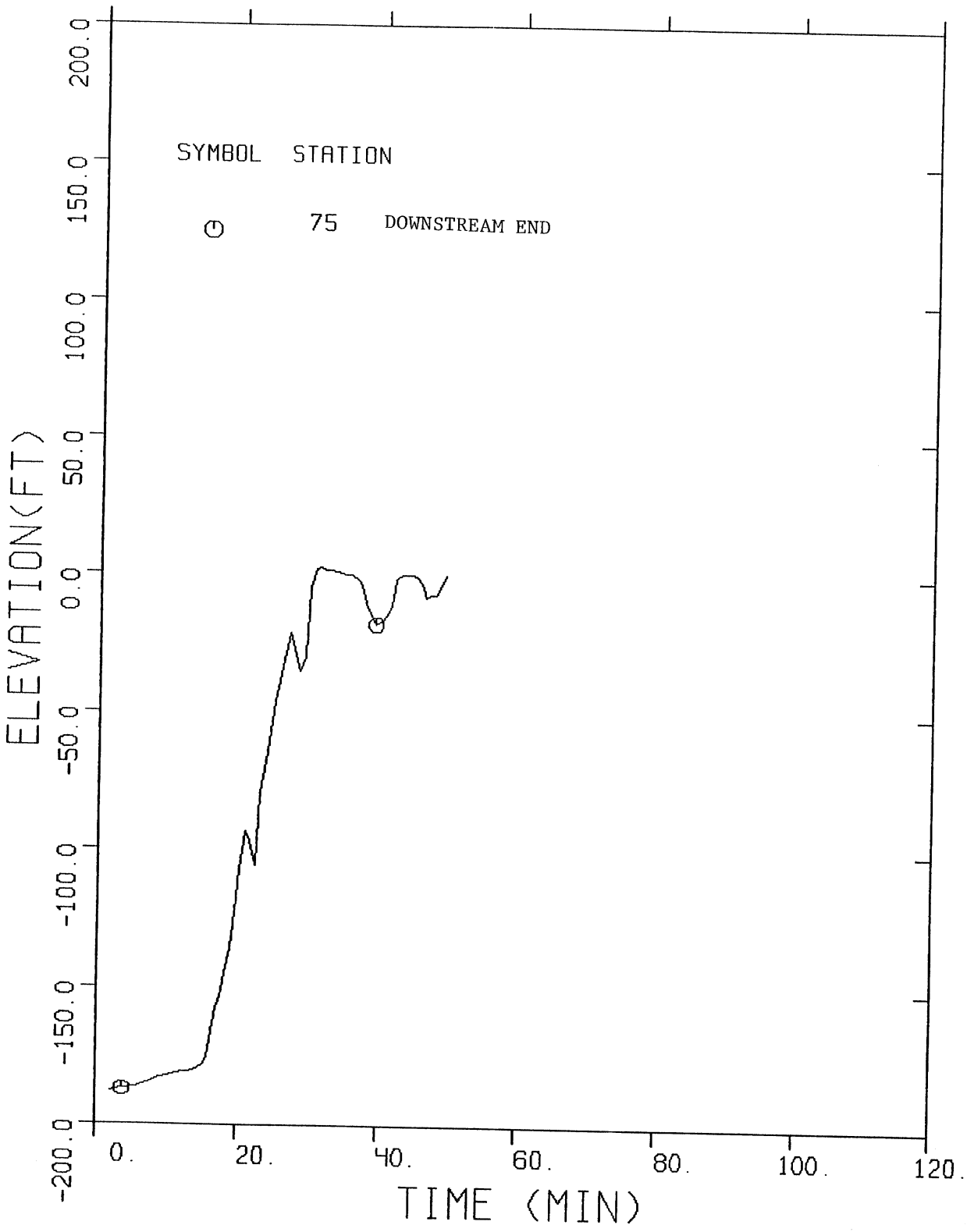

Fig. 70. Time variation of water surface elevation at downstream end, dropshaft design capacity inflow.

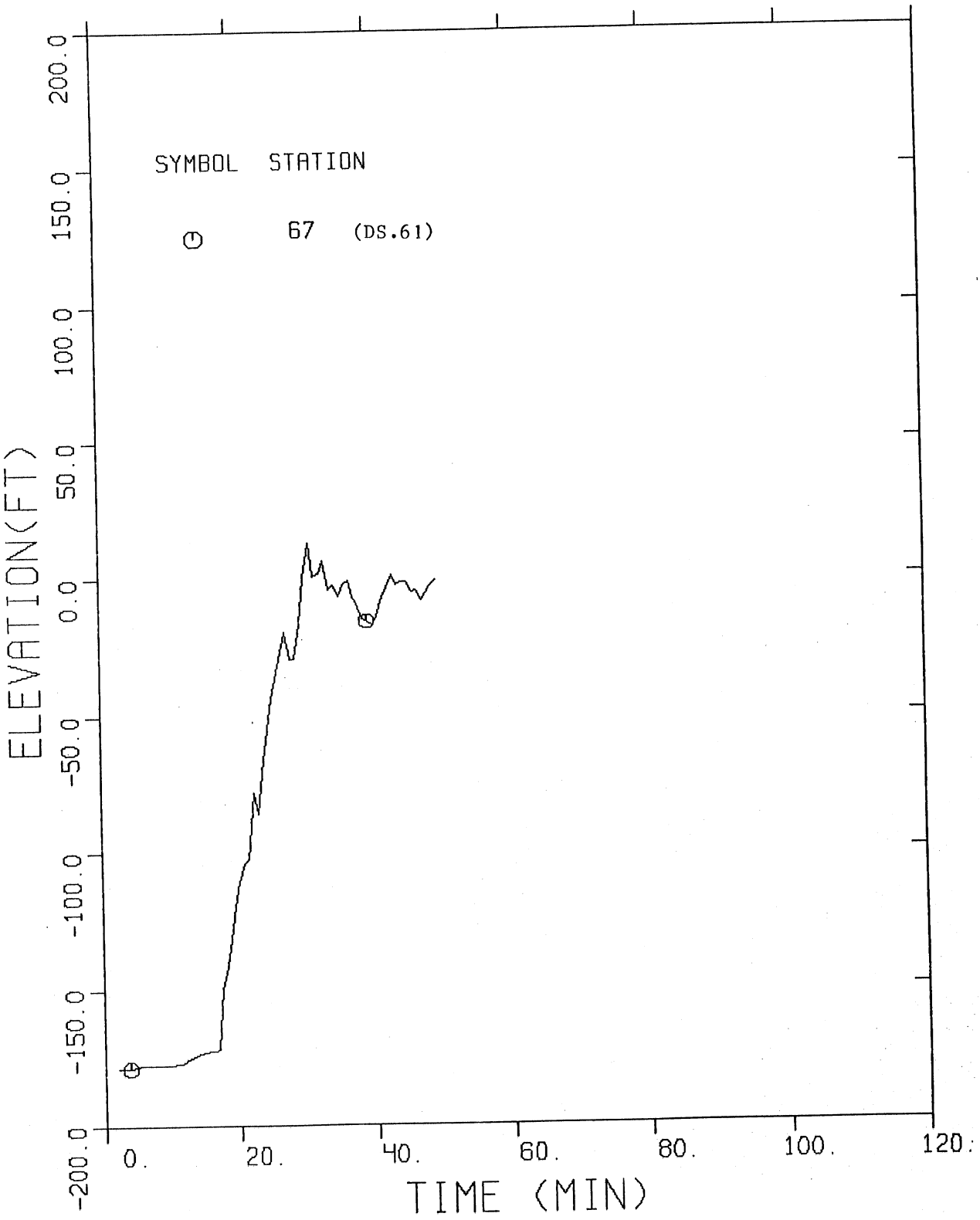

Fig. 71. Time variation of water surface elevation of DS.61, dropshaft design capacity inflow.

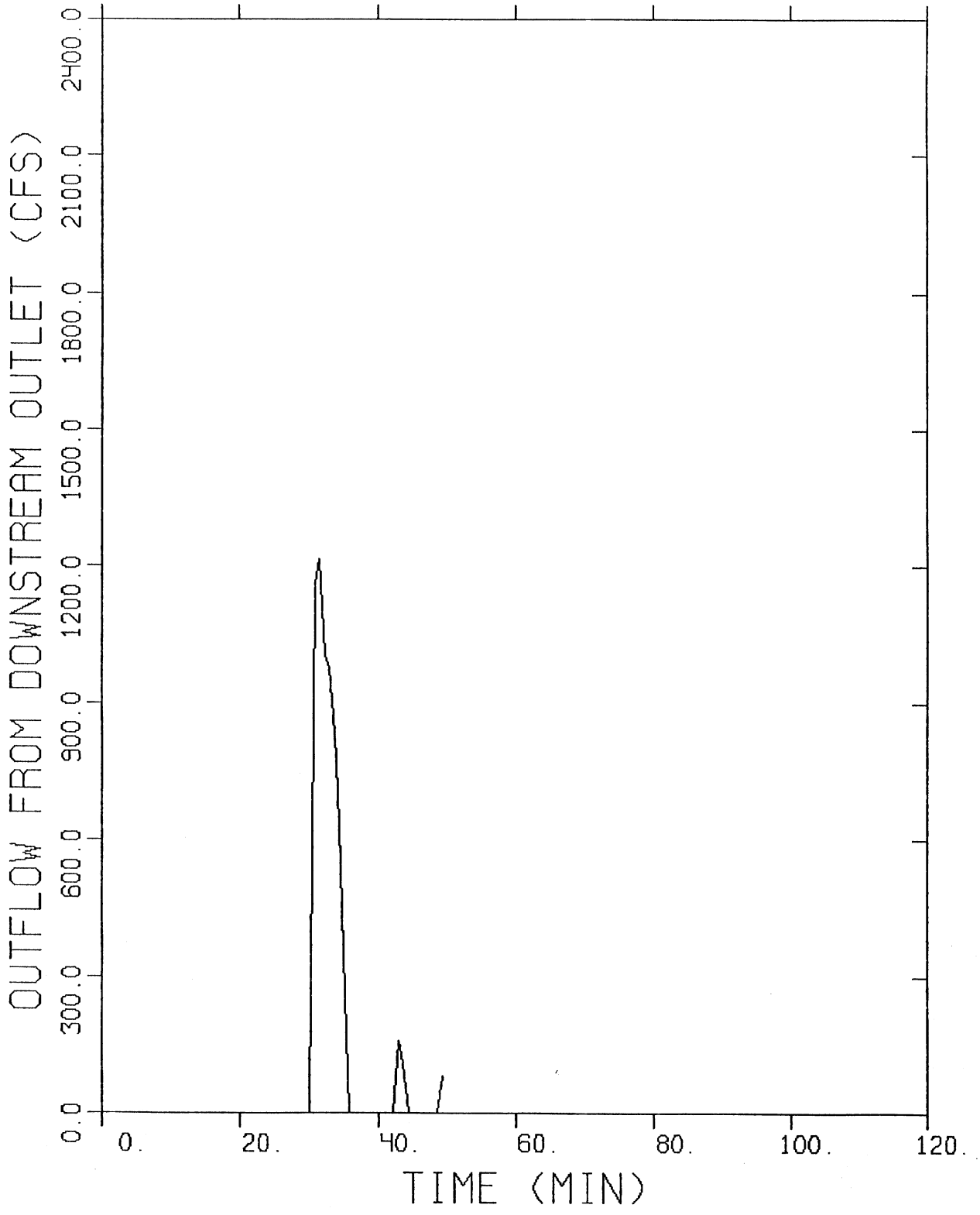

Fig. 72. Overflow hydrograph from 13A tunnel, dropshaft design capacity inflow.

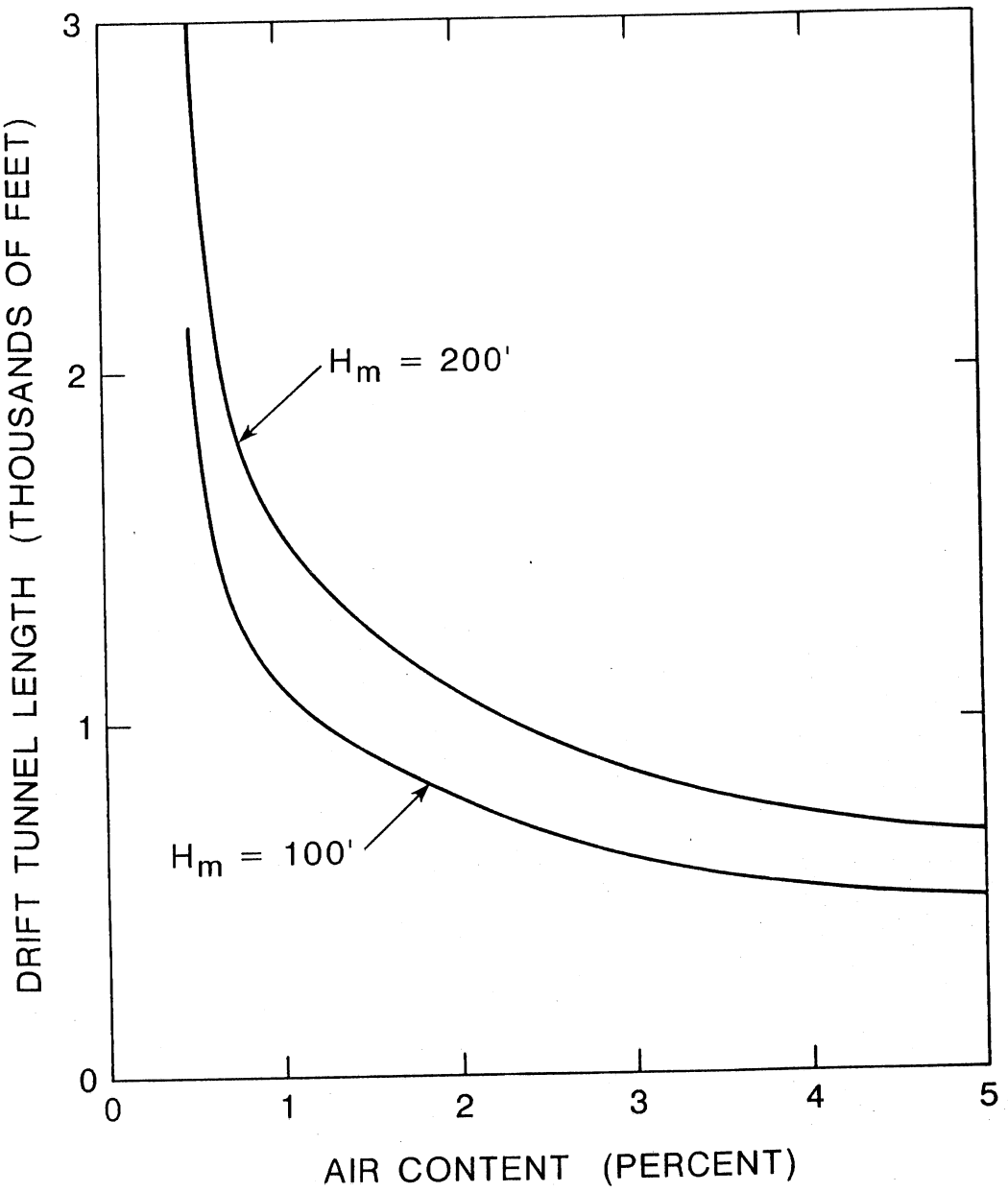

Fig. 73. Conditions for dropshaft-drift tube resonance.